12-15-2014

Toward the Combinatorial Development of Hydrophobic-Tagged Antifolate-Directed Degradation of Human Thymidylate Synthase

Daniel J. Menasco
University of South Carolina - Columbia

TOWARD THE COMBINATORIAL DEVELOPMENT OF HYDROPHOBIC-TAGGED ANTIFOLATE-DIRECTED DEGRADATION OF HUMAN THYMIDYLATE SYNTHASE

by

Daniel J. Menasco

Bachelor of Science
Southern Oregon University, 2000

Submitted in Partial Fulfillment of the Requirements

For the Degree of Doctor of Philosophy in

Chemistry

College of Arts and Sciences

University of South Carolina

2014

Accepted by:

Qian Wang, Major Professor

James M. Sodetz, Committee Member

Maksymilian Chruszcz, Committee Member

Kim Creek, Committee Member

Lacy Ford, Vice Provost and Dean of Graduate Studies

DEDICATION

To my girls: the center of my universe.

ACKNOWLEDGEMENTS

I would like to take this opportunity to acknowledge my mentor, Qian Wang, for his forbearance, sagacity, and the unsolicited counsel that he provided in times of my own personal tumult. His determined and relentless pursuit to provide opportunities with his the intrepid tact, have undoubtedly left an indelible impression of appreciation and pride. I would also like to thank Dr. Gary Horvath and Karen Barbour both of whom I hold in the highest regards for their work ethic, measured personality, and their keen depth of insight. The knowledge they've passed on to me was integral to the pursuit of my own personal research. Moreover, I thoroughly enjoyed their company and their exceptional sense of humor.

I would like to express my sincere gratitude towards the following professors, colleagues, undergraduates, and former lab members for their mentorship and support: Professor Franklin G. Berger, Professor Lukasz Lebioda, Professor Kazunori Kataoka, Associate Professor Caryn E. Outten, Associate Professor Campbell McInnes, R. James Christie, Ph.D., Josh Bolger, Ph.D., Eve Nisaraporn Suthiwangcharoen, Ph.D., Leslie Lovelace, Ph.D. Jun Hu, Ph.D., Jillian Clarire, Boyd Baxter Lever III, Phirun Cheng, Enoch Adolga, Nick Mank, and of course Andrew "Twinky" Lee, Ph.D.

Lastly, I want to thank my family: my brother for his unwavering support, love, and his exceptional fidelity, my mother for her resolute drive to care for and love her granddaughters in their father's absence, and my spritely little girls Hana and Hina; without your laughter and love I couldn't have accomplish so much. Both of you will

always be my proudest achievements. Lastly, a true friend: my beautiful loving wife whose ebullience and equanimity kept me focused and measured under the mos nsurmountable circumstances. Her remarkable love and unflinching support will remain ineffable, as they cannot be compared.

ABSTRACT

Direct post-translational control over a protein of interest (POI) can be exploited by manipulating the cells protein quality-control systems responsible for either intracellular turnover through ubiquitination (POI half-life) or repairing and degrading misfolded proteins.[1] In an effort to target and degrade a high value POI we selected the enzyme human thymidylate synthase (TS) for post-translational degradation through ligand-directed ubiquitination and hydrophobic tagging.

Thymidylate synthase catalyzes the reductive methylation of 2'-deoxyuridine monophosphate (dUMP) to 2'-deoxythymidine monophosphate (dTMP). As the *de novo* source of dTMP the regulation of intracellular TS is strictly controlled by ubiquitin-independent proteasomal degradation mediated by an internal TS-degron sequence.[2,3] Using conventional peptide synthesis and the TS-directed antifolate, raltitrexed (RTX), we designed a series of a high affinity RTX-directed conjugates that specifically recruited TS to the von Hippel Linadau (VHL) E3 ligase in order to facilitate ubiquitin-dependent proteasomal degradation. These protein suppression conjugates are known as PROteolysis TArgeting Chimera's (PROTAC). These conjugates were challenged against TS and TS overexpressing cell lines with their inhibition and ubiquitination events monitored by half-life and Western blot analyses. However, no evidence of ubiquitin-mediated proteasomal degradation was found.

Contrary to the reliance of ubiquitination by the PROTAC's system, we sought to simplify our approach and "tag" TS with a hydrophobic probe. The seminal driving force behind protein folding and stabilization is the burial of core hydrophobic residues.[4] While these residues are critical to maintaining the native folding state, partial denaturation results in their exposure, leading to incomplete folding events and proteasomal degradation.[5,6] In an effort to mimic this endogenous event and promote active TS proteasomal degradation, we generated a small library of RTX linked hydrophobic tags using the Kenner safety-catch handle under solid phase peptide synthesis. In this study we found that the general length of both the linkage and surface area of the hydrophobic tag were essential to growth inhibition of TS bearing cells. The implications of these findings, with regards to both the synthetic endeavors and their respective biological results, are discussed.

Table of Contents

LIST OF TABLES

LIST OF FIGURES

List of Abbreviations

5FU 5-fluorouracil

5mTHF ..... 5'-methyltetrahydrofolate

Ala ..... Alanine

Arg ..... Arginine

ATP ..... Adenosine Triphosphate

Asp ..... Aspartic Acid

CB3717 ..... 10-propargyl-5,8-dideazafolic acid

CDK ..... Cyclin Dependent Kinase

CRC ..... Colorectal Cancer

$CH_2H_4PteGlu$ ..... N^5,N^{10}-methylenetetrahydrofolate

DHFR ..... Dihydrofolate Reductase

DNA ..... Deoxyribonucleic Acid

ecTS ..... *Escherichia coli* Thymidylate Synthase

ERAD ..... ER-associated degradation

eYFP ..... Enhanced Yellow Fluorescent Protein

dUMP ..... 2'-deoxyuridine monophosphate

dTMP ..... 2'-deoxythymidine monophosphate

dUTP ..... 2'-deoxyuridine triphosphate

E ..... Glutamic Acid

E. Coli ..... *Escherichia coli*

FBP ..... F box protein

FdUMP ..... 5-fluoro-2'-deoxyuridylate

FdUTP ..... 5-fluoro-2'-deoxyuridyltriphosphate

FPGS ..... Folylpolyglutamate Synthetase

GFP ..... Green Fluorescent Protein

Gly ..... Glycine

Glu ..... Glutamic Acid

hA ..... α-Helix

HIF1α ..... Hypoxia Inducible Factor 1α

H_2PteGlu ..... dihydrofolate

H_4PteGlu ..... tetrahydrofolate

hTS ..... human Thymidylate Synthase

IDR ..... Intrinsically Disordered Region

IKK ..... IκBa Kinase

IPP ..... IκBa phophopeptide

kDa ..... kilo Daltons

L ..... Leucine

LV ..... 5'-formyltetrahydrofolate

MetAP-2 ..... Methionine aminopeptidease-2

mRNA ..... Messenger Ribonucleic Acid

MTX ..... Methotrexate

NADPH ..... Nicotinamide adenine dinucleotide phosphate

ODC ..... Ornithine Decarboxylase

OVA ..... Ovalicin

P ..... Proline

PDB ..... Protein Database

PgA ..... Propargyl Amine

PLP ..... Pyridoxal-5'-Phosphate

PLX ..... Plevitrexed

PMX ..... Pemetrexed

POI ..... Protein of Interest

Pro ..... Proline

PHD ..... Proline Hydroxylase

PROTAC ..... Proteolysis Targeting Chimera

TS ..... Thymidylate Synthase

Tyr ..... Tyrosine

R ..... Arginine

RFC ..... Reduced Folate Carrier

RNA ..... Ribonucleic Acid

RTX ..... Raltitrexed

SCF ..... Skp-Cul1-F-Box Family

SHMT ..... Serine Hydroxymethyltransferase

Ub ..... Ubiquitin

UGD ..... Uracil-DNA-Glycosylase

UPR ..... Unfolded Protein Response

UPS ..... Ubiquitin-Proteasome System

YFP ..... Yellow Fluorescent Protein

Val ..... Valine

VHL ..... von Hippel-Lindau

CHAPTER 1

INTRODUCTION

1.0 THYMIDYLATE SYNTHASE: FUNCTION AND MECHANISIM

Since the early 90's human thymidylate synthase (hTS) [EC 2.1.1.45] has been a high profile drug target for colorectal cancer.[7] A concerted effort has been made to delineate the relationship between its structural biology and pharmacological potential, as hTS is responsible for the *de novo* production of thymidine, a process which is invariably highjacked by malignant cells and other tissue specific neoplasms. Through the tandem coupling of the nucleoside 2'-deoxyuridine monophosphate (dUMP) and the cofactor N^5,N^{10}-methylenetetrahydrofolate ($CH_2H_4PteGlu$), hTS catalyzes the reductive methylation of dUMP to produce one of the four nucleoside-phosphates necessary for genetic inheritance: 2'-thymidine monophosphate (dTMP) (Figure 1.1).

The highly evolutionary conserved human thymidylate synthase is a 70 kDa committed dimer complex with each monomer (35 kDa) interface consisting of an extremely tight interaction between each of the two six-stranded β-sheets - one from each subunit.[8] The back walls of each active site, where the catalytic cysteine resides, sit at the surface opposite of the β-sheet interface.[8] Each catalytic cysteine occupies position 195 (Cys198 in *E.coli*) at the base of the fourth β-strand in the catalytic loop 181-197. Crystal structures have shown the catalytic loop placing Cys195 outside the active site,

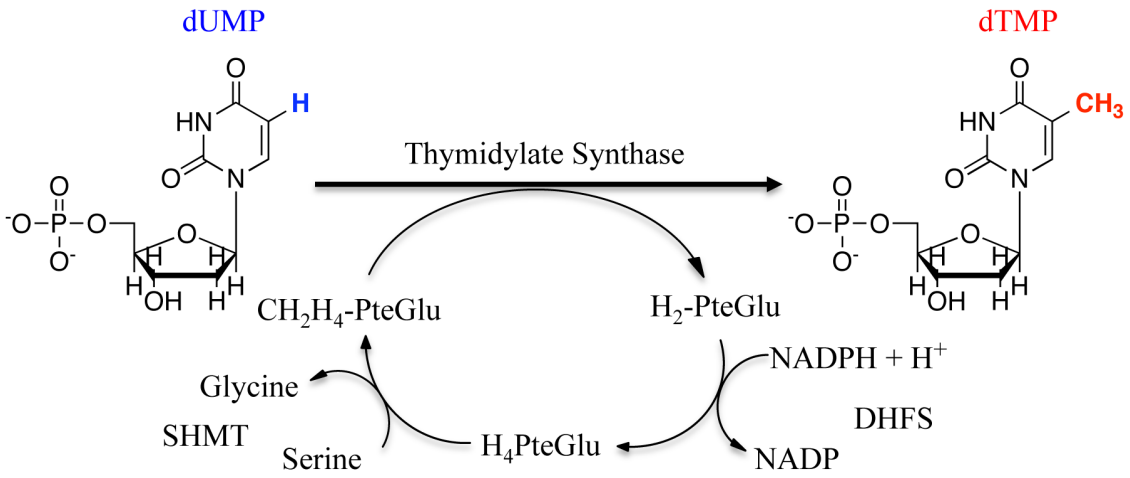

Figure 1.1. A Representative schematic for the synthesis of deoxythymidine monophosphate (dTMP) from deoxyuridine monophosphate (dUMP) by hTS. The metabolic turnover of dUMP coupled with its cofactor, N^5,N^{10}-methylenetetrahydrofolate ($CH_2H_4PteGlu$), to produce dTMP and dihydrofolate ($H_2PteGlu$), which is subsequently reduced by NADPH through dihydrofolate reductase (DHFR). Its product, tetrahydrofolate ($H_4PteGlu$) is used to regenerate $CH_2H_4PteGlu$ through a reaction with the PLP-dependent enzyme serine hydroxymethyltransferase (SHMT) and the amino acid L-serine.

indicating that the conformer is inactive. In concert with this inactive conformation was the disordered state of loop 108-129, which is perpendicular to the catalytic loop 181-197.[8] Conversely, upon ligand binding, loop 181-197 is rotated 180° toward the active site pocket and inserts the nucleophilic Cys195 residue with a concomitant ordering of loop 108-129 (Figure 1.2).[9] The order and mobility of the two loops work in concert to foment the catalytic turnover of dUMP. In between this dynamic mobility hTS forms an asymmetrical alignment, which is believed to act as a guide for both substrates and assist in docking with in the active site.

This shift in conformation subsequently renders the opposite monomer unit incapable of binding substrates, hence, the binding of substrates to hTS creates a dynamic active/inactive population. In another word, the concerted order (or disorder) of loops 181-197 and 108-129 renders each monomer as active or inactive.[10] Post-substrate binding, a significant structural adjustment occurs where specific active site residues are repositioned toward the incoming ligands. The ordered sequential manner in which the substrates bind relies upon the pyrimidine dUMP binding first, followed by the cofactor, CH_2H_4PteGlu. Once the substrate and co-substrate are bound, hTS catalyzes the reductive methylation of dUMP followed by the sequential release of H_2PteGlu and the product, dTMP (Figure 1.3).

Interestingly, hTS catalyzes the first step in the cyclic process devoted to the transfer of single carbon moieties, which are found under three different oxidation states of CH_2H_4PteGlu: formate, formaldehyde, and methanol. The transfer at the formaldehyde oxidation state, which is equivalent to the transfer of a hydroxymethyl group, is catalyzed by hTS as CH_2H_4PteGlu is in the correct oxidation state to transfer a hydroxymethyl

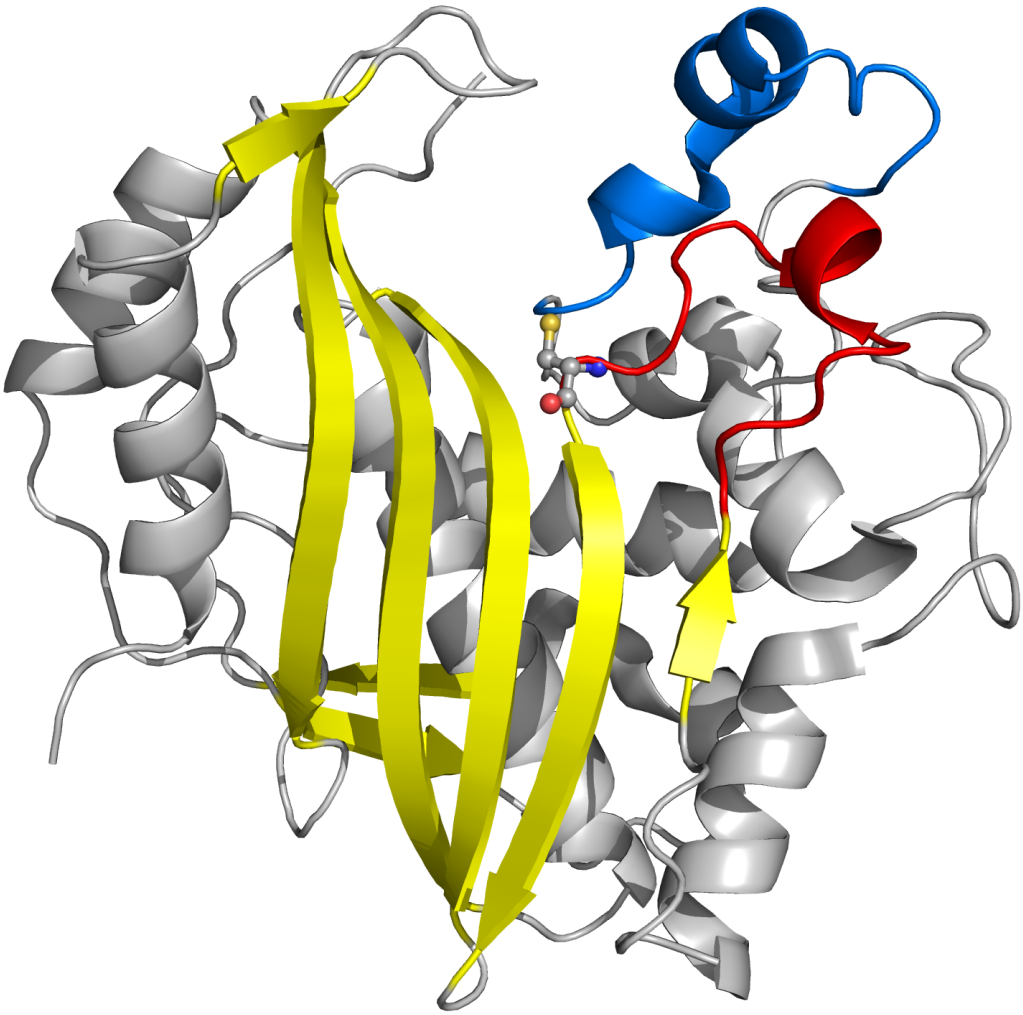

Figure 1.2. Active conformation of thymidylate synthase monomer (PDB 1HYV). The four β-strands (yellow) generate a tight interface between monomer units. At the top of the first β-strand resides the catalytically active Cys195, which is currently positioned in the active state with both loops, 181-197 (red) and 108-127 (blue) occupying the same active conformation.[9]

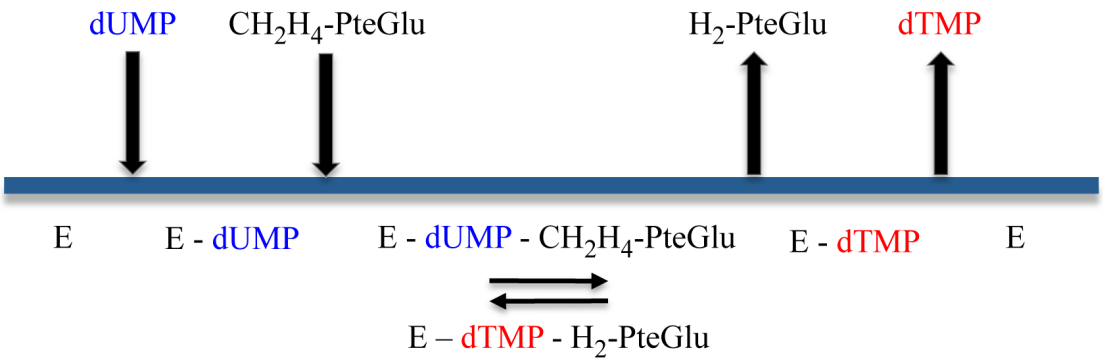

Figure 1.3. A pseudo-Cleland diagram illustrating the sequential ordered binding and release of dUMP/CH_2H_4-PteGlu followed by H_2-PteGlu/dTMP, respectively. (E represents human thymidylate synthase).

group (originally from L-serine). Here hTS catalyzes the transfer of the single carbon unit and a lone hydride from different sites of the cofactor $CH_2H_4PteGlu$. However, the final product is methylated rather than hydroxymethylated, corresponding to a reduction of dTMP and the subsequent oxidation of $CH_2H_4PteGlu$ to $H_2PteGlu$. The mechanistic process is achieved through the dynamic alignment and realignment of the substrate and co-substrate throughout a series of steps in the catalytic domain of hTS (Figure 1.4).

The steps demonstrating the mechanistic anatomy of TS were realized upon the investigative efforts surrounding the 25 conserved residues within the active site.[11] Contrary to the premise of nature conserving residues across multiple species, it was determined that only five residues proved to be irreplaceable: Arg218 (dUMP stabilization), Asp221 (cofactor stabilization), Cys198 (nucleophile in Michael Addition to C6 of dUMP, intermediate I), Tyr146 (active base that abstracts C5 proton from intermediate III), and Glu60 (cofactor elimination from ternary complex).[11] The guanidinium groups of four conserved arginine's produce an electrostatic anchor that surrounds the phosphate of dUMP in a tetrahedral arrangement, securing dUMP for the impending arrival of the cofactor.[11] In addition to stabilizing dUMP, Arg218 acts as a physical "buttress" through the hydrogen bonds between its guanidinium head group and two loops within the active site.

Formation of the ternary complex is accomplished upon cofactor binding, which causes a conformational shift, directing segments of the primary structure to form the core of the active catalytic binding site around the reactants through maximizing hydrophobic interactions and sequestering the substrates from the bulk solvent.[11] Hence,

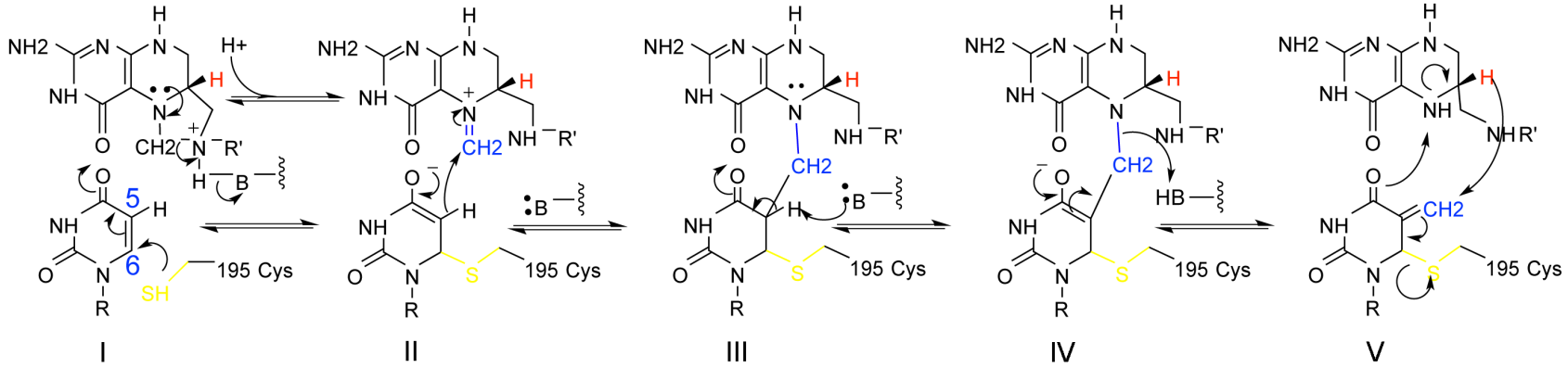

Figure 1.4. The catalytic mechanism for the reductive methylation of dUMP by hTS with the cofactor $CH_2H_4PteGlu$. (I) Cys195 covalently activates C6 of dUMP by nucleophilic Michael addition with concomitant ring-opening formation of the iminum at N5 of the pterin ring. (II) Upon formation of the iminum ion, the enolate attacks the resulting Mannich base generating the covalent linkage between the two substrates. (III) Tyr146 abstracts the C5 proton on dUMP reconstituting the active enolate. (IV) The enolate subsequently collapses eliminating the covalent bridge and transferring the methylene moiety to C5. (V) Finally, a hydride-transfer from C6 of the pterin ring reforms the C5-C6 unsaturation, releasing Cys195 and forming dTMP.[1]

the binding cavity isn't fully formed until (i) dUMP is sequestered, (ii) a number of hydrophobic side chains are within van der Waals contact with either the pterin ring system (2-aminopteridin-4(3*H*)-one) or *p*-aminobenzylic acid/thiophene substituent of the cofactor, (iii) electrostatic side chains or water-mediated hydrogen bond network has coordinated with the cofactors glutamate(s), and (iv) Asp221 has coordinated with the pterin ring and additional hydrogen bonds through amino acid side chains and water.[11] The conserved binding mechanism, in which TS successfully mediates a convoluted reaction coordinate, is paid through an entropic reduction mediated by cofactor binding and its effects upon closing the active site, aligning the reactants, and solvent sequestration.[11]

1.1 Antimetabolites of Thymidylate Synthase

Antimetabolites are currently the most widely applied treatment for both viral infections and cancer therapies. In general, they [antimetabolites] are analogs of natural metabolites that either directly or indirectly play a role in the metabolism or biosynthesis of DNA and RNA.[12] Antimetabolites are of strategic importance regarding their applications in cancer. This is due to the unmitigated proliferation that many cancers exhibit in order to maintain their rapid and incongruous expansion.

As a malignancy develops, it requires a vast carriage of nutrients and a steady source of carbon. In order to maintain this rate of expansion, cells located in the tumor parenchyma establish aberrant vasculature networks, which act as industrial highways for the import of carbon.[13] The dramatic intake is complemented by increased DNA

synthesis and replication, cell division, and overall tumor survival. Progression of tumor growth correlates to altered genetic expression and gene-product production, a process that is intrinsically relevant to the metabolic fate of folic acid and the genes encoding their respective binding and import proteins.[14] As the centerpiece in DNA/RNA biosynthesis and repair, folic acid is an essential cofactor as demonstrated by its supplementation for expecting mothers and its routine use as an antifolate in oncology clinics.

Dietary folic acid is chiefly found in leafy green vegetables, fruits, legumes, and liver. Upon ingestion, folic acid primarily accumulates in the intestine with adsorption occurring in the jejunum. Here they are transferred across the apical membrane, as well as in the kidneys, and released into circulation as 5-methyl tetrahydrofolate (5mTHF).[15] The cellular acquisition of 5mTHF allows for the metabolic methylation of homocysteine to produce methionine and H_4PteGlu (THF). The cofactor THF is the responsible unit for the one carbon donation in biosynthesis of the nucleoside dTMP.[15]

Of consideration to this research are the pyrimidine and folate (Vitamin B_9) analogs, which suppress the catalytic capacity of thymidylate synthase – the *de novo* source of thymidine. In the absence of dTMP, inhibition of hTS leads to a reduction in the intracellular thymidine pools disrupting DNA synthesis and leads to cell death – a phenomenon known as 'thymineless death.'[16] This metabolic bottleneck represents a prime opportunity for the development for chemotherapeutics directed at inactivating hTS. Clinically, the most widely used anti-TS agent is the suicide inhibitor 5-fluorouracil (5FU). It's clinical presence was based on the observation that uracil metabolism was used more widely in tumors than normal tissues, strongly indicating a potential

therapeutic opportunity.[17] Post-systemic delivery, 5FU is anabolized as a pro-drug to its active form 5-fluoro-2'-deoxyuridylate (FdUMP) within the cell. Here, FdUMP's cytotoxicity is realized by the irreversible ternary complex that forms upon is binding to hTS. The inhibition of hTS depletes the dTMP pools and induces severe destabilization of the other three deoxynucleotide pools through separate feedback controls.[18] Ultimately, this perturbation fractures DNA synthesis and repair, allowing the cell to initiate apoptotic events.

Consequently, the blockade induced by FdUMP also leads to increased levels of dUMP's precursor metabolite: dUTP. Both the 5FU intermediate FdUTP and dUTP can be incorporated into DNA causing strand breaks while maintaining a relative "immunity" from the action of nucleotide excision repair by uracil-DNA-glycosylase (UGD).[18] While it appears that FdUMP possesses more than one mechanism to halt hTS turnover, thymidylate kinase can salvage resident thymidine pools through phosphorylation to reinstate dTMP, thus circumnavigating any intracellular depletion or inactivated hTS and yielding a mechanism of resistance.

The over all response rates under the administration of single anticancer agent are typically low and, in colorectal cancer (CRC), are approximately 10-15% with 5FU.[19] Combining therapies to increase the therapeutic response to CRC and surpass potential routes of resistance has dramatically improved 5FU's intrinsic value. Specifically, the use of antifolates has compounded the efficacy of 5FU's and as a result it has maintained its clinical presence from the late 1950's. The cooperatively displayed by co-administration of antifolates and 5FU lies within the cells requirement to maintain high endogenous levels of reduced folate ($CH_2H_4PteGlu$). In order to maintain optimal binding conditions

of FdUMP to hTS the antifolate Leucovorin (LV, 5'-formyltetrahydrofolate) was administered to supplement the intracellular expansion of reduced folate. Uptake of LV is mediated by the reduced folate carrier (RFC) and is then subsequently (poly)glutamylated by folylpolyglutamate synthetase (FPGS). This enzyme, FPGS, affixes multiple glutamic acid residues to the gamma-carboxylate of LV, which serves to increase the solubility of LV and prevent premature export.[20] Moreover, the addition of glutamic acid residues to LV, and other notable reduced folate analogs, enhances the stability of the hTS•FdUMP•LV complex. It was shown in large meta-analyses of CRC that while the LV/FdUMP co-administration generated excellent response rates, this didn't translate in any significant extension of survival.[21]

In order to circumvent the deleterious effects of fluoro-pyrimidine resistance, alternate hTS-targeting strategies were developed and focused on TS cofactor analogs. Structural analogs of CH_2H_4PteGlu were designed around modification of the pterin ring system, the number of methylene spacers between the ring system and the central aromatic unit, and to a lesser extent, the modification of the terminal glutamic acid moiety (Figure 1.5).

Raltitrexed (RTX, Tomudex or ZD1694) is a specific quinazolinone inhibitor of hTS that demonstrated high affinity for hTS and improved cellular retention in addition to low off-target activity when compared to its hTS analog counterparts (Figure 1.5). Clinically, RTX showed promising results against breast, pancreas, hepatic, gastric, and CRC with response rates ranging from 14-30%.[22] Curiously, as a single therapeutic in a CRC trial, RTX yielded a slightly lower median survival when compared to 5FU despite

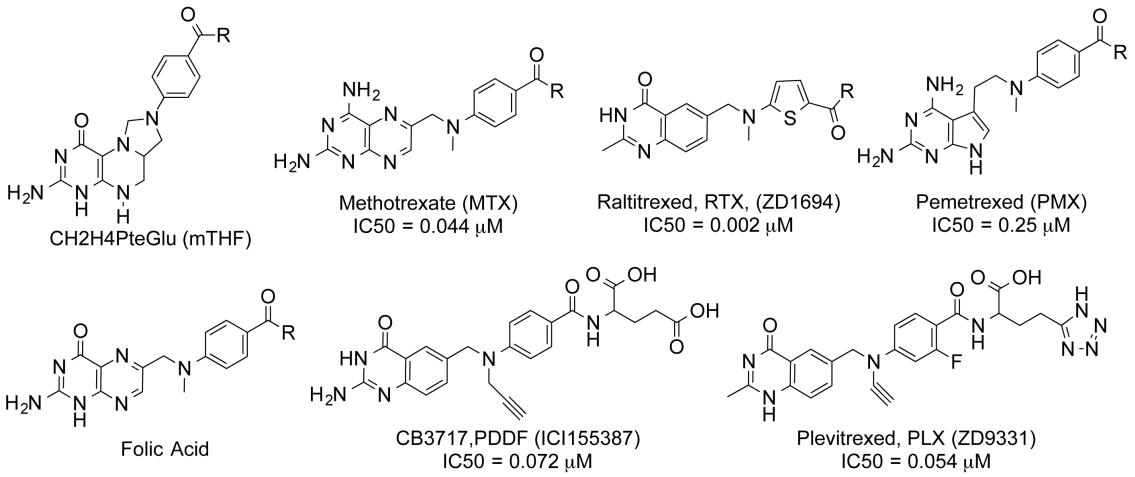

Figure 1.5. Antifolate inhibitors of thymidylate synthase and their respective half-maximal inhibitory concentrations (R = Glutamic Acid).

producing a superior toxicity profile.[23] Nonetheless, as of the fall of 2014 there five active clinical trials registered with the clinical trials database, *Clincialtrials.gov*, all of which pair the co-adminstration of RTX with taxanes, platins, and radiation therapy or a combination of angiogenic inhibitors, platins, and 5FU.

Raltitrexed was closely modeled after CB3717. Despite holding great promise as an hTS inhibitor, CB3717 demonstrated life-threatening nephro and dose-limiting hepatic toxicity, prematurely terminating its clinical development.[20] Synthetic alterations of CB3717 resulted in the rational design of RTX, which formed the ternary complex hTS•FdUMP•RTX (Figure 1.6). Modifications of CB3717 included replacing the 2'-amino group on the pterin ring, the methylenepropargyl at N^{10}, and the benzene ring system with two methyl groups and thiophene moiety, respectively (Table 1.1) These modifications altered the compounds partition coefficient, which improve aqueous solubility and reduced it to a benign nephrotoxicity profile. As with CB3717, RTX is a structural analog of $CH_2H_4PteGlu$, but it lacks the key methylene moiety involved in dTMP synthesis and therefore, it cannot participate in DNA synthesis or in its inhibitory action, which is dependent upon dUMP accumulation.[20]

Raltitrexed is transported into the cell through the RFC as shown by its resistance to enter cells (cell line L1210:1565) with impaired RFC function. Once inside the cell RTX undergoes γ-polyglutamylation processing by FPGS where glutamic acid residues are sequentially ligated via γ-linkages to the gamma-carboxylate of RTX. Against cell lines unable to polyglutamylate reduced folates, the IC_{50} of RTX increased from 0.009 to >100 μM, demonstrating the synergistic relationship between γ-polyglutamylation and

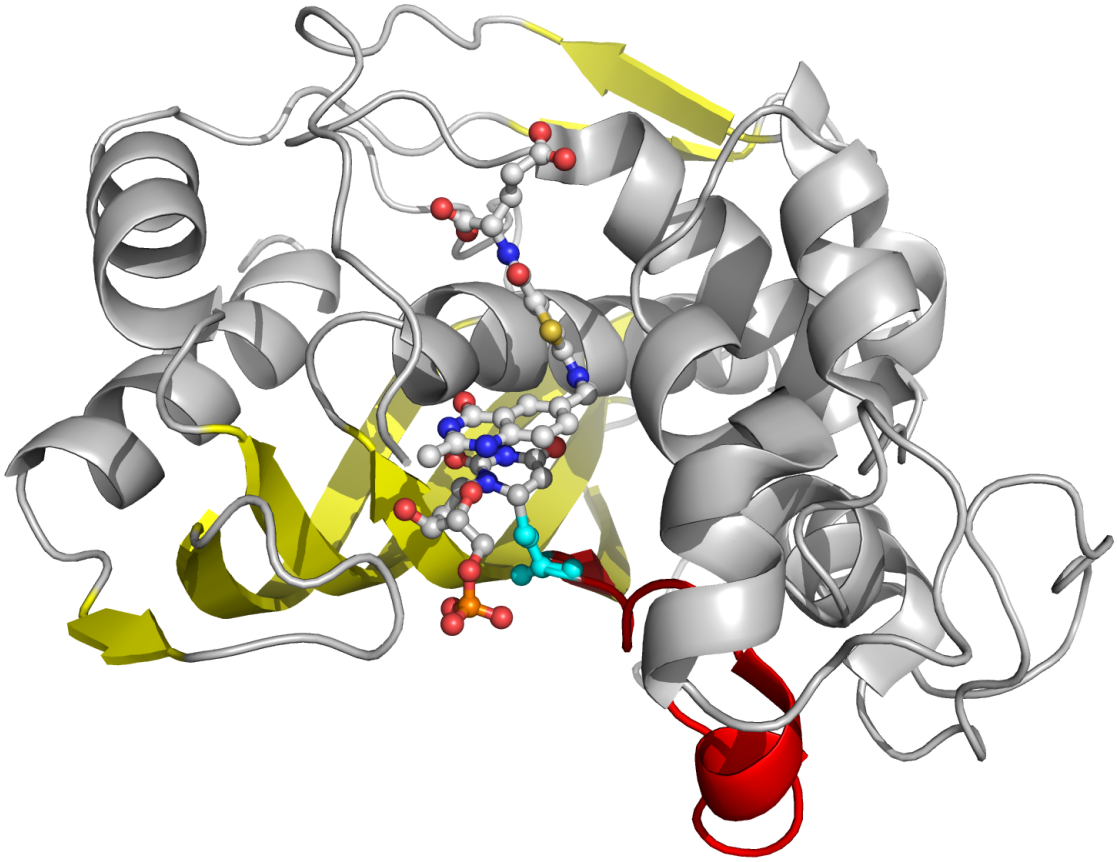

Figure 1.6. Ternary structure of Thymidylate synthase monomer (PDB 1HYV), RTX, and dUMP. At the base of the binding pocket, C6 of dUMP is covalently attached to the sulfhydryl of Cys195 (magenta). Directly above dUMP is the planar face of the quinazolinone ring system of RTX, which sits directly above and offset of the nucleosides ribose. The thiophene and glutamic acid moiety of RTX are rotated 90° with respect to the quinazolinone and 45° into the plane of the crystal structure. The catalytic loop (residues 181-197) is in red.[9]

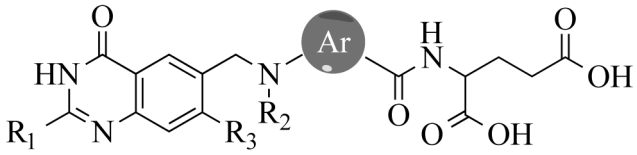

Table 1.1. Relationship between the structural substitutions in raltitrexed and their corresponding effects upon cellular uptake by the RFC and polyglutamylation as measured by growth inhibitory properties compared to ICI 198583 and CB3717.

ID	C2 R_1	C7 R_2	N10 R_3	Aryl Group	Growth Inhibition, IC_{50} (μM)		
					L1210	L1210:1565 (RFC^{neg})	L1210:MB3 ($FPGS^{neg}$)
RTX	CH_3	H	CH_3	Thiophene	0.009	0.92	70
2-NH_2	NH_2	H	CH_2	Thiophene	0.72	0.5	94
7-CH_3	CH_3	CH_3	CH_3	Thiophene	1.6	43	9
ICI 198583	CH_3	H	PgA	Benzene	0.13	8	2.7
CB3717	NH_2	H	PgA	Benzene	5.5	5.5	13
7-CH_3	CH_3	CH_3	PgA	Benzene	0.2	8	0.6

antifolate potency.[24] Notably, it was determined that within a 30-minute window roughly 90% of the drug was in mono-triglutamate form. After 24-hours only 30% of the tritiated material was lost with the remaining consisting of tetra, penta, and hexaglutamate forms.[20] This concludes that the rate of FPGS processing is faster than rate of RTX export and it estimates that the number of γ-glutamate associated with RTX is determining factor in prolonging drug sequestration. It was noted that if the cells were resuspended in fresh, drug-free media for 4 hours after the 24-hour incubation period that 40% of TS activity returned. This may be interpreted in two ways: (a) the FPGS process was retarded, thus the rate of processing was slowed; and (b) that although the γ-polyglutamate forms of RTX enable cellular retention, constant drug exposure may be required.[20] Nonetheless, the mixed noncompetitive inhibition exhibited by RTX sees a dramatic improvement in inhibitory potency (hTS affinity) with the addition of each corresponding γ-glutamylation.

The therapeutic value of RTX lies in its ability to maintain an intracellular presence, thus increasing tissue residency. The result of which has been attributed to the 4-7 γ-connected glutamic acid residues to RTX. Using ecTS (*E. coli* Thymidylate Synthase) and a tetraglutamate analog of CB3717 Kamb et al. showed that polyglutamylation alters the kinetics of ligand binding through minimal hydrogen bonding and van der Waals contacts; although the majority of these contacts were devoted to Glu-1 (glutamic acid) via a water-mediated hydrogen bond network to ecTS. Both Glu-2 and Glu-3 (Glu-4 density was ambiguous) were found to be loosely fit, suggesting that the γ-polyglutamyl tail is largely mobile and didn't rely on any specific ligand-protein interaction.[25] This is likely due to the random-coil formation that

polyglutamate peptides adopt at physiological pH. Therefore, a high entropic threshold is likely pronounced during the formation of the ternary complex. Interestingly, the overall fold improvement regarding the number of glutamic acid residues added with respect to TS inhibition were found to vary between species.[25]

1.2 Ubiquitin-independent proteosomal degradation

The homeostasis of intracellular protein levels is primarily maintained by the proteasome. Located in both the cytosol and the nucleus, the proteasome acts as a disposal system responsible for destroying unwanted, aged, over saturated, and misfolded proteins that, if left unregulated, would generate a toxic cellular environment. However, its spatial and temporal control of key cellular cycles and regulatory system substrates is its prime directive. Hence, cell division, environmental stress response, and apoptosis are, in part, under the direction of the proteasome. Although the physical function of the proteasome is proteolysis, it is a member of a much more complex and diverse system of protein quality assurance.

It's generally assumed that substrates are polyubiquitylated, via the covalent linkage to ε-amino group of the substrates lysine, through a series of enzymes-complexes that ultimately designate proteins for direct degradation (Figure 1.7). The proteasome-ubiquitin system (UPS) possesses an additional layer of organizational molecular-recognition systems that are independent of degradation. Monoubiquitylation, for example, is necessary for the trafficking of proteins, receptor internalization, virus

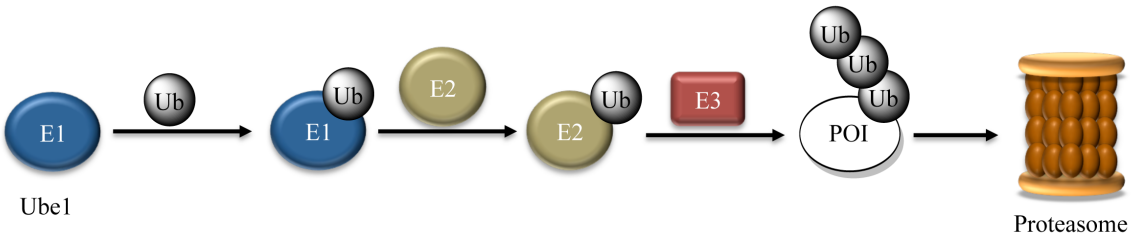

Figure 1.7 General mechanism for ubiquitin-dependent proteasomal degradation. The first step involves the E1 enzyme, Ube1, activation (via ATP) of ubiquitin (Ub) through the conjugation of a free cysteine on E1 and the carboxy terminus of Ub. Once activated, one of the 30-members of the E2 enzyme family can either directly transfer the Ub unit to the protein of interest (POI) or interact with one of the 700 substrate-specific E3 ligases through two avenues: (i) the E3 ligase can directly conjugate to the activated Ub and ubiquitinate the POI, (ii) the E3 ligase can form a complex with E2-Ub where it facilitates the transfer of Ub from E2 unit to the POI.

budding, and histone modification.[26-29] Moreover, the ubiquitin-proteasome relationship may also require adaptor proteins or molecular chaperones in order to corroborate substrate identity as post-translational modifications substantially alter the proteome's diversity.[30]

Contrary to ubiquitin-dependent proteasomal degradation pathway(s) there exists a small population of protein substrates that undergo proteasome recognition, but without involvement of the complex network of activating and ligating enzymes. This subset of degradation targets is independent of ubiquitin conjugation and therefore undergoes ubiquitin-independent proteasomal degradation. Thymidylate synthase (TS) is a non-ubiquinated proteasomal substrate that falls directly into the same aforementioned category as Ornithine decarboxylase (ODC), calmodulin, p53 tumor suppressor protein, and the CDK inhibitor $p21^{Cip1}$.[31-34]

In an unbound state the half-life of hTS is approximately 6-10 hours. However, inhibitors such as FdUMP and RTX stabilize the ternary complex and extend the enzyme's half-life to 20-24 hours, presumably altering the proteasome's capacity to degrade TS. This phenomenon was initially attributed as the result in an autoregulatory response mechanism due to the exposure of the previously mentioned TS inhibitors. It was postulated that exposure to TS inhibitors resulted in a 2-4 fold induction of enzyme as a result of disrupting hTS-mRNA complex, thus blocking translational repression and facilitating translational progress presenting a mechanism of resistance.[35] It was found that fluoropyrimidines do not alter ribosome binding to TS mRNA. Nor did altering the binding domain of mRNA for the ribosome affect induction of TS.[36]

The particular structural features of the N-terminus of TS, which is extended in mammalian TS, appeared to regulate the enzymes intracellular half-life through ubiquitin-independent proteasome degradation with 26S regulatory complex.[37] Further investigation confirmed the ubiquitin-independent proteolysis of the TS polypeptide through site-directed modification of all internal lysine's generating a 'lysineless' TS via a K→R modification.

Under the lysineless mutant, administration of FdUMP still yielded an inhibitory ternary-complex, thus the catalytic activity of TS was retained; additional evidence of its ubiquitin-independence was corroborated under proteasomal inhibitors where the wtTS half-life was restored upon their administration.[38] Structurally, the intrinsically disordered region (IDR) of the N-terminus is comprised of 45 residues possessing a proline-rich region spanning positions 9-15 (^{9}PRRPLPP^{15}) and 24-27 with two-conserved arginine's at positions 10-11. Downstream of the flexible domain is a highly conserved amphipathic 15-residue α-helix (hA) from residues 31-45. Although hA functions as a structural scaffolding in tandem with the IDR rather than in a sequence specific manner.[39] Together, these 45 residues function as an independent degradation signal or degron sequence.[2]

Although the domain is highly disordered, and therefore not found in crystal structures, deletion of the degron sequence does not abrogate its catalytic activity, but instead stabilizes the enzyme. Certain residues were found to possess critical features that supported its ability to act as a degradation signal. Located at the penultimate position of the N-terminal polypeptide lays a proline, which with the exception of *M. musculus*, is conserved in mammals, and whose substitution only serves to stabilize TS (except under

Pro2→Gly2 or Pro2→Val2 point mutations). Hence, the degron sequence requires proline in the second position, and to a lesser extent, valine or glycine.[3] TS also undergoes post-translational excision of the Met initiator, but doesn't experience N-α-acetylation (it's noted that acetylation of the N-terminal residue inhibits ubiquitylation and thus, proteasomal degradation[40-42]) of the N-terminal amino acid leaving Pro2 free. Conversely, Pro2→Leu2 or Pro2→Ala2 substitutions promote acetylation and stabilize the TS polypeptide. This strongly suggests that the absence of acetylation and the presence of proline at the penultimate position are critical to the intracellular half-life of TS.[3]

Further evidence of the critical nature of the arginine dipeptide was demonstrated through the half-life analyses of phylogenically related TS. Lacking this motif, arginine point mutations were introduced to the N-terminus of cow, rabbit, platypus, and armadillo TS where they demonstrably converted the N-termini of non-primate TS into active degrons. Thus, the absence of the Arg-Arg motif is responsible TS stability in these species.[2] Taken together, the hTS degron functions as a bipartite degradation system composed of two domains within the N-terminus: the IDR, which possesses the critical residues Pro2 and 9-15 (^{9}PRRPLPP^{15}), along with the preceding α-helix. Both domains are required and are the key determinants in the post-association steps leading to the ubiquitin independent proteasomal processing of hTS.[43]

1.3 TARGETING AND HYDROPHOBIC TAGGING OF CELLULAR PROTEINS

As with any intracellular regulatory system, its spatial and temporal control can be subjected to 'reprogramming' through tumorigenesis. Of particular interest are the established systems that manage protein turnover in order to maintain a healthy proteome and modulate protein homeostasis. The strict regulation of protein turnover is typically mediated by the proteasome and its ancillary system of substrate-specific ligases and ubiquitin-conjugation enzymes colloquially referred to as the Ubiquitin-Proteasome System (UPS).

The UPS asserts posttranslational control through four distinct mechanisms: (i) activation of ubiquitin in an ATP-dependent reaction to the ubiquitin-activation enzyme (E1), (ii) conjugation (or transfer) of ubiquitin to the ubiquitin-conjugation enzyme (E2) from E1, (iii) ligation of ubiquitin to the substrate-specific ligase (E3) from E2 with concomitant identification of the substrate by the E3 ligase, and lastly (iv) translocation and proteolysis of the substrate via the proteasome. This indispensable identification and degradation system governs cell cycle progression, apoptosis, DNA double-strand repair, and angiogenesis, which are, notably the primary systems which cancer appropriates to modulate its own malignant proliferation.[44-48]

Reports correlating cancer and the involvement of the E1 and E2 enzymes are sparse. However, a large body of research has clearly linked the deregulation of the E3 ligases to multiple forms of disease and cancer.[49-52] Checkpoint activation, cell-cycle progression, and apoptosis are all potential points of oncogenic manipulation where the E3-Ub machinery is readily commandeered, making it a therapeutic target.[53, 54] An E3

ligase of particular interest is the modular Skp-Cullin-F-box (SCF) or SCF complex. This Ub-E3 ligase is composed of a heterotetrameric complex consisting of a Cullin subunit Cul1, which forms a u-shaped complex that simultaneously interacts at its N-terminus with the adaptor protein Skp1 (S-phase-kinase-associated protein-1), and its C-terminus with the Rbx1: an ancillary zinc-binding RING finger where the E2 conjugating enzyme docks. The final component, the F-box, is tethered to Skp1 and functions as an adaptor protein where it recruits the POI and supply's substrate specificity.[55]

Asserting control over the SCF complex via external tunable pharmacological agents has provided a unique opportunity to control protein function through these external posttranslational modifications. This technology has been developed by a number of investigators. Crews et al. have pioneered some of the more simplistic and facile protein degradation technologies.[56-59] Using the SCF complex with the mammalian F box protein (FBP) β-TRCP/E3RS ($SCF^{\beta\text{-}TRCP}$), they were able to target and promote Ub-directed degradation of an off target POI: methionine aminopeptidease-2 (MetAP-2) [[60]].

This was accomplished due to the intrinsic capability of $SCF^{\beta\text{-}TRCP}$ to identify a 10-residue amino acid signal located on IκBα, a negative regulator of the transcriptional modulator NFκB. Upon environmental inflammation, $SCF^{\beta\text{-}TRCP}$ promotes Ub-directed degradation of IκBα, thus activating NFκB.[61] The inflammatory response induces IκBα kinase (IKK) to phosphorylate both serines within the 10-mer-signal peptide of IκBα , thus promoting its [phosphorylated IκBα] complexation with β-TRCP.[62-64]

The IκBa phophopeptide (IPP) can be used recruit β-TRCP to the $SCF^{\beta\text{-}TRCP}$ complex. To determine if the $SCF^{\beta\text{-}TRCP}$ complex could successfully target and degrade MetAP-2, a high affinity MetAP-2 covalent inhibitor, ovalicin (OVA), was connected to IκBα, generating a bifunctional targeting system termed proteolysis-targeting chimeric system (PROTAC-1). This system demonstrated the direct ubiquitination and degradation of a foreign substrate, MetAP-2, through the chemical control of the endogenous E3-ligase SCF system.[65] The PROTAC itself was the result of the facile linkage of the angiogenic MetAP-2 inhibitor OVA to the IκBα peptide via the commercially available disuccinimidyl suberate-glycine linker using standard FMOC chemistry.

This strategy has provided an alternative technique to interrogate the inner space of proteome without resorting to the more quixotic mutational or targeted screens used to generate a specific phenotype. The PRTOAC posttranslational technology has seen further applications to knock down both the androgen and estrogen receptors using the IκBα-estradiol and IκBα-dihydroxytestosterone PROTACT-2 and PROTAC-3, respectively, with the $SCF^{\beta\text{-}TRCP}$ complex.[66]

Alternative E3 domains have also been successfully employed, such as the von Hippel-Lindau (VHL) tumor suppressor E3-Ligase, which recognizes the central hydroxylated proline of the seven amino acid sequence: -ALAPYIP- of hypoxia inducible factor 1α (HIF1α). Under normoxic conditions a proline hydroxylase (PHD) catalyzes the hydroxylation of the central proline in the aforementioned seven-mer of HIF1α. The VHL recognizes the modification and constitutively ubiquinates HIF1α until cellular conditions shift to hypoxic levels where the transcription factor is freed and mobilizes

downstream system necessary for cell survival.[67] Similar to the SCF complex, the VHL has also seen use in the knockdown of the steroid hormone receptor using PROTACs constructed of DHT and estradiol with the hydroxylated HIF1α peptide LAPYI.[68] Treatment of breast ERα-dependent breast cancer cells and androgen dependent prostate cancer cells with these PROTACs, respectively, resulted in cell cycle arrest, inhibiting the proliferation of both cells lines.[68]

Although the PROTAC approach provides a novel and robust system for posttranscriptional control, its limitations are easily realized when comparing the potential number of therapeutic targets to readily available ligands directed at disease-causing substrates, oncogenic products, or pathogens.[69] Hence, the ability to regulate a specific member of the proteome through a global application will require the appropriation of a quality control system inherent to living systems.

Currently, there are methods that target specific proteins for degradation in the absence of a direct targeting ligand: (i) in *Arabidopsis thaliana* the hormone auxin can be used to dimerize a SCF^{TIR1} complex to an AXR3 transcriptional repressor. When the repressor is genetically fused to a POI the E3-ligase can promote proteolysis of the fusion construct.[70] (ii) To induce GFP targeted degradation a chimeric FBP from Slmb (a *Drosophila melanogaster* FBP) was engineered by fusing the N-terminal of Slmb to a single-domain antibody (VhhGFP4), which is directed to GFP, YFP, or eYFP.[71] This $SCF^{Slmb\text{-}VhhGFP4}$ fusion E3-ligase targeted GPF constructs in *drosophila* embryos and was not only readily accessible to the UPS, but devoid of any deleterious effects upon the embryos. Interestingly, this method demonstrated the ability to rapidly phenocopy loss-of-function mutations on both cytoplasmic and nuclear proteins.[71]

The systems mentioned above necessitate genetic modification to generate a fusion system capable of targeting a POI. Although such systems remain relevant to the exploration of protiec structure-function relationships, they don't address the need to capture more of the 'undruggable' portion of the proteome. To address this, a general method that utilizes small molecules capable of targeting proteins in the cellular milieu is necessary. Specifically, this method should examine a quality control system that is fundamental to the intrinsic nature of all proteins.

This characteristic is apparent within the core of a protein's tertiary structure, where the burial of hydrophobic residues generates a cumulative stabilizing force. However, partially folded or misfolded protein states can lead to the exposure of unstructured hydrophobic regions that would otherwise be buried in their native states. These aberrant events can promote aggregation of amorphous aggregates or oligomers in a concentration specific manner, which can increase the cellular distribution of unfolded endoplasmic reticulum (ER) and cytosolic proteins.

To protect and sustain protein homeostasis within the cells secretory pathway, the ER and Golgi apparatus turn to a sentinel intracellular signaling system that monitors folding and unfolding events: the Unfolded Protein Response (UPR) pathway. Here, the UPR can coordinate the processing of metastable or misfolded proteins which can be reprocessed back into the folding cycle or, if proper folding is not restored, they enter the ER-associated degradation (ERAD) pathway, which prepares the substrate for ER-translocation and ultimately cytosolic proteolysis via the UPS.[72, 73] Should an imbalance of misfolded proteins continue and overwhelm the ER processing machinery, the UPR will modulate three main responses: (i) brief attenuation of global translational output via

PERK/eiF2α phosphorylation, (ii) transcriptional activation of ER protein folding capacity by up-regulating chaperones and preventing ER-bound mRNA translocation (via IRE1) while simultaneously increasing the rate of degradation of misfolded proteins (via ERAD), and (iii) in the event where the first two responses are either prolonged or disrupted, cell death may be initiated.[74, 75]

Externally, as opposed to within the ER landscape, the translational production, of nascent polypeptides is also at risk of misfolding and aggregation. To avoid such deleterious outcomes and ensure the conformational integrity of proteins and overall protein homeostasis (proteostasis), cells invest in a plexus of highly specialized eukaryotic chaperones: HSP40, HSP60 (TriC), HSP70s (BiP), HSP90s, and HSP100s.[76, 77] These versatile and structurally unique macromolecules can be mobilized to directly recognize and bind hydrophobic moieties in an effort to facilitate proper folding or refolding under ribosomal-mediated proteogenesis and stress-inducible scenarios. In order to govern a coordinated proteostasis network, synergistic action between multiple pathways, such as the UPR of the ER and UPS mediated proteolysis, must be inherent (Figure 1.8).

Manipulation of this protein surveillance system may serve as a potential mechanism for therapeutic application. Induction of proteolysis by mimicking protein destabilization through hydrophobic exposure may systematically degrade "hydrophobic tagged" proteins via the proteasome. Indeed Neklesa *et al*. have demonstrated the ability to impersonate a partially denatured or unfolded state of a protein and its subsequent proteolysis using the HaloTag dehalogenase fusion system. By appending a hydrophobic adamantane moiety (HyT13) to a haloalkane reactive linker, which possesses high avidity

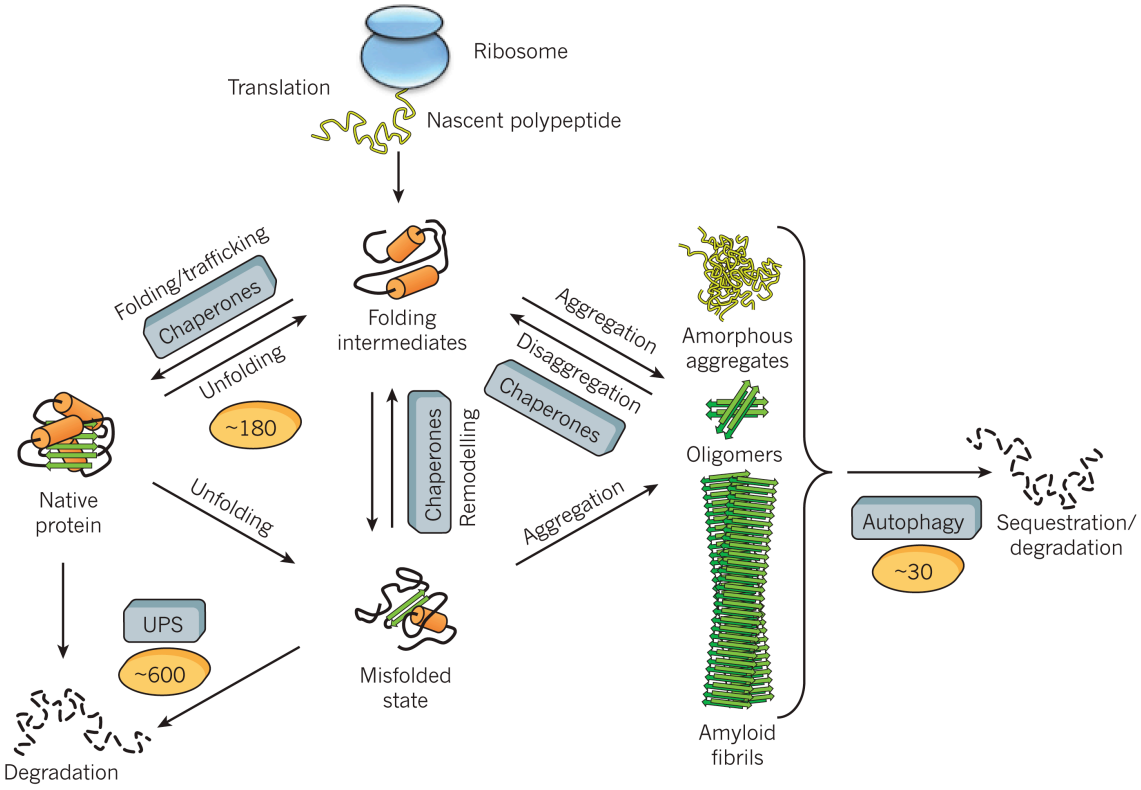

Figure 1.8 The integrated proteostasis network comprised (counterclockwise) of the trafficking, UPS, remodeling, and aggregation/disaggregation components which serve to interrogate and mediate protein fate. Under trafficking, approximately 180 chaperones and their adaptors contribute to the production of properly folded systems, whereas the UPS and autophagy systems possess over 600 and 30 components, respectively.

for the HaloTag dehalogenase, excellent translational control of various intracellular fusion proteins was maintained including transmembrane and zebrafish proteins and targeted POI's in tumor burdened mice.[78, 79]

The functional utility of this system was applied to both *in vitro* and *in vivo* systems targeted against the proto-oncogene, HRAS1, a small GTPase that possess elevated tumorigenic potency under the absence of intracellular signaling.[80, 81] A key diagnostic attribute of the mutant HRAS1^{G12V} allele is that the ectopic expression of this gene can produce a transformed phenotype that clearly distinguishes *Hras*^{1G12V} expression. Thus, when *Hras*^{1G12V} expressing cells are incubated under low serum conditions, their ability to maintain cell-to-cell contact is attenuated and they form distinct colonies rather than their native monolayer formation.

Moreover, their [*Hras*^{1G12V} expressing cells] utility is also realized in immunocompromised mice where these cells are capable of tumor formation upon systemic administration.[82] Suppression of the colony forming capability of Hras1^{G12V} in NIH-3T3 was analyzed with a HA-HaloTag-Hras1^{G12V} fusion and a negative control that was incapable of binding the haloalkane (HA-HaloTag-Hras1^{D106A}).

Upon treatment with the haloalkane-HyT13, the HA-HaloTag-Hras1^{G12V} expressing cells had reverted to their native monolayer state, whereas the negative control produced distinct colonies indicating that their haloalkane-HyT13 tag had successfully eliminated Hras1^{G12V} fusion protein, *in vitro*. *In vivo* examination of this system was performed in nude mice injected with stably transfected HA-HaloTag-Hras1^{G12V} in NIH-3T3 cells with concomitant administration of the haloalkane-HyT13. Tumor formation

was monitored for 13 days prior to dosing, where members of the treatment group reported that the average tumor size was 16% of those in vehicle control group.[83] While the HaloTag fusion system has clearly shown the ability to induce hydrophobic mediated degradation, the system is unable to degrade endogenous proteins unless the HaloTag system has been fused to the target protein.[83]

Nonetheless, applying this *tour-de-force* strategy to a system whose degradation is mediated by the proteasome, but in an ubiquitin-independent manner, would demonstrate the direct applicability of hydrophobic-tagging toward endogenous proteins using readily available and modifiable ligands with out a genetically transfected fusion construct.

1.4 References

1. Lins, L. & Brasseur, R. The Hydrophobic Effect in Protein-Folding. *Faseb J.* **9**, 535-540 (1995).

2. Melo, S.P., Yoshida, A. & Berger, F.G. Functional dissection of the N-terminal degron of human thymidylate synthase. *Biochem. J.* **432**, 217-226 (2010).

3. Pena, M.M.O. et al. The Intrinsically Disordered N-terminal Domain of Thymidylate Synthase Targets the Enzyme to the Ubiquitin-independent Proteasomal Degradation Pathway. *J. Biol. Chem.* **284**, 31597-31607 (2009).

4. Fenton, W.A. & Horwich, A.L. GroEL-mediated protein folding. *Protein Sci.* **6**, 743-760 (1997).

5. Dobson, C.M. Protein folding and misfolding. *Nature* **426**, 884-890 (2003).

6. Kubota, H. Quality Control Against Misfolded Proteins in the Cytosol: A Network for Cell Survival. *J. Biochem.* **146**, 609-616 (2009).

7. Rustum, Y.M. et al. Thymidylate synthase inhibitors in cancer therapy: Direct and indirect inhibitors. *J. Clin. Oncol.* **15**, 389-400 (1997).

8. Schiffer, C.A., Clifton, I.J., Davisson, V.J., Santi, D.V. & Stroud, R.M. Crystal structure of human thymidylate synthase: A structural mechanism for guiding substrates into the active site. *Biochemistry* **34**, 16279-16287 (1995).

9. Lovelace, L.L., Minor, W. & Lebioda, L. Structure of human thymidylate synthase under low-salt conditions. *Acta Crystallogr. Sect. D-Biol. Crystallogr.* **61**, 622-627 (2005).

10. Anderson, A.C., O'Neil, R.H., DeLano, W.L. & Stroud, R.M. The structural mechanism for half-the-sites reactivity in an enzyme, thymidylate synthase, involves a relay of changes between subunits. *Biochemistry* **38**, 13829-13836 (1999).

11. Finer-Moore, J.S., Santi, D.V. & Stroud, R.M. Lessons and conclusions from dissecting the mechanism of a bisubstrate enzyme: Thymidylate synthase mutagenesis, function, and structure. *Biochemistry* **42**, 248-256 (2003).

12. Peters, G.J. Novel Development in the use of Antimetabolites. *Nucleosides Nucleotides Nucleic Acids* **33**, 358-374 (2014).

13. Fang, J., Nakamura, H. & Maeda, H. The EPR effect: Unique features of tumor blood vessels for drug delivery, factors involved, and limitations and augmentation of the effect. *Adv. Drug Deliv. Rev.* **63**, 136-151 (2011).

14. Kelemen, L.E. The role of folate receptor alpha in cancer development, progression and treatment: Cause, consequence or innocent bystander? *Int. J. Cancer* **119**, 243-250 (2006).

15. Matherly, L.H., Hou, Z.J. & Deng, Y.J. Human reduced folate carrier: translation of basic biology to cancer etiology and therapy. *Cancer Metastasis Rev.* **26**, 111-128 (2007).

16. Grogan, B.C., Parker, J.B., Guminski, A.F. & Stivers, J.T. Effect of the Thymidylate Synthase Inhibitors on dUTP and TTP Pool Levels and the Activities of DNA Repair Glycosylases on Uracil and 5-Fluorouracil in DNA. *Biochemistry* **50**, 618-627 (2011).

17. Heidelberger, C. et al. Fluorinated Pyrimidines, A New Class of Tumor-Inhibitory Compounds *Nature* **179**, 663-666 (1957).

18. Longley, D.B., Harkin, D.P. & Johnston, P.G. 5-Fluorouracil: Mechanisms of action and clinical strategies. *Nat. Rev. Cancer* **3**, 330-338 (2003).

19. Johnston, P.G. & Kaye, S. Capecitabine: a novel agent for the treatment of solid tumors. *Anti-Cancer Drugs* **12**, 639-646 (2001).

20. Jackman, A.L. et al. ICI-D1694, A Quinazoline Antifolate Thymidylate Synthase Inhibitor that is a Potent Inhibitor of L1210 Tumor-Cell Growth-In vitro and In vivo - A New Agent for Clinical Study.. *Cancer Res.* **51**, 5579-5586 (1991).

21. Piedbois, P. et al. Modulation of Fluorouracil by Leucovorin in Patients with Advanced Colorectal-Cancer - Evidence in Terms of Response Rate. *J. Clin. Oncol.* **10**, 896-903 (1992).

22. Scagliotti, G.V. & Selvaggi, G. Antimetabolites and cancer: emerging data with a focus on antifolates. *Expert Opin. Ther. Patents* **16**, 189-200 (2006).

23. Cocconi, G. et al. Open, randomized, multicenter trial of raltitrexed versus fluorouracil plus high-dose leucovorin in patients with advanced colorectal cancer. *J. Clin. Oncol.* **16**, 2943-2952 (1998).

24. Jackman, A.L. et al. ZD1694 (Tomudex) - A New Thymidylate Synthase Inhibitor with Activity in Colorectal-Cancer. *Eur. J. Cancer* **31A**, 1277-1282 (1995).

25. Kamb, A., Moore, J.F., Calvert, A.H. & Stroud, R.M. Structural Basis for Recognition of Polyglutamyl Folates by Thymidylate Synthase. *Biochemistry* **31**, 9883-9890 (1992).

26. Jason, L.J.M., Moore, S.C., Lewis, J.D., Lindsey, G. & Ausio, J. Histone ubiquitination: a tagging tail unfolds? *Bioessays* **24**, 166-174 (2002).

27. Haglund, K., Di Fiore, P.P. & Dikic, I. Distinct monoubiquitin signals in receptor endocytosis. *Trends Biochem.Sci.* **28**, 598-603 (2003).

28. Hicke, L. Protein regulation by monoubiquitin. *Nat. Rev. Mol. Cell Biol.* **2**, 195-201 (2001).

29. Dupre, S., Urban-Grimal, D. & Haguenauer-Tsapis, R. Ubiquitin and endocytic intemalization in yeast and animal cells. *Biochim. Biophys. Acta-Mol. Cell Res.* **1695**, 89-111 (2004).

30. Farras, R., Bossis, G., Andermarcher, E., Jariel-Encontre, I. & Piechaczyk, M. Mechanisms of delivery of ubiquitylated proteins to the proteasome: new target for anti-cancer therapy? *Crit. Rev. Oncol./Hematol.* **54**, 31-51 (2005).

31. Murakami, Y., Matsufuji, S., Hayashi, S., Tanahashi, N. & Tanaka, K. Degradation of ornithine decarboxylase by the 26S proteasome. *Biochem. Biophys. Res. Commun.* **267**, 1-6 (2000).

32. Tarcsa, E., Szymanska, G., Lecker, S., O'Connor, C.M. & Goldberg, A.L. Ca2+-free calmodulin and calmodulin damaged by in vitro aging are selectively degraded by 26 S proteasomes without ubiquitination. *J. Biol. Chem.* **275**, 20295-20301 (2000).

33. Sheaff, R.J. et al. Proteasomal turnover of p21(Cip1) does not require p21(Cip1) ubiquitination. *Mol. Cell.* **5**, 403-410 (2000).

34. Asher, G., Lotem, J., Sachs, L., Kahana, C. & Shaul, Y. Mdm-2 and ubiquitin-independent p53 proteasomal degradation regulated by NQ01. *Proc. Natl. Acad. Sci. U. S. A.* **99**, 13125-13130 (2002).

35. Chu, E. & Allegra, C.J. The vole of thymidylate synthase as an RNA binding protein. *Bioessays* **18**, 191-198 (1996).

36. Kitchens, M.E., Forsthoefel, A.M., Rafique, Z., Spencer, H.T. & Berger, F.G. Ligand-mediated induction of thymidylate synthase occurs by enzyme stabilization - Implications for autoregulation of translation. *J. Biol. Chem.* **274**, 12544-12547 (1999).

37. Forsthoefel, A.M., Pena, M.M.O., Xing, Y.Y., Rafique, Z. & Berger, F.G. Structural determinants for the intracellular degradation of human thymidylate synthase. *Biochemistry* **43**, 1972-1979 (2004).

38. Pena, M.M.O., Xing, Y.Y., Koli, S. & Berger, F.G. Role of N-terminal residues in the ubiquitin-independent degradation of human thymidylate synthase. *Biochem. J.* **394**, 355-363 (2006).

39. Melo, S.P., Barbour, K.W. & Berger, F.G. Cooperation between an Intrinsically Disordered Region and a Helical Segment Is Required for Ubiquitin-independent Degradation by the Proteasome. *J. Biol. Chem.* **286**, 36559-36567 (2011).

40. Meinnel, T., Peynot, P. & Giglione, C. Processed N-termini of mature proteins in higher eukaryotes and their major contribution to dynamic proteomics. *Biochimie* **87**, 701-712 (2005).

41. Meinnel, T., Serero, A. & Giglione, C. Impact of the N-terminal amino acid on targeted protein degradation. *Biol. Chem.* **387**, 839-851 (2006).

42. Mayer, A., Siegel, N.R., Schwartz, A.L. & Ciechanover, A. Degradation of Proteins with Acetylated Amino Termini by the Ubiquitin System. *Science* **244**, 1480-1483 (1989).

43. Barbour, K.W., Xing, Y.Y., Pena, E.A. & Berger, F.G. Characterization of the bipartite degron that regulates ubiquitin-independent degradation of thymidylate synthase. *Biosci. Rep.* **33**, 165-U205 (2013).

44. Nakayama, K.I. & Nakayama, K. Ubiquitin ligases: cell-cycle control and cancer. *Nat. Rev. Cancer* **6**, 369-381 (2006).

45. Muratani, M. & Tansey, W.R. How the ubiquitin-proteasome system controls transcription. *Nat. Rev. Mol. Cell Biol.* **4**, 192-201 (2003).

46. Krogan, N.J. et al. Proteasome involvement in the repair of DNA double-strand breaks. *Mol. Cell.* **16**, 1027-1034 (2004).

47. Adams, J. The proteasome: A suitable antineoplastic target. *Nat. Rev. Cancer* **4**, 349-360 (2004).

48. Vlachostergios, P.J., Patrikidou, A., Daliani, D.D. & Papandreou, C.N. The ubiquitin-proteasome system in cancer, a major player in DNA repair. Part 1: post-translational regulation. *J. Cell. Mol. Med.* **13**, 3006-3018 (2009).

49. Okamoto, Y. et al. UbcH10 is the cancer-related E2 ubiquitin-conjugating enzyme. *Cancer Res.* **63**, 4167-4173 (2003).

50. Lisztwan, J., Imbert, G., Wirbelauer, C., Gstaiger, M. & Krek, W. The von Hippel-Lindau tumor suppressor protein is a component of an E3 ubiquitin-protein ligase activity. *Genes Dev.* **13**, 1822-1833 (1999).

51. Satija, Y.K., Bhardwaj, A. & Das, S. A portrayal of E3 ubiquitin ligases and deubiquitylases in cancer. *Int. J. Cancer* **133**, 2759-2768 (2013).

52. Vucic, D., Dixit, V.M. & Wertz, I.E. Ubiquitylation in apoptosis: a post-translational modification at the edge of life and death. *Nat. Rev. Mol. Cell Biol.* **12**, 439-452 (2011).

53. Pray, T.R. et al. Cell cycle regulatory E3 ubiquitin ligases as anticancer targets. *Drug Resist. Update* **5**, 249-258 (2002).

54. Jia, L. & Sun, Y. SCF E3 Ubiquitin Ligases as Anticancer Targets. *Curr. Cancer Drug Targets* **11**, 347-356 (2011).

55. Cardozo, T. & Pagano, M. The SCF ubiquitin ligase: Insights into a molecular machine. *Nat. Rev. Mol. Cell Biol.* **5**, 739-751 (2004).

56. Pratt, M.R., Schwartz, E.C. & Muir, T.W. Small-molecule-mediated rescue of protein function by an inducible proteolytic shunt. *Proc. Natl. Acad. Sci. U. S. A.* **104**, 11209-11214 (2007).

57. Banaszynski, L.A., Chen, L.C., Maynard-Smith, L.A., Ooi, A.G.L. & Wandless, T.J. A rapid, reversible, and tunable method to regulate protein function in living cells using synthetic small molecules. *Cell* **126**, 995-1004 (2006).

58. Bonger, K.M., Chen, L.C., Liu, C.W. & Wandless, T.J. Small-molecule displacement of a cryptic degron causes conditional protein degradation. *Nat. Chem. Biol.* **7**, 531-537 (2011).

59. Raina, K. & Crews, C.M. Chemical Inducers of Targeted Protein Degradation. *J. Biol. Chem.* **285**, 11057-11060 (2010).

60. Suzuki, H. et al. I kappa B alpha ubiquitination is catalyzed by an SCF-like complex containing Skp1, cullin-1, and two F-box/WD40-repeat proteins, beta TrCP1 and beta TrCP2. *Biochem. Biophys. Res. Commun.* **256**, 127-132 (1999).

61. Deshaies, R.J. SCF and cullin/RING H2-based ubiquitin ligases. *Annu. Rev. Cell Dev. Biol.* **15**, 435-467 (1999).

62. Yaron, A. et al. Identification of the receptor component of the I kappa B alpha-ubiquitin ligase. *Nature* **396**, 590-594 (1998).

63. Yaron, A. et al. Inhibition of NF-kappa B cellular function via specific targeting of the I kappa B-ubiquitin ligase. *Embo J.* **16**, 6486-6494 (1997).

64. Karin, M. & Ben-Neriah, Y. Phosphorylation meets ubiquitination: The control of NF-kappa B activity. *Annu. Rev. Immunol.* **18**, 621-+ (2000).

65. Sakamoto, K.M. et al. Protacs: Chimeric molecules that target proteins to the Skp1-Cullin-F box complex for ubiquitination and degradation. *Proc. Natl. Acad. Sci. U. S. A.* **98**, 8554-8559 (2001).

66. Sakamoto, K.M. et al. Development of protacs to target cancer-promoting proteins for ubiquitination and degradation. *Mol. Cell. Proteomics* **2**, 1350-1358 (2003).

67. Schneekloth, J.S. et al. Chemical genetic control of protein levels: Selective in vivo targeted degradation. *J. Am. Chem. Soc.* **126**, 3748-3754 (2004).

68. Rodriguez-Gonzalez, A. et al. Targeting steroid hormone receptors for ubiquitination and degradation in breast and prostate cancer. *Oncogene* **27**, 7201-7211 (2008).

69. Hopkins, A.L. & Groom, C.R. The druggable genome. *Nat. Rev. Drug Discov.* **1**, 727-730 (2002).

70. Nishimura, K., Fukagawa, T., Takisawa, H., Kakimoto, T. & Kanemaki, M. An auxin-based degron system for the rapid depletion of proteins in nonplant cells. *Nat. Methods* **6**, 917-U978 (2009).

71. Caussinus, E., Kanca, O. & Affolter, M. Fluorescent fusion protein knockout mediated by anti-GFP nanobody. *Nat. Struct. Mol. Biol.* **19**, 117-U142 (2012).

72. Chakrabarti, A., Chen, A.W. & Varner, J.D. A Review of the Mammalian Unfolded Protein Response. *Biotechnol. Bioeng.* **108**, 2777-2793 (2011).

73. Vembar, S.S. & Brodsky, J.L. One step at a time: endoplasmic reticulum-associated degradation. *Nat. Rev. Mol. Cell Biol.* **9**, 944-U930 (2008).

74. Ron, D. & Walter, P. Signal integration in the endoplasmic reticulum unfolded protein response. *Nat. Rev. Mol. Cell Biol.* **8**, 519-529 (2007).

75. Walter, P. & Ron, D. The Unfolded Protein Response: From Stress Pathway to Homeostatic Regulation. *Science* **334**, 1081-1086 (2011).

76. Hartl, F.U., Bracher, A. & Hayer-Hartl, M. Molecular chaperones in protein folding and proteostasis. *Nature* **475**, 324-332 (2011).

77. Gething, M.J. Role and regulation of the ER chaperone BiP. *Semin. Cell Dev. Biol.* **10**, 465-472 (1999).

78. Los, G.V. et al. HatoTag: A novel protein labeling technology for cell imaging and protein analysis. *ACS Chem. Biol.* **3**, 373-382 (2008).

79. Noblin, D.J. et al. A HaloTag-Based Small Molecule Microarray Screening Methodology with Increased Sensitivity and Multiplex Capabilities. *ACS Chem. Biol.* **7**, 2055-2063 (2012).

80. Bos, J.L. RAS Oncogenes in Human Cancer - A Revew.. *Cancer Res.* **49**, 4682-4689 (1989).

81. Krontiris, T.G., Devlin, B., Karp, D.D., Robert, N.J. & Risch, N. An Association between the Risk of Cancer and Mutations in the HRAS1 Minisatellite Locus. *N. Engl. J. Med.* **329**, 517-523 (1993).

82. Parada, L.F., Tabin, C.J., Shih, C. & Weinberg, R.A. Human EJ Bladder-Carcinoma Oncogene is Homolog of Harvey Sarcoma-Virus RAS Gene. *Nature* **297**, 474-478 (1982).

83. Neklesa, T.K. et al. Small-molecule hydrophobic tagging-induced degradation of HaloTag fusion proteins. *Nat. Chem. Biol.* **7**, 538-543 (2011).

CHAPTER 2

REGIOSELECTIVE MODIFICATION OF RALITREXED

2.0 INTRODUCTION

The quinazoline-based antifolate Raltitrexed (RTX, ZD1694) exerts its cytotoxic effect upon the enzyme thymidylate synthase (TS, EC 2.1.1.45) by noncovalent inhibition, thus preventing dTMP turnover and, ultimately, apoptosis. It was designed to be a robust, water-soluble analog of the clinically tested CB3717 antifolate, synthesized to encourage polyglutamylation of it's gamma-carboxylate in order to retain high intracellular concentrations and increased cytotoxic potency.[1]

Several strategies have been applied to generate polyglutamylate analogs of antifolates via solution or solid phase peptide synthesis (SPPS).[2-4] Solution phase approaches typically necessitate either direct cleavage of the aryl-glutamic acid moiety from the pterin ring or employ stereospecific enzymatic cleavage of the parent monoglutamate in order to re-conjugate the (poly)glutamyl tail that was retroactively synthesized.[5, 6]

Conversely, the formation of pyroglutamates and their subsequent mono-, di-, and tri(N^{15})glutamates followed by condensation to the pterin-aryl group has also been described for the use as NMR probes.[7] Moreover, coupling methods that involved DCC/NHS or tertiary amines such as triethylamine or 4-methylmorpholine, proved

incapable of controlled regioselective amidation and, furthermore, can support racemization under conditions for esterification.[8-10] The necessity of regioselective placement upon antifolate analogs is paramount to their biological activity.[11-14] Alternative approaches that don't involve the deconstruction of antifolate synthons, yet still maintain the regionselectivity required for biological applications, should focus on the synthetic modification of the end product of pharmacological agents.[15]

Specifically, N-protected glutamic anhydrides have proved useful where their formation activates the carboxylate carbonyls toward specific nucleophilic attack. Following anhydride formation, activation of the accessible carbonyl is followed by nucleophilic addition, thus regioselective opening occurs with concurrent release of the newly modified isomer. The resultant regioselectivity will yield a mixture of α and γ products that require further isolation and purification.

Altering the reactions conditions can control regioselectivity of N-protected glutamic anhydrides: polar aprotic or nonpolar solvents can favor γ versus α–selectivity, respectively, in addition to the steric involvement of both the nucleophile and the N-associated protecting group.[16, 17] The aforementioned routes could easily apply to the regioselective modification of RTX without altering the pharmacological activity of the antifolate. By selecting the γ-carboxylate of RTX, multiple synthetic alterations could be employed. Of specific interest is the facile Cu(I) catalyzed azide-alkyne cycloaddition (CuAAC) labeling system. Selectively amidating the γ-carboxylate of RTX with propargylamine (PgA) would render the compound receptive to non-fluorogenic azide dyes. Upon cycloaddition of the azide-alkyne ligation, the formation of the triazole complex would produce a highly fluorescent TS specific probe. Here, we describe the

synthetic route to construct a highly specific thymidylate synthase fluorescent probe using a known anticancer compound and evaluate its *in vitro* potential for cellular localization of TS.

2.1 Results and Discussion

2.1.0 Synthesis and Characterization of RTXγ-PgA by DCC/NHS Coupling

Initial coupling experiments with **1a** and PgA were performed altering between EDCI and DCC with NHS coupling in order to trap the γ-carboxylate (Figure 2.1). However, this method produced poor regioselectivity and low yields despite DCC-NHS stoichiometry. Crude analysis via reverse phase chromatography showed the presence of excess dicyclourea (DCU), and confirmed the presence of four products (Figure 2.2). Under UV/Vis detection at 341 nm, and confirmed by LC/MS (data not shown), the crude material of the DCC/NHS coupling produced four peaks at **1a** (23.67 min), **1b** (24.69 min), **1b** (24.84 min), and **1d**: at (25.77 min), resulting in approximately 75% conversion to both alpha (**1b**) and gamma isomers (**1c**) in addition to dual α/γ modification (**1d**). The remaining 25% was unreacted starting material (**1a**) and was recycled for further use (Table 2.1). The final α/γ content was 1:1.3 or slightly 50% of biologically active product was generated as measured by all observable UV_{341} peaks. Purification of the conjugates was stifled due to the fastidious nature of the acylurea by-product, DCU, necessitating multiple injections. Nonetheless, the crude products were separated and purified over a reverse phase semi-preparatory HPLC. Each collected fraction was further analyzed via

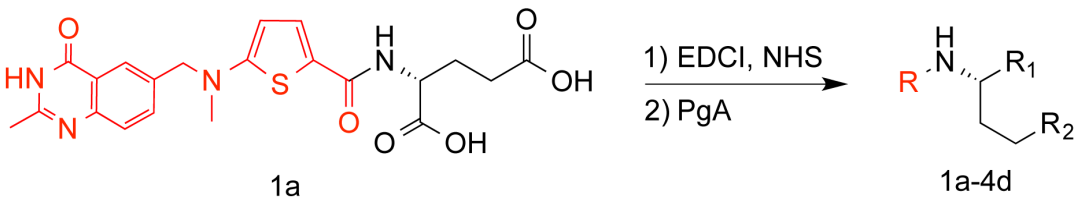

Figure 2.1. General synthetic scheme for the pseudo-selective amidation of **1a** using EDCI and NHS coupling reagents and PgA. Prospective regioselectivities were verified by LCMS and yields calculated via UV_{341}. (R = aminopterin-thiophene of **1a**)

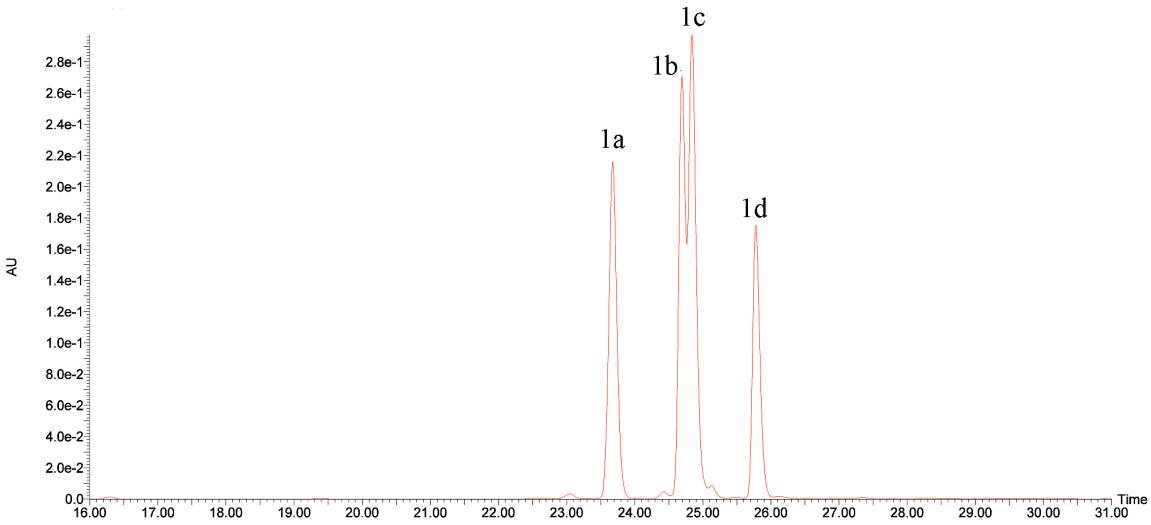

Figure 2.2 Reverse phase HPLC trace of the crude RTX-PgA conjugates synthesized using EDC/NHS. All compounds were monitored at 341 nm. (x-axis in minutes)

Table 2.1 Random regioselectivity was demonstrated using DCC/NHS coupling with **1a** and PgA. Multiple substitutions in coupling reagents (DCC/NHS, HOBt/HBTU) failed to improve selectivity.

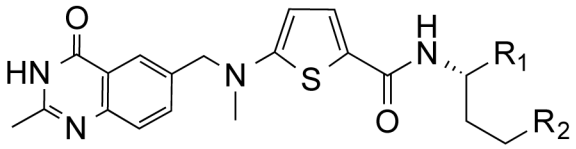

DCC/NHS Selective Amidation			RT	
Product	R_1	R_2	(min)	% isomer
1a	COOH	COOH	23.67	25
1b	PgA	COOH	24.69	25
1c	COOH	PgA	24.84	32
1d	PgA	PgA	25.77	18

LC/MS for their predicted $[M+H]^+$ at 459, 496, and 533 for **1a-d,** respectively (data not shown). The fractions were then dried and prepped for ^1H NMR characterization. In the interest of characterization and future scaling, only compounds **1a** and **1c** were analyzed. Key peaks in the structural assignment of **1a** were the diasterotopic methylenes at 2.0 and 2.2 ppm (b,b') along with 2.4 (a,a'), which were proposed to experience a slight upfield shift upon amidation at the gamma position, but not the alpha (Figure 2.3) In agreement with this hypothesis, both sets of methylene protons of **1c** produced a slight shift in addition to no observable change in the lone stereocenter **c** at 4.5 ppm, thus conferring γ-conjugation (Figure 2.4).

2.1.1 Synthesis and Characterization of RTXγ-PgA by DCC/DMAP Coupling

To further enhance the selectivity, **1a** was subjected to additional steps to ensure complete γ-regioselectivity without enduring its total synthesis.[18] Therefore, the regioselective opening of glutamic anhydride by PgA using stoichiometric amounts of DMAP was pursued (Figure 2.5).[10] Coupling conditions were sought to completely dissolve **1a** prior to its dilution into dichloromethane (DCM) followed by the drop-wise addition of DCC in order to slowly form the predicted **1a**-anhydride. The **1a**-anhydride reacts at -40 °C with PgA in the presence of DMAP under a jacket of argon. The resulting **2b** and **2c** isomers yielded a profound increase in selectivity shifting to 1:9 α/γ. The crude mixture of compounds **2a-d** was quickly identified by HPLC-UV with an elution order of **2a** (23.10 min), **2b** (24.31 min), **2c** (24.49 min), and **2d** (25.67 min). All compounds were monitored at 341 nm (Figure 2.6) and characterized by LC/MS (data not

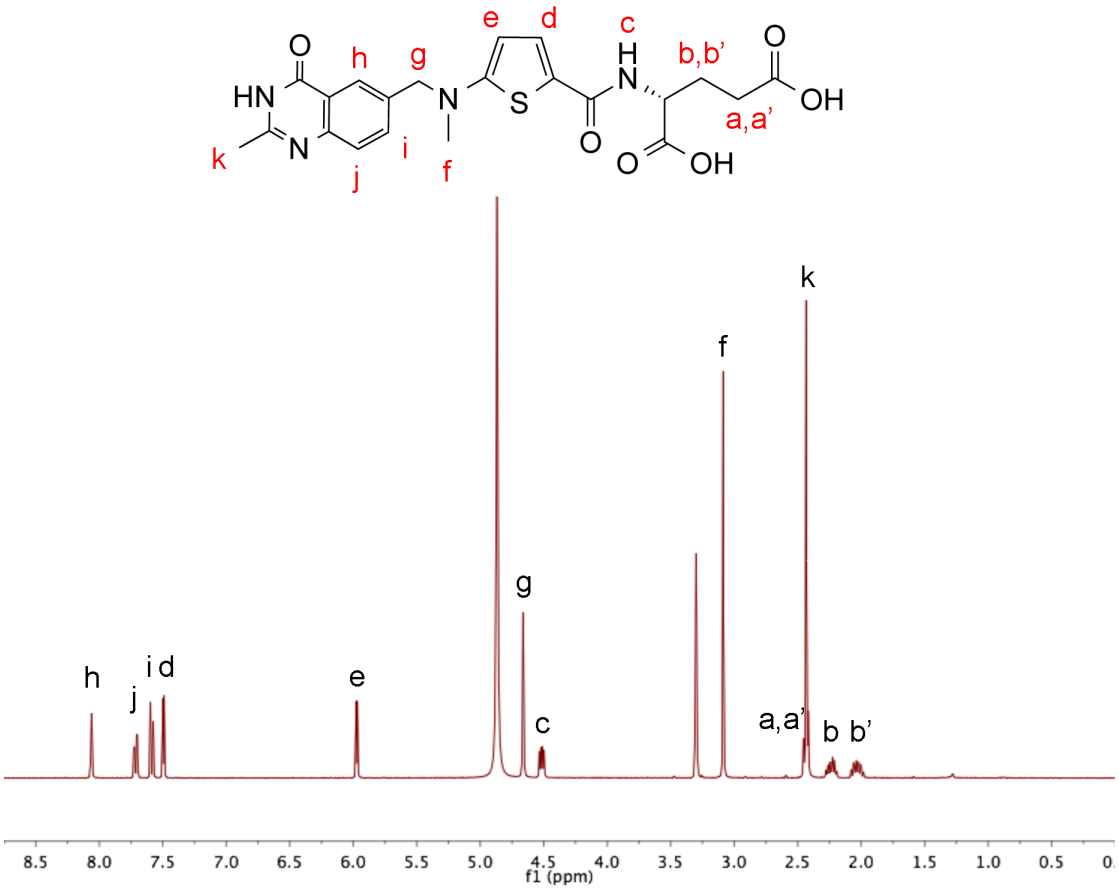

Figure 2.3 ^{1}H NMR spectra of **1a**. Solvent: CD_3OD; Concentration: 6.5 mg mL^{-1}.

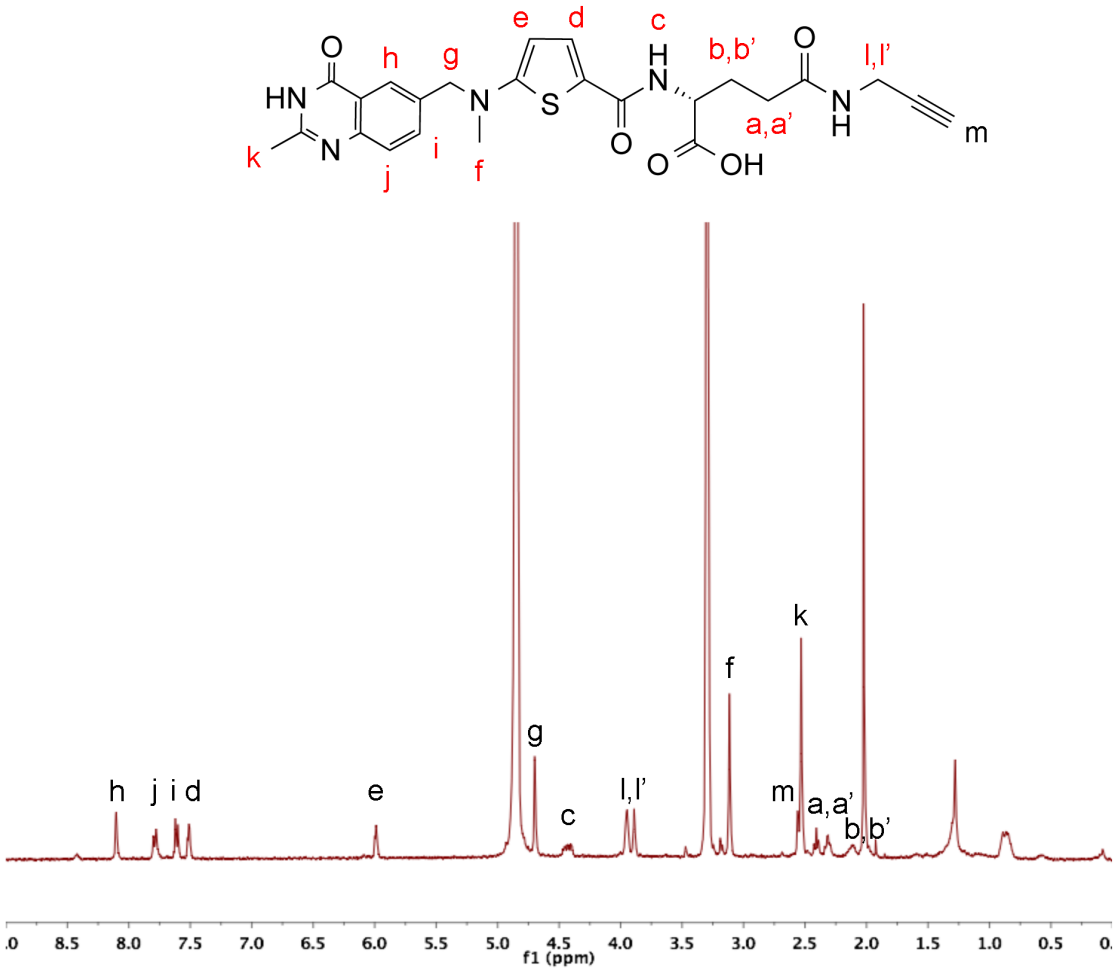

Figure 2.4 ^{1}H NMR spectra of **1c**. Solvent: CD_3OD; Concentration: 3.2 mg mL^{-1}.

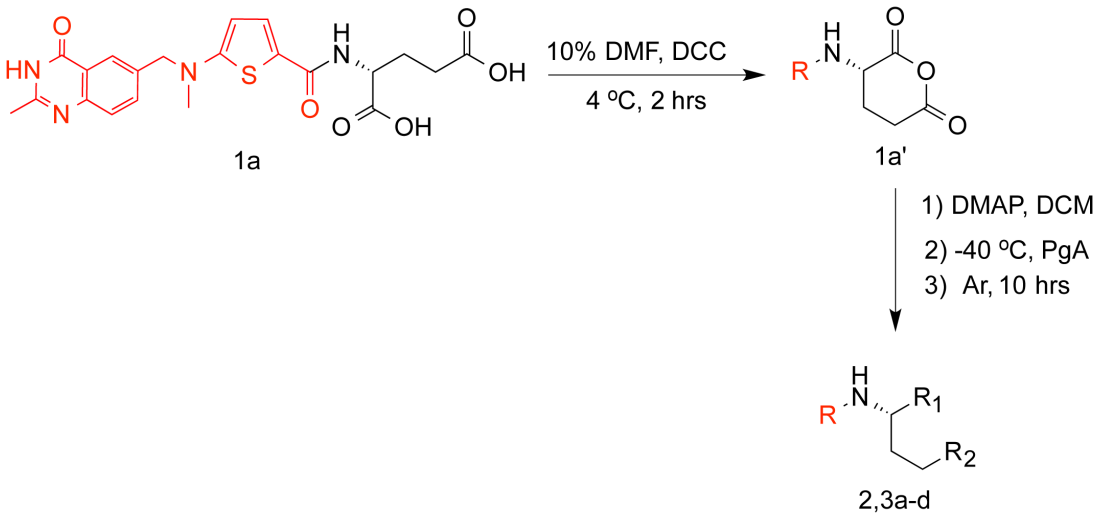

Figure 2.5 General synthetic scheme for the selective amidation via anhydride (**1a'**) of **1a** using DCC and DMAP coupling reagents. Under the polar-aprotic DMF the γ-carboxylate was positioned for direct nucleophilic attack by PgA. Prospective regioselectivities were verified by HPLC-UV. (R = aminopterin-thiophene of **1a**)

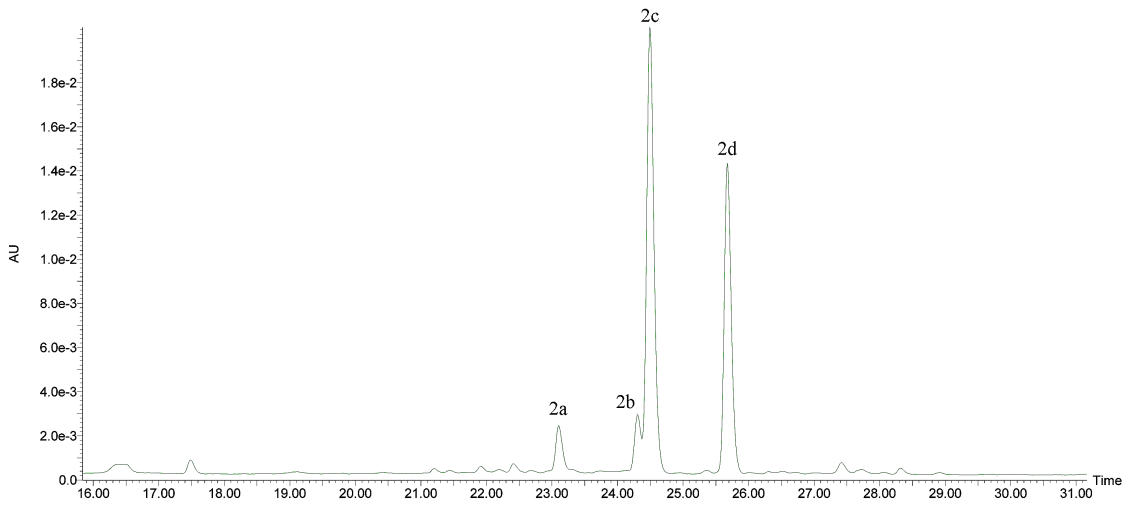

Figure 2.6 Reverse phase HPLC trace of RTX-PgA conjugates synthesized using DCC/DMAP. (x-axis in minutes)

shown). Given previous characterization (Figure 2.3, 2.4), no attempt was made to procure their NMR spectra. The concomitant production of the dual modified antifolate **2d** was still present. From a synthetic and biological propose, **2d** is incompatible as it is devoted to quenching any potential single modification and it's α-modification is pharmacologically inert toward TS. To remove any prospect of forming **2d**, PgA equivalents were paired with **1a** (Table 2.2). The synthetic scheme was scaled to 100 μM and confirmed the reproducibility of achieving enhanced γ-selectivity (1:9 α/γ). Moreover, compound **2d** had completely receded with an accompanying increase in **1a**. Given **3a** (21.00 min) is the starting material, it was easily recovered and recycled for additional syntheses (Figure 2.7). Under DCC/DMAP coupling the ratio of the isomers **3b** (22.48 min) and **3c** (22.71 min) was shifted from 1:1.3 to 1:9 α/γ by direct cooling to -40 °C in the presence of DMAP and purified under preparatory HPLC to yield 100% purity **4b** with 90% γ-character (Figure 2.7).

2.1.2 Binding Fidelity of RTXγ-PgA

To determine if any of the pharmacokinetic or dynamic parameters of **1a** had been altered, isothermal titration calorimetry was performed on **4b** and compared to **1a** (Figure 2.8). Both compounds produced a sinusoidal path resulting from their exothermic interaction with the dUMP-hTS complex. The enzyme was previously analyzed against dUMP and trace contents of DMF to alleviate any signal from their dilution: no signal. overlap was detected. Compound **1a** bound to the dUMP-hTS complex in a 1:2.4 ratio with a disassociation constant of 0.068 μM. Both parameters were expected as at

Table 2.2 Resulting regioselectivity improved under the auspice of a polar aprotic system, which enabled the regioselective ring opening of the intermediate anhydride (**1a'**) to favor the gamma position.

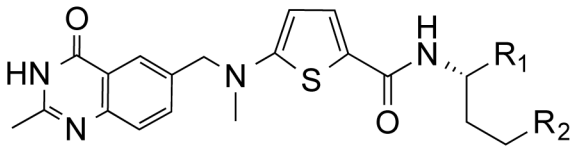

DCC/DMAP Selective Amidation			Regiochemistry (PgA equivalents)	
Product	R_1	R_2	2a-d (1.8)	3a-d (1.0)
2-3a	COOH	COOH	5	41
2-3b	PgA	COOH	7 (9%)	6 (10%)
2-3c	COOH	PgA	52 (91%)	53 (90%)
2-3d	PgA	PgA	36	0

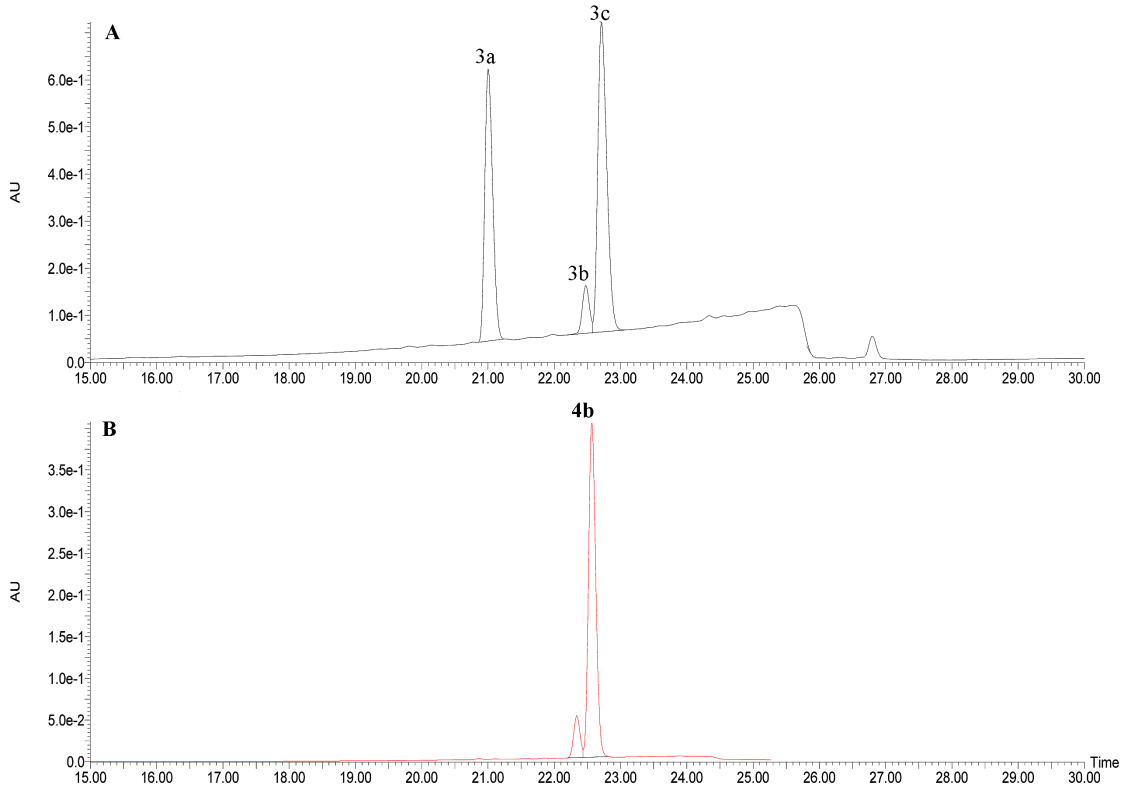

Figure 2.7 (A) HPLC trace of the crude reaction products using equimolar amounts of starting material, **1a**, and PgA. (B) HPLC trace of post purification of **3b** and **3c**, yielding high purity **4b** at 90% γ-regioselectivity. (x-axis in minutes)

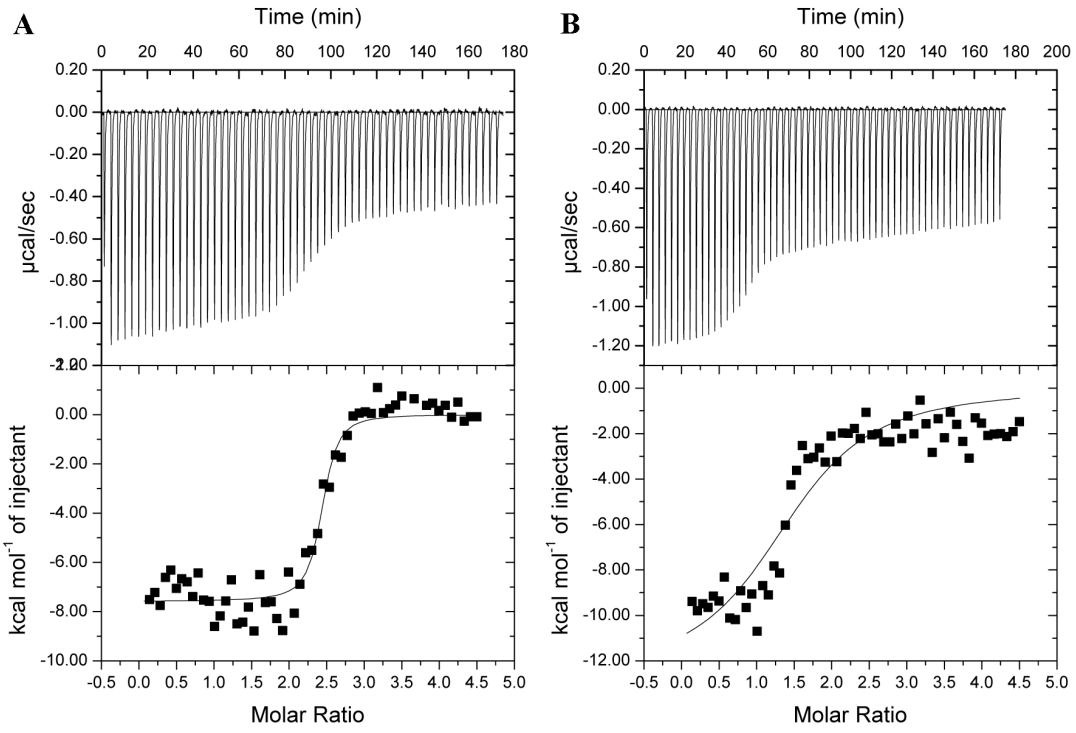

Figure 2.8 The top section within each panel is raw exothermic calorimetric output of each compound recorded over time. The lower section of each panel is the binding isotherm for each titrant. (A) Bottom panel: binding isotherm of **1a** (300 µM) with dUMP (100 µM) and hTS (15 µM). (B) Bottom panel: binding isotherm of **4b** (300 µM) with dUMP (100 µM) and hTS (15 µM).

saturating conditions hTS can bind both monomers with exceptional fidelity.[19] The Gibbs free energy (-9.8 Kcal), enthalpy (-7588 ± 142 cal mol^{-1}), and entropic parameters (7.47 cal mol^{-1}/deg) reported optimal hydrophobic and hydrogen binding which are all strongly indicative of selective binding.

However, the behavior of **4b** deviated from **1a** with the γ-propargylation of its carboxylate. The addition of the large sp-sp hybridized system may have disrupted hydrophobic stability of the terminal end of the conjugate, leading to an increase in the entropic threshold to -17.2 cal mol^{-1}/deg. This, in turn, yielded a poor binding avidity of **4b** and increasing the disassociation constant from 0.068 μM to 3.8 μM. Although still within the binding capability of hTS (ΔG, -7.4 kcal; ΔH, $-1.258X10^4$ ± 1195 cal mol^{-1}; N, 1.6), the **4b** dUMP-TS system was evaluated spectrophotometrically to evaluate its inhibitory capabilities. It was demonstrated that **4b** still possessed inhibitory capabilities and functioned as a capable inhibitor (personal communication with Dr. Leslie Lovelace).

The 57-fold decrease in binding suggests that alteration of the gamma unit of **1a** must take into account the enzyme's surface and active site environment. Based on the crystal structure of **1a** with dUMP-TS, the selective placement of the gamma-carboxylate is seen to coordinate through water-networked hydrogen bonds.[20] Although speculative without a crystal structure, it is likely that inserting the bulky electrophilic alkyne where the columbic coordination is perturbed is the contributing factor to the deterioration of **1a** binding characteristics.

2.1.3 In situ CuAAC Reaction with RTXγ-PgA and Az42

Our effort to synthesize a potential biological probe resulted in the synthesis, characterization, and biophysical evaluation of compound **4b**. To determine its *in vitro* efficacy, **4b** was introduced to TS overexpressing cells (CHL^{-TS} PJZ205/200) using a novel fluorogenic coumarin dye (**5a**, 3-azido-7-hydroxycoumarin) which lays dormant until it undergoes Cu(I)-catalyzed alkyne-azide cycloaddition (CuAAC) reaction with a reactive alkyne [[21]]. This bioorthogonal reaction is highly specific due to the selective reactivity between azides and alkynes, which are not endogenous elements in nature.[22] (Figure 2.9)

The confocal analysis of the CuAAC reaction was evaluated under various conditions in which the reagents, **4b**, and **5a**, were tested for background fluorescence (Figure can be see in Figure 2.10 and 2.11). Panel C showed a sharp increase in fluorescence indicating the CuAAC reaction had taken place. Within the overlay of panel C the propidium iodide nuclear stain clearly demarcates the perimeter of the nucleus and the presence of the click conjugate **6a** is revealed by the pink hue generated from the blue and red overlap (Figure 2.10). This suggests the CuAAC reaction had taken place while **4b** was in a ternary complex with TS and dUMP. Of particular interest are panels F-G, where both **4b** and **5a** are incubated as separate components (Figure 2.11).

Neither panels produced any notable fluorescence in the DAPI channel where the **6a** conjugate is expected to actively fluoresce after the CuAAC reaction. Moreover, it was speculated that the combination of the azide-alkyne might possess a low order of propinquity and efficient ligand-alignment to undergo *in situ* CuAAC.[23]

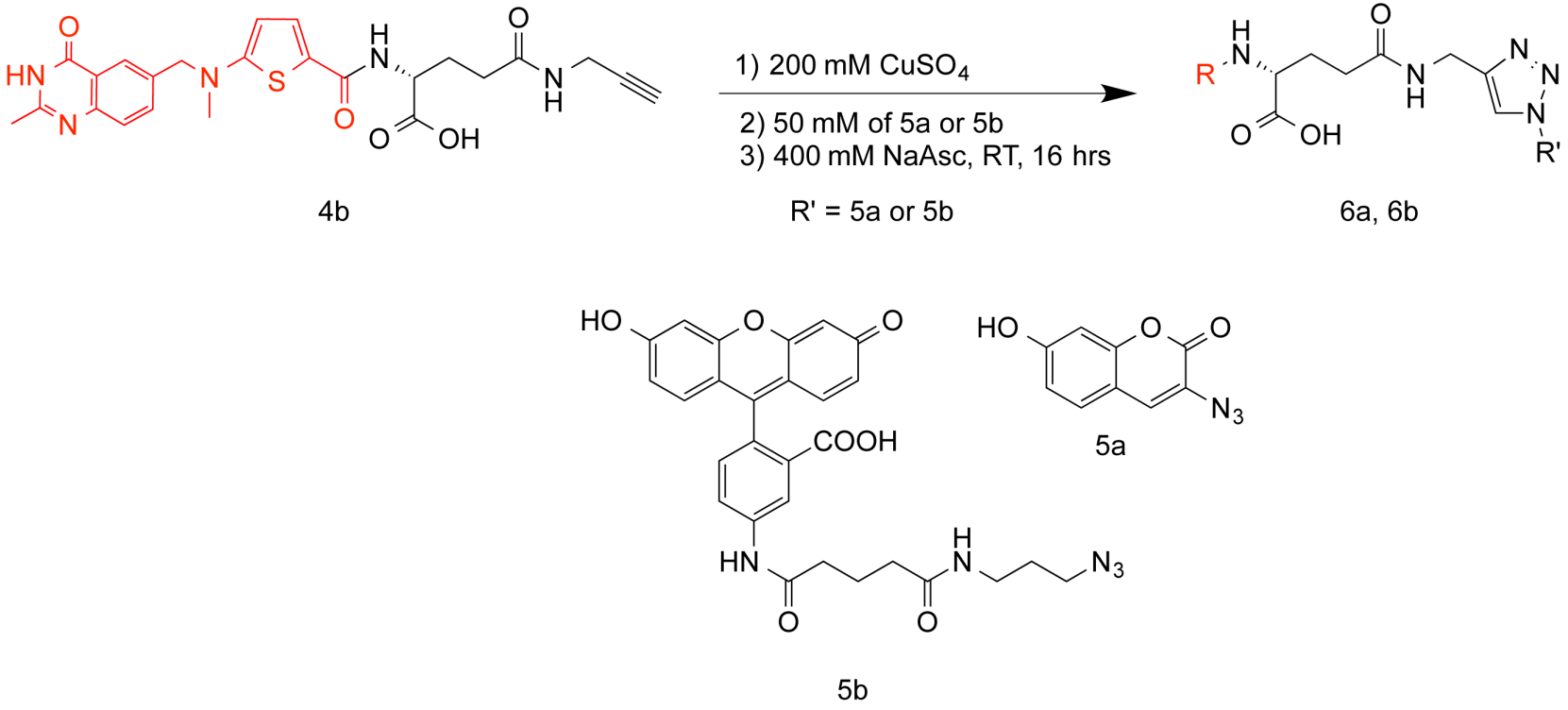

Figure 2.9 General scheme for the CuAAC reaction with Az42 (**5a**) and N_3-APOP-FITC (**5b**) to yield **6a** and **6b**, respectively.

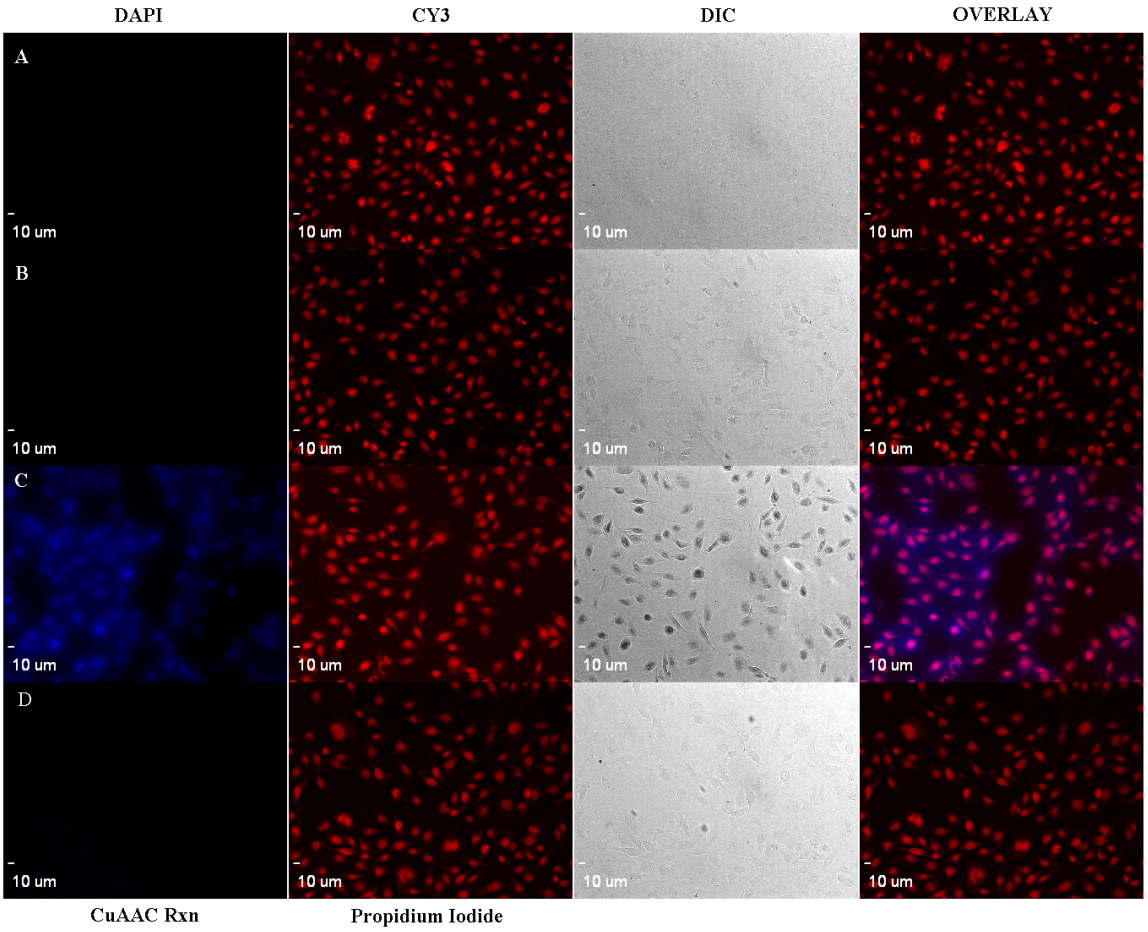

Figure 2.10 Confocal analyses of the CuAAC reaction with compound **4b** and **5a** in CHL^{-TS} PJZ205/200 cells. Conditions: (A) no reagents or dyes. (B) **4b** and $CuSO_4$. (C) **4b**, TCEP, $CuSO_4$, **5a**. (D) TCEP, $CuSO_4$. Panel C clearly indicates a strong presence of the CuCAA reaction in hTS overexpressing cells. All wells counter stained with propidium iodide for nuclear representation. Scale bars are 10 μm.

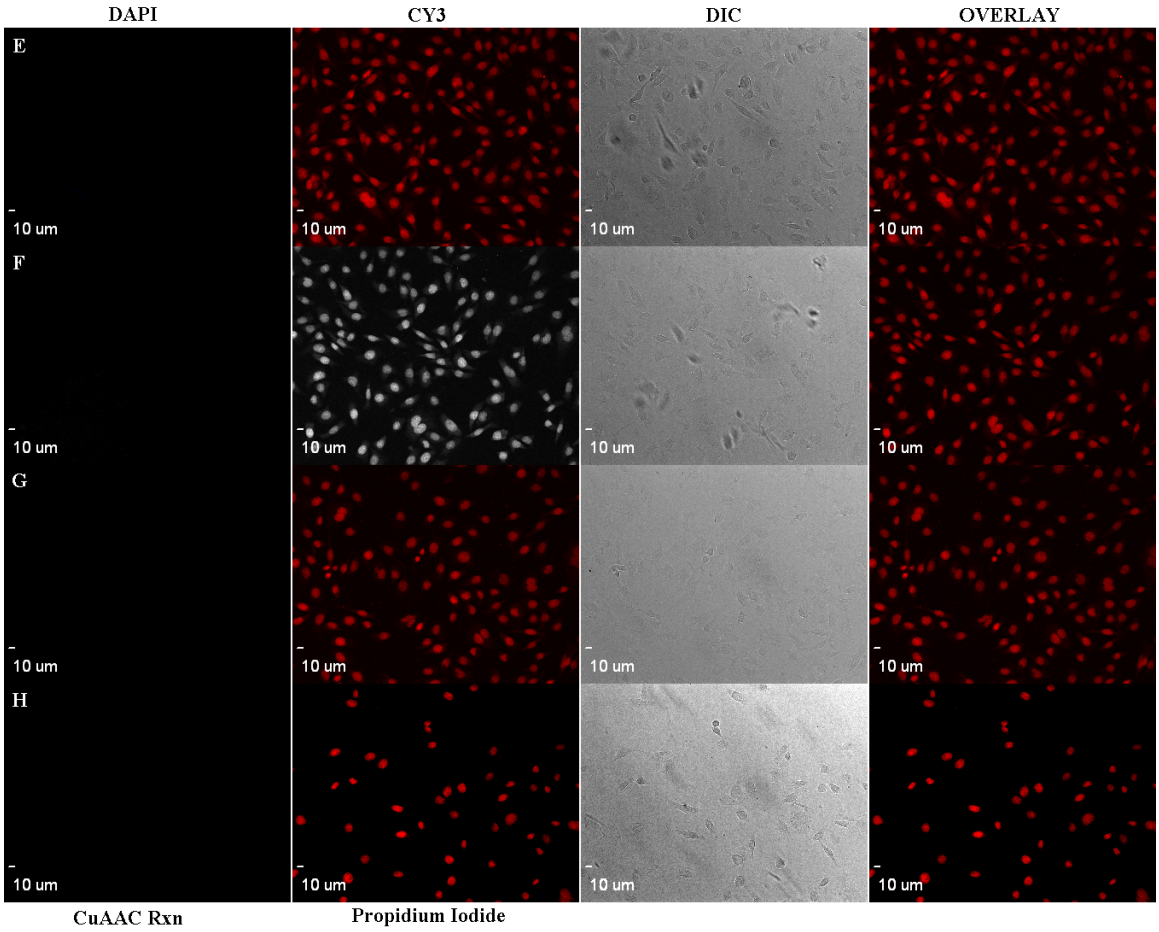

Figure 2.11 Confocal analyses of the CuAAC reaction with compound **4b** and **5a** in CHL^{-TS} PJZ205/200 cells. (E) **4b**, TCEP, $CuSO_4$. (F) **4b**. (G) **5a**. (H) **4b** and **5a**. All wells counter stained with propidium iodide for nuclear representation. Scale bars are 10 μm.

However, given the entropic parameters of **4b**, the lack of fluorescence in panel H (Figure 2.11) confirms that both a reducing agent (TCEP or Sodium Acorbate) and Cu(I) are required to facilitate the 1,3-Hugsien cycloaddition, which forms the 1,2,3-triazole is responsible for the fluorogenic activation of **5a**.[24]

To validate the previous findings, the experiments above were repeated in CHL^{-TS} PJZ205/200 and CHL^{-TS} Null cell lines in addition to the application of a TS-specific antibody (Ab^{+TS}-647) for co-localization (Figure 2.12). Panel A shows the resultant fluorescence from the **6a** product with overlap noted within the same regions as those stained with the TS-specific antibody (Figure 2.12). However, panel B, the negative control, shows some low levels of fluorescence from either **4b** or **5a.** In comparison with the TS stain of panel B, it can be seen that the background fluorescence does not correlate entirely with the signal produced by the TS Ab^{+TS}-647. Thus, it is unlikely that either component exhibits any characteristics of random fluorescence. Importantly, panels C and D confirm that fluorescence exhibited in panel A and, therefore, in panel C of figure 2.6, is due to the presence of TS, as the **6a** conjugate does not display non-specific binding or off-targeting capabilities. This is reaffirmed by the lack of signal in both Ab^{+TS}-647 fluorescent micrographs. (Figure 2.12)

Due to the low background exhibited by **4b** in figure 2.8 and the close proximity with which **5a** must aligned with the active alkyne of **4b**, an alternative longer wavelength dye with a extended linker was proposed. The N_3-APOP-FITC (**5b**) linker-dye was used to demonstrate the viability of an alternate probe and to alleviate the potential for false positive CuAAC between the blue emitting **5a** and **4b**. The linker possesses a terminal azide moiety for active CuAAC, which is tethered to two three-

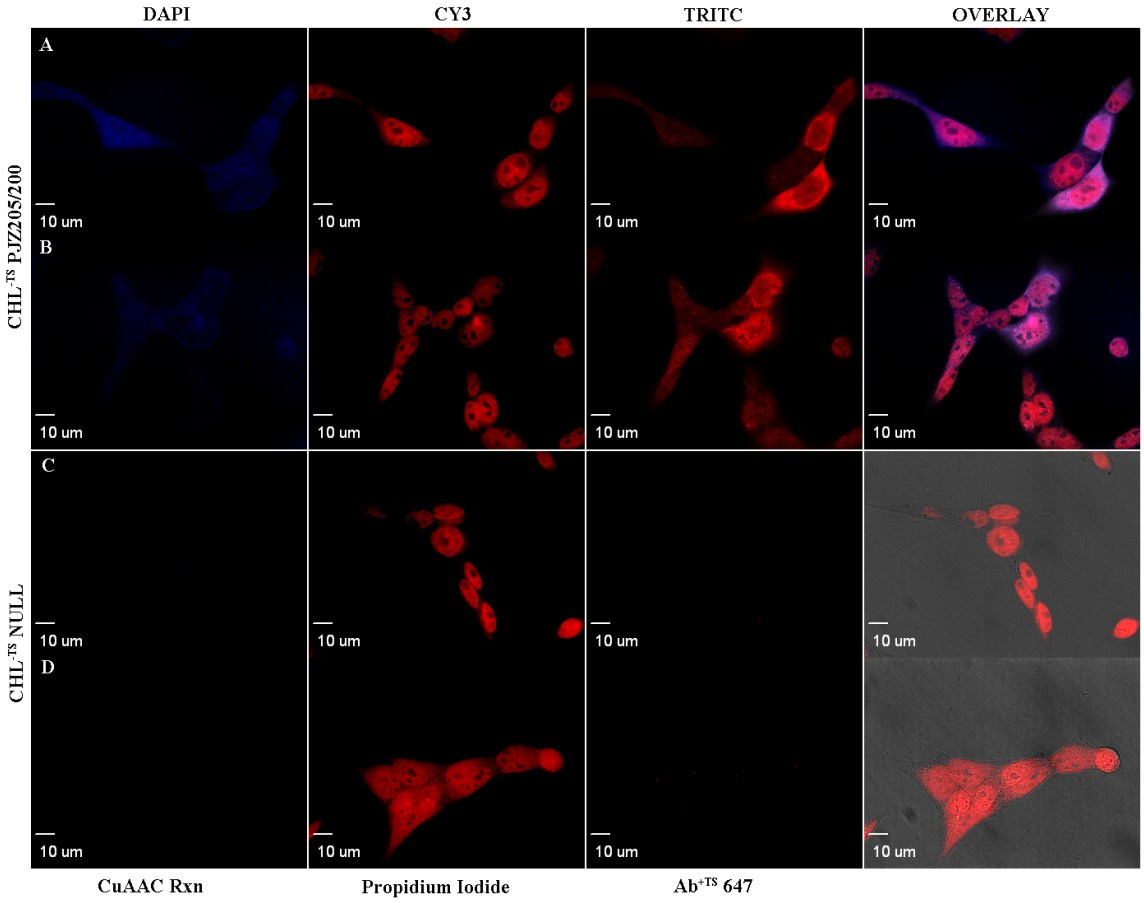

Figure 2.12 Fluorescent confocal micrographs of **6a** in CHL TS overexpressing and null cell lines. (A) **6a** CuAAC in TS overexpressing cells are clearly visible and detected with the +TS 647-conjugated Ab (third column). (B) CuAAC negative control (no catalysts) shows low background. (C, D) TS null cells show no signal of any **6a** fluorescence or TS (third column). The overlay of C and D includes their respective DIC. All cells counter stained with propidium iodide (second column). Scale bar is 10 μm. Taken with 60× Apo Oil.

methylene spacers with an internal amide and the carboxy-terminus of the linker conjugated to FITC. In panels A-D a sharp increase in the fluorescence within the DAPI filter is seen to increase in a concentration dependent manner (Figure 2.13). Although the GFP channel records the presence of the **5b** CuAAC reaction (no background within the inset for free dye), the same corresponding reaction shows activity in the DAPI filter.

This phenomenon indicates that **4b** might be fluorescent, but only in relationship to the levels external dye is administered and, therefore, is dependent on the CuAAC or triazole formation. This is because the addition of **4b** was constant (25 μM) and free **5b** (insets in all panels) did not produce any activity in either the DAPI or GFP filters. (Figure 2.13) Potentially, channel overlap, or bleed, appears to occur at the expense of the CuAAC reaction. However, it stands to be more reasonable to assume the triazole itself possesses fluorescent properties because, as the threshold of CuAAC rose in proportion to the amount of azide-dye added, there was an accompanying increase in signal within the DAPI channel. Provided with this posit, it was pertinent to further investigate the role of **4b** and its potential cross-fluorescence.

In order to investigate the fluorescent relationship between **4b** and **5b**, flow cytometry was used to measure their prospective interactions in CHL^{-TS} pJZ205/200 cells (Figure 2.14). Here, 25 μM of **4b** and **5b** was applied to cells as the signal and spatial representation of the dye at this concentration was superior to those at the other three concentrations seen in figure 2.13. Plot A2 illustrates the CuAAC signal from both the 488 (**5b**) and 405 (**4b**) channels, demonstrating that the reaction occurred as evidenced by the population in the second quadrant, Q2. Interestingly, both negative controls seen in plots A3 and A4 are free **5b** and **4b**, respectively, with Q3 of plot A3 occupying the most

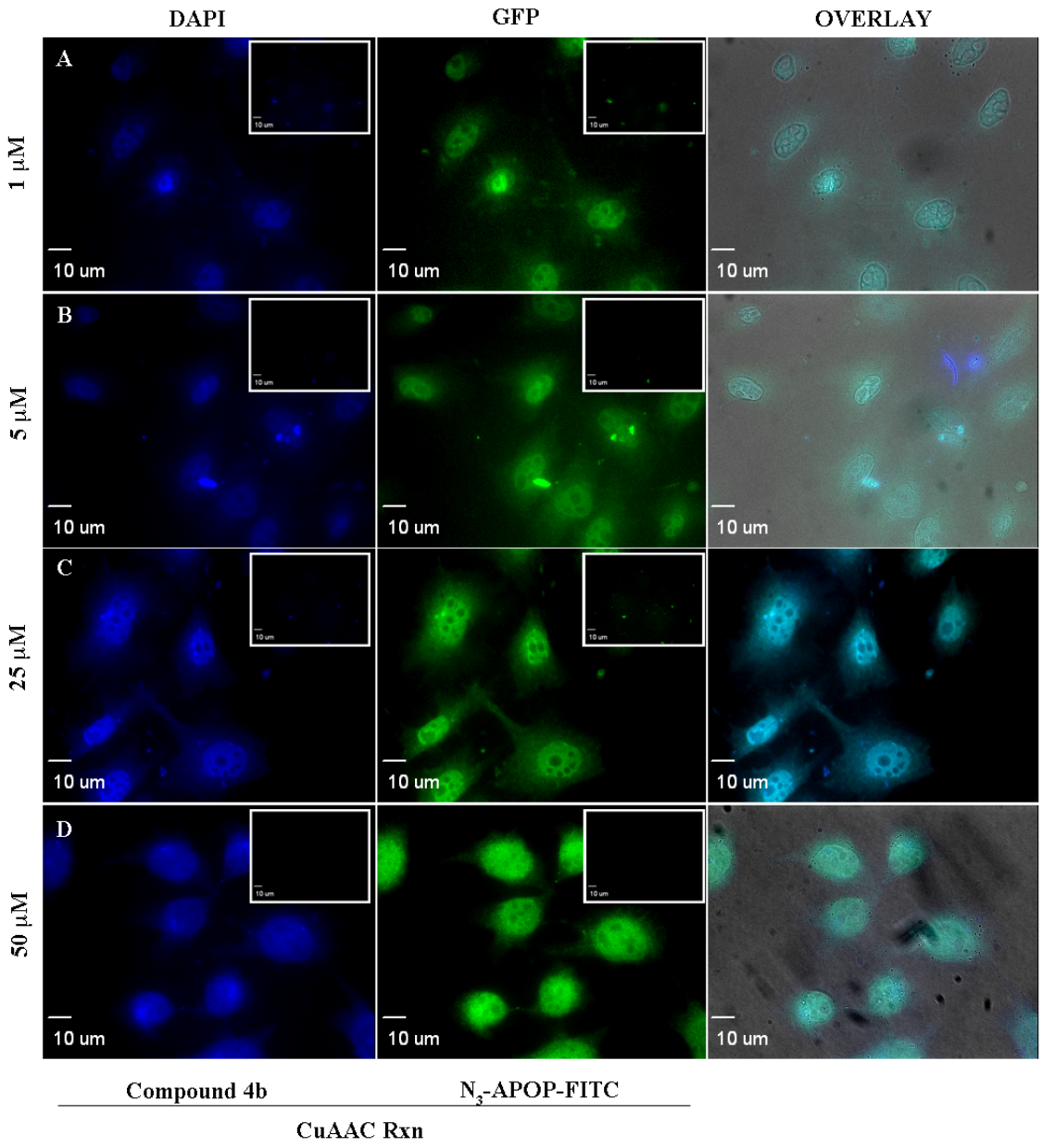

Figure 2.13 Fluorescence micrograph of the CuAAC reaction with **4b** and the extended linker **5b**. (A-D) Concentration of **5b** varied for each CuAAC rxn demonstrating maximum signal strength and cellular visualization. Both the DAPI and GFP filters represent the CuAAC reaction between compound **4b** and the dye-linker with negative controls for the latter (inset). Scale bar is 10 μm. Taken with 60× Apo Oil lens.

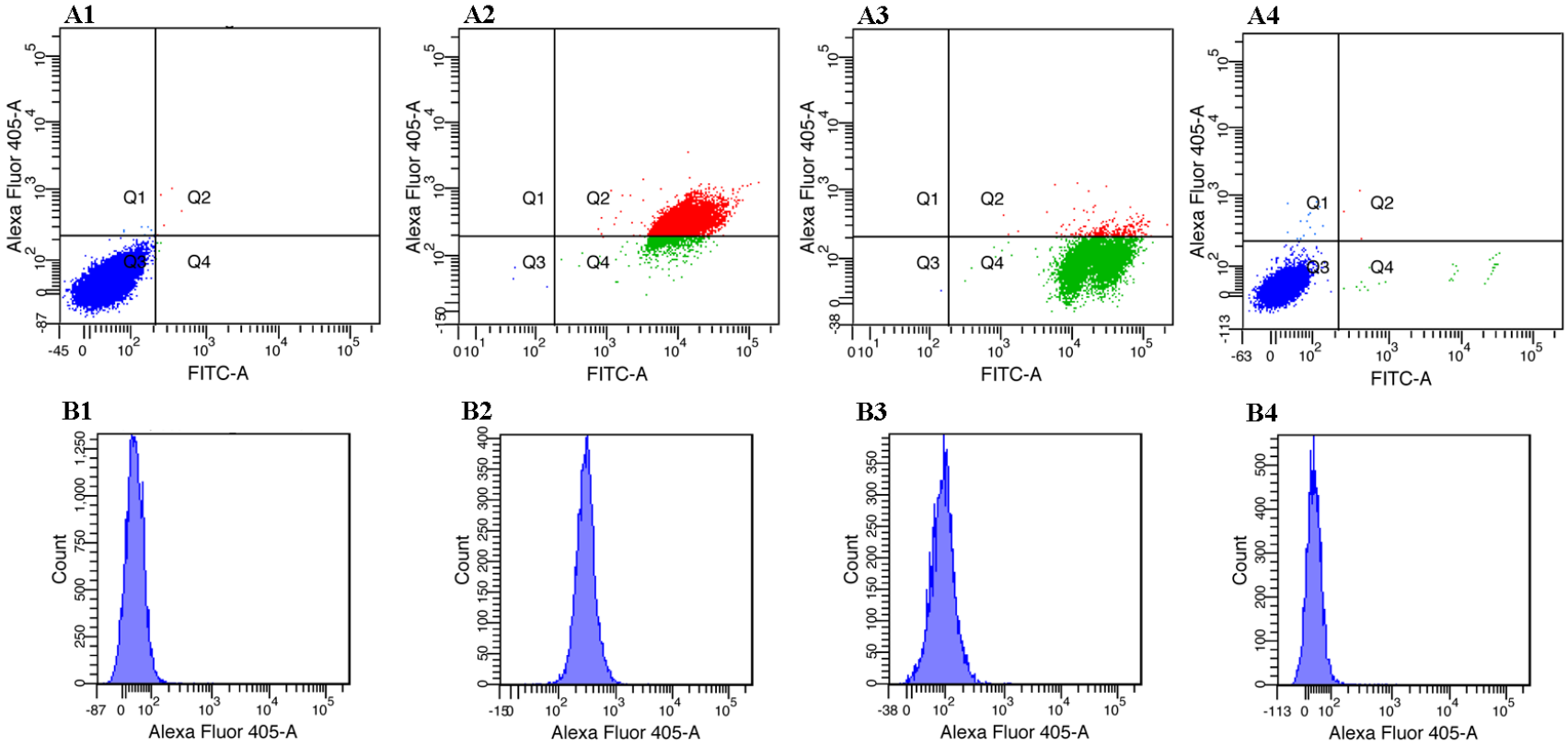

Figure 2.14 (A) Flow cytometry dot plots for compound **4b** and 25 μM **5b** dye in CHL^{-TS} pJZ205/200 cells: (A1) Negative control. (A2) Representative CuAAC reaction. (A3) 25 μM **5b** dye. (A4) 25 μM compound **4b**. (B) Histogram flow analysis for compound **4b** (Alexa Fluor 405-A) in in CHL^{-TS} pJZ205/200 cells demonstrates the fluorescence transmission of **4b** (A4, B4) is significantly altered when compared the transmission generated for the CuAAC reaction (A2, B2). The designation for histograms B1-B4 follows those of the dot plots for A1-A4.

signal and not for **4b**. These controls show **4b** is not a fluorescent product under the 405-channel nor has the azide-dye undergone any type of CuAAC reaction. The relevance to whether **4b** is fluorescent will only be apparent under conditions where (i) triazole formation occurs without an azide-fluorophore or (ii) triazole formation can only be detected at a narrow emission that precludes counter fluorescence from either **4b** or azide-associated compounds.

Under CuAAC conditions, histogram A2 shows a distinct shift under the 405-channel from the negative control, A2. This suggests that formation of the triazole, and not **4b** itself, is responsible for generating a fluorescent signal. Additionally, histogram 4B, the negative control for **4b**, mirrors that of histogram A2, clearly supporting the non-fluorescent nature of free **4b** (Figure 2.14). Lastly, it's unlikely that **4b** could exhibit any proportional signal while bound in a ternary complex with dUMP-TS. The potential to reach any point of conjugation necessary for fluorescence can only be accessed by the triazole, as it is presumably solvent exposed, whereas the buried pterin ring system or the thiophene moiety are deep within the binding pocket of the **6b**•dUMP•TS ternary complex.

2.2 Experimental

2.2.0 Synthesis and Characterization of RTXγ-PgA by EDCI/NHS Coupling

Dr.'s Jiangli Fan, Yi Chen, and Honglin Li graciously performed the synthesis of **4b** for the use of all cell assays. The following is a brief analysis of their synthetic **4b** for

the use of all cell assays. The following is a brief analysis of their synthetic protocol. In a 500 mL round bottom flask, 2.1 mmol (1 g) of **1a** was dissolved in 10 mL of DMF and cooled in a water-ice bath. To the reaction, 2.5 mmol (0.260 g) of NHS and 2.5 mmol (0.44 g) of EDCI were added. The resulting mixture was stirred will in the ice bath for 0.5 hrs until a white precipitate formed. A solution of PgA (0.124 g, 2.25 mmol) in 5 mL of DMF was added. The resulting mixture was allowed to come to room temperature and stirred for 24 hrs. The reaction mixture was poured into water (100 mL) and stirred for 30 min to form a precipitate. The crude product was purified over a RP C_{18} 10.0 x 250mm, 10 μm column at 6 mL min^{-1}using a 25% ACN (0.05% TFA) to 90% gradient in 60 min. Peaks were detected at 220 nm and confirmed via ESI LC/MS. Fractions were collected, pooled, and dried under lyophilization to yield **4b** as a brown-yellow solid; ^{1}H NMR (400 MHz, CD_3OD) δ 1.98 (1H, m) 2.15 (1H, m), 2.31 (1H, m), 2.41 (1H, m), 2.52 (3H, s), 2.5 (1H, d, J = 9.2 Hz), 3.12 (1H, s), 3.89 (1H, s), 3.95 (1H, s), 4.7 (1H, s), 6.0 (1H, d, J = 4.4 Hz), 7.6 (1H, d, J = 8.4 Hz), 7.7 (1H, d, J = 8.2 Hz), 8.1 (1H, s); Compound **1a** purchased from Sequoia Research Ltd.; ^{1}H NMR (400 MHz, CD_3OD) δ 2.0 (1H, m), 2.2 (1H, m), 2.0 (1H, m), 2.4 2.0 (1H, m), 3.1 (3H, s), 4.5 (1H, m), 4.66 (2H, s), 5.97 (1H, d), 7.49 (1H, s), 7.5 (1H, d, J = 9.5 Hz), 7.7 (1H, d, J = 8.1 Hz), 8.06 (1H, s).

2.2.1 Synthesis and Characterization of RTXγ-PgA by DCC/DMAP Coupling

To a 100 mL round-bottom flask were added **1a** (47 mg, 103 μmol) in 2 mL of DMF under argon and cooled to 4 °C followed by the drop-wise addition of 6 mL of DCM with DCC (20 mg, 97 μmol) over 60 min. The flask brought to -40 °C in a dry ice-

acetonitrile bath and where DMAP (12 mg, 99 μmol) in DCM was added via the septum. To the flask, the primary amine PgA (6.4 μL, 100 μmol) was added and reaction was run for 3 hours at -40 °C then allowed to reach to room temperature over night. The reaction was extracted 2× in 15 mL of water with DCM and pooled using a 250 mL separation funnel. The pooled water was evaporated under reduced pressure at 52 °C with ACN until dry. All samples were prepared for analytical and preparatory HPLC-UV using the corresponding methods. Analytical: Inject 20 μL over a RP C_{18} 4.6 × 250 mm, 5 μm column from 10-80% ACN with 0.1% TFA at 1 mL min^{-1} in 45 min, monitoring peaks at 269 and 341 nm. For preparatory purification inject 94 μL over a RP C_{18} 10.0 × 250-mm, 5 μm column from 10-80% ACN with 0.1% TFA at 4.7 mL min^{-1} monitoring peaks at 269 and 341 nm. Peaks were identified and collect using MassLynx FractionLynx software.

2.2.2 Enzyme Purification

Thymidylate synthase was partially purified according to the protocol previously reported.[19]

2.2.3 Isothermal titration calorimetry

Isothermal titration calorimetry (ITC) was performed on a VPITC instrument (Microcal Corp.) with a 250 μL syringe. All ITC measurements were carried out at in degassed solutions at 26 °C. Approximately 52, 5 μL injections were made with 6-second

duration and 120 seconds spacing. The macromolecule (TS) concentration was 15 μM in 50 mM Tris-HCl, pH 7.4 with 1 mM EDTA and 20 μM BME, which is referred to as "Buffer A." Titration was carried out in buffer A with the following reagents: 100 μM dUMP and 300 μM of either **1a** or **4b**. The data was processed using the manufacturers software ORIGIN.

2.2.4 Cell Prep

All cells were provided by Dr. Franklin G. Berger (University of South Carolina, Department of Biological Sciences). All cells were grown in a T75 flask under 10% fetal bovine serum (FBS) in high glucose Dulbecco's Modified Eagle's medium (DMEM) with 100 U of penicillin-streptomycin (Pen-Strep) at 37 °C and humidified at 5% CO_2. Cell line RJK33.13, a TS-deficient derivative of V79 Chinese hamster lung cells (CHL^{-TS} pJZ205, CHL^{-TS} pJZ205/200, CHL^{-TS} Null) were grown to confluency and passaged at either 1:10 or 1:20 with 0.25% trypsin. CHL^{-TS} Null cells were supplemented with 10 μM thymidine.

2.2.5 CuAAC Assay and Image Analysis with Lab-TEKII Prep

CHL-TS pJZ205/200 cells were seeded at 1×10^5 cell/well into a Lab-TEKII 8-well chamber (Nalgene) that was coated with 10 μg/mL of fibronectin at 4 °C for 24 hours. Cells were incubated for 6 hrs at 37 °C and then prepped for 30 min incubation with reagents according column A in table 2.3. Immediately after incubations wells were

Table 2.3 CuAAC conditions for confocal analyses with compound **4b** and **5a** in CHL^{TS} PJZ205/200 cells.

Panel ID	A	B: $CuSO_4$ (µL)	C: TCEP (µL)	D: 5a (µL)	E⌘
Fig 2.10, A	§	0	0	0	800 µL
Fig 2.10, B	160 µL **4b** + §	160	0	0	640 µL
Fig 2.10, C	160 µL **4b** + §	160	320	20	300 µL
Fig 2.10, D	20 µL **5a** + §	160	320	0	320 µL
Fig 2.11, E	160 µL **4b** + §	160	320	0	320 µL
Fig 2.11, F	160 µL **4b** + §	0	0	0	800 µL
Fig 2.11, G	20 µL **5a** + §	0	0	0	800 µL
Fig 2.11, H	160 µL **4b** + §	0	0	20	780 µL

(Stock conc. = **4b**, 500 µM; **5a**, 2 mM; TCEP, 1 mM; $CuSO_4$, 1 mM)

§ Adj to 800 µL with DMEM

⌘ Final volume to 800 µL with 100 mM TRIS-HCl, pH 8.0

aspirated, washed 2× with phosphate buffered saline (PBS) and fixed with 250 μL of 3.7% paraformaldehyde (pfa) for 10 min at room temperature. After fixation, cells were washed 2× with PBS and counterstained with propidium iodide (PI) at 2 μL/mL. Cells were washed 3× with PBS and dye-labeled by sequentially adding reagents according to columns B→E in table 2.3.

The slide was wrapped in aluminum foil and incubated at room temperature (RT) for 60 min. The cells were aspirated and wash 3× in PBS. Approximately 10 μL of the antioxidant 1,4-diazabicyclo[2.2.2]octane (DABCO) was added per well and the chamber was released and covered with a 22x50 mm glass coverslip and sealed with nail polish. All data was collected on an Olympus IX81 confocal fluorescent microscope with either a 10× air objective or 60× apo oil lens.

2.2.6 CuAAC Assay and Image Analysis with 12-well Prep

Glass coverslips were added to a twelve-well plate and washed in ethanol followed by 3× washes with PBS. Each well was seeded with 1×10^5 cells and incubated overnight. All wells were prepped for 30 min incubation with **5a** or **5b** according column A in table 2.4 and 2.5, respectively. Immediately after incubations wells were aspirated, washed 3x with PBS and fixed with 250 μL of 3.7% pfa for 10 min at (RT). After fixation, cells were washed 2× with PBS and counterstained with PI at 2 μL/mL. Cells were washed 3× with PBS and dye-labeled by sequentially adding reagents (B→D) according tables 2.4 or 2.5. The trays were wrapped in aluminum foil and incubated at

Table 2.4 CuAAC conditions for confocal analyses with compound **4b** and **5b** in CHL^{-TS} PJZ205/200 and CHL^{-TS} Null cells.

Pre IHC		Post IHC			
ID	A	B: **5b** (µL)	B: 1x PBS (µL)	C: $CuSO_4$ (µL)	D: NaAsc (µL)
Fig 2.12, A	100 µL 4b + §	25	300	200	400
Fig 2.12, B	100 µL 4b + §	25	900	0	0
Fig 2.12, C	100 µL 4b + §	25	300	200	400
Fig 2.12, D	100 µL 4b + §	25	900	0	0

(Stock conc. = **4b**, 1 mM; **5a**, 2 mM; TCEP, 1 mM; $CuSO_4$, 1 mM)

§ Adj to 1000 mL with DMEM in 10% FBS

Table 2.5 CuAAC conditions for confocal analyses with compound **4b** and **5b** in CHL^{-}_{TS} PJZ205/200 cells to determine relationship between concentration of **5b** and image resolution.

Pre IHC		Post IHC			
ID	A	B: **5b** (µL)	B: 1x PBS (µL)	C: $CuSO_4$ (µL)	D: NaAsc (µL)
Fig 2.13, A	100 µL 4b + §	2	298	200	400
Fig 2.13, B	100 µL 4b + §	10	290	200	400
Fig 2.13, C	100 µL 4b + §	50	250	200	400
Fig 2.13, D	100 µL 4b + §	100	300	200	400

(Stock conc. = **4b**, 1 mM; **5b**, 2 mM; TCEP, 1 mM; $CuSO_4$, 1 mM)

§ Adj to 1000 mL with DMEM in 10% FBS

RT for 15 hrs. The cells were aspirated and wash 3× in PBS. Individual cover slips were removed and dried and set with 10 μL of DABCO or 15 μL of VectaShield and sealed with nail polish. All data was collected on an Olympus IX81 confocal fluorescent microscope with either a 10× air objective or 60× apo oil lens.

2.2.7 Immunohistochemistry with 12-well Prep

Immediately after fixation, cells were washed 3× in PBS at 37 °C and permeabilized with 0.1% Triton X100 for 5 min. Cells were washed 3× in PBS and blocked in 10% goat serum with 50 mg mL^{-1} sucrose and 20 mg mL^{-1} bovine serum albumin (BSA, Rockcreek) in PBS for 90 min at RT. Cells were washed 3X in PBS and probed for 60 minutes with hTS primary antibody T-106 [1:40] in 5% goat serum with 1% BSA in PBS.

Cells were washed 3×, 5 minutes each in PBS followed by secondary probe Cy5-ab-642 goat anti-mouse at 1:2000 in the same solution as the primary probe. Cells were washed 3 ×, 5 minutes each in PBS and counter stained with PI at 2 μL mL^{-1}. Cells were washed with 3× with PBS and prepared for CuAAC reaction according to table 2.4 AND 2.5. The trays were wrapped in aluminum foil and incubated at RT for 15 hrs. The cells were aspirated and wash 3× in PBS.

Individual cover slips were removed and dried and set with 10 μL of DABCO or 15 μL of VectaShield and sealed with nail polish. All data was collected on an Olympus IX81 confocal fluorescent microscope with either a 10× air objective or 60× apo oil lens.

2.2.8 Flow cytometry Cell Prep for CuAAC Reaction

Cells were prepped as previously described in section 2.3.4. Cells were seeded in a 12-well plate at 1×10^5 cells per well and incubated at 37 °C at 5% CO_2 for 24 hours. Cells were inoculated with 25 μM **4b** in six wells filled with 1 mL DMEM and incubated for 60 min. Cells were washed with 1 mL, 1× in 37°C PBS and then lifted with 150 μL of 0.25% trypsin for 3 min at 37 °C. Cells were centrifuged at 100 RCF for 3 min, aspirated and washed with 1% BSA in PBS at 37 °C. Additional centrifugation followed at 200 RCF for three min where the cells were then aspirated and fixed in 100 mL of 3.7% pfa at 37 °C for 15 min at RT. Cells were washed again with 1% BSA in PBS and pelleted at 200 RCF for 3 min followed by permeabilization with 100 μL of Triton X-100 for 15 min. Cells were washed again with 1% BSA in PBS and pelleted at 200 RCF for 3 min then prepped for CuAAC reaction.

2.2.9 Flow cytometry of CuAAC Reaction

To each positive control 100 μL of 1 mM $CuSO_4$ and 250 μL of 2 mM histidine were pooled together and added to each well. All wells were then diluted with 240 μL of PBS followed by 10 μL of 2.5 mM **5b**. The CuAAC reaction proceeded upon the addition of 400 μL of 1 mM sodium ascorbate. The reaction was incubated for 30 min at RT with no light. Post CuAAC, the samples were washed with 1% BSA in PBS and pelleted at 200 RCF for 3 min. The samples were aspirated and resuspended in 400 μL of PBS and analyzed immediately.

2.3 REFERENCES

1. Jackman, A.L. et al. ICI-D1694, A Quinazoline Antifolate Thymidilate Synthase Inhibitor that is a Potent Inhibitor of L1210 Tumor-Cell Growth-Invitro and Invivo - A New Agent for Clinical-Study. *Cancer Res.* **51**, 5579-5586 (1991).
2. Meienhof.J, Jacobs, P.M., Godwin, H.A. & Rosenber.Ih Synthesis of Hepta-Gamma-L-Glutamic Aacid by Conventional and Solid-Phase Techniques. *J. Org. Chem.* **35**, 4137-4140 (1970).
3. Piper, J.R., McCaleb, G.S. & Montgomery, J.A. A Synthetic Approach to Poly(Gamma-Glutamyl) Conjugates of Methotrexate. *J. Med. Chem.* **26**, 291-294 (1983).
4. Nair, M.G., Nanavati, N.T., Kumar, P., Gaumont, Y. & Kisliuk, R.L. Synthesis and Biological Eevaluation of Poly-Gamma-Glutamyl Metabolites of 10-Deazaaminopterin and 10-Ethyl-10-Deazaaminopterin. *J. Med. Chem.* **31**, 181-185 (1988).
5. Bisset, G.M.F., Pawelczak, K., Jackman, A.L., Calvert, A.H. & Hughes, L.R. Synthesese And Thymidylate Synthase Inhibitory Activity of the Poly-Gamma-Glutamyl Conjugates of N- 5- N-(3,4-Dihhydro-2-Methyl-4-Oxoquinazolin-6-ylmethyl)-N-Methylamino -2-Thenoyl -L-Glutamic Acid (ICI D1694) and Other Quinazoline ANTIFOLATES. *J. Med. Chem.* **35**, 859-866 (1992).
6. Bader, H. & Rosowsky, A. 1st Use of the Taylor Pteridine Synthesis as a Route to Polyglutamate Derivatives of Antifolates .45. *J. Org. Chem.* **56**, 3386-3391 (1991).

7. Forsch, R.A. & Rosowsky, A. Synthesis of gamma- N-15 -L-glutamyl derivatives of 5,10-dideazatetrahydrofolate. *J. Label. Compd. Radiopharm.* **42**, 1103-1117 (1999).

8. Wang, S., Lee, R.J., Mathias, C.J., Green, M.A. & Low, P.S. Synthesis, purification, and tumor cell uptake of Ga-67-deferoxamine-folate, a potential radiopharmaceutical for tumor imaging. *Bioconjugate Chem.* **7**, 56-62 (1996).

9. Dhaon, M.K., Olsen, R.K. & Ramasamy, K. Esterification of N-Protected Alpha-Amino-Acids With Alcohol/Carbodiimide/4-(Dimethylamino)-Pyridine - Racemization of Aspartic And Glutamic-Acid Derivatives. *J. Org. Chem.* **47**, 1962-1965 (1982).

10. Martin, D.M.G. & Siedlecki, P.S. Preparation of the key intermediate in a novel synthesis of ZD9063P: The chemical component of ADEPT, a targeted cytotoxic therapy. *Org. Process Res. Dev.* **4**, 259-263 (2000).

11. Hoffbran.Av, Tripp, E., Houlihan, C.M. & Scott, J.M. Studies on Uptake of Synthetic Conjugated Folates by Human Marrow Cells. *Blood* **42**, 141-146 (1973).

12. Schirch, V. & Strong, W.B. Interaction of Folylpolyglutamates with Enzymes in One-Carbon Metabolism. *Arch. Biochem. Biophys.* **269**, 371-380 (1989).

13. Jackman, A.L. et al. ZD1694 (Tomudex) - A New Thymidilate Synthase Inhibitor with Activity in Colorectal-Cancer. *Eur. J. Cancer* **31A**, 1277-1282 (1995).

14. Kamb, A., Moore, J.F., Calvert, A.H. & Stroud, R.M. Structural Basis for Recognition of Polyglutamyl Folates by Thymidilate Synthase *Biochemistry* **31**, 9883-9890 (1992).

15. Francis, C.L. et al. Total synthesis of methotrexate-gamma-TRIS-fatty acid conjugates. *Aust. J. Chem.* **55**, 635-645 (2002).

16. Huang, X.C., Luo, X.H., Roupioz, Y. & Keillor, J.W. Controlled regioselective anilide formation from aspartic and glutamic acid anhydrides. *J. Org. Chem.* **62**, 8821-8825 (1997).

17. Deguest, G., Bischoff, L., Fruit, C. & Marsais, F. Regioselective opening of N-Cbz glutamic and aspartic anhydrides with carbon nucleophiles. *Tetrahedron: Asymmetry* **17**, 2120-2125 (2006).

18. Cao, S.L., Wan, R. & Feng, Y.P. New synthesis of thymidylate synthase inhibitor Raltitrexed. *Synth. Commun.* **33**, 3519-3526 (2003).

19. Lovelace, L.L., Gibson, L.M. & Lebioda, L. Cooperative inhibition of human thymidylate synthase by mixtures of active site binding and allosteric inhibitors. *Biochemistry* **46**, 2823-2830 (2007).

20. Phan, J. et al. Human thymidylate synthase is in the closed conformation when complexed with dUMP and raltitrexed, an antifolate drug. *Biochemistry* **40**, 1897-1902 (2001).

21. Le Droumaguet, C., Wang, C. & Wang, Q. Fluorogenic click reaction. *Chem. Soc. Rev.* **39**, 1233-1239 (2010).

22. Hong, V., Presolski, S.I., Ma, C. & Finn, M.G. Analysis and Optimization of Copper-Catalyzed Azide-Alkyne Cycloaddition for Bioconjugation. *Angew. Chem.-Int. Edit.* **48**, 9879-9883 (2009).

23. Lewis, W.G. et al. Click chemistry in situ: Acetylcholinesterase as a reaction vessel for the selective assembly of a femtomolar inhibitor from an array of building blocks. *Angew. Chem.-Int. Edit.* **41**, 1053-1057 (2002).

24. Sivakumar, K. et al. A fluorogenic 1,3-dipolar cycloaddition reaction of 3-azidocoumarins and acetylenes. *Org. Lett.* **6**, 4603-4606 (2004).

CHAPTER 3

ANTIFOLATE-PROTAC INDUCED DEGRADATION OF THYMIDYLATE SYNTHASE

3.0 INTRODUCTION

The importance of protein-protein interactions in regards to the etiology of disease cannot be understated. The ability to mitigate or disrupt these interactions relies heavily on the pharmacology of biopharmaceuticals or peptide conjugates.[1, 2] Although examples of efficient small molecule targeted therapies have been shown, the ability to successfully influence these interaction remains difficult given the immense diversity protein substrates display on their surface or active site.[3-5] Contrary to more classically targeted systems such as enzymes and transmembrane receptors, protein-protein actions are not dependent on small pharmacophore interactions. Rather, they undergo reciprocal interactions that are mediated through spatial recognition of surface exposed non-contiguous amino acids.

A bifunctional molecule that recruits rather than disrupts protein-protein interaction has potential, should the substrate and the recruiting machinery coalesce to yield a therapeutic response.[6] Such systems have shown great utility in cell free systems, fusion constructs, and drug-peptide/carbohydrate conjugates.[7] Specifically the drug-peptide chimera holds great appeal due to its bioorthogonal capacity and its reliance upon the endogenous machinery inherent to many cell types, but without any genetic assault.

This system, qualified as the Proteolysis Targeting Chimera System (PROTACs) asserts targeted degradation via chemical control over the translational conscripts to which it targets.[8]

At one pole of the chimeric compound is a substrate-specific ligand, designed to actively recruit a protein of interest (POI). Tethered by a chemical linker to the opposite pole of the chimera is a peptide signal-sequence designed to enlist an ubiquitin-protein E3-ligase, thus targeting the POI for ubiquitin-dependent proteasomal-degradation.[9] The serviceable nature of the ligase is compounded, given there are over 600 E3-ligases of which the Skp1-Cullin-F-box (SCF) and von Hippel-Landau (VHL) are more widely studied.[10-12] These systems have asserted direct *in vitro* protein degradation of steroid hormone receptors, aminopeptidases, aryl hydrocarbon-receptors, and hypoxia-molecular switches.[8, 10, 13, 14]

The VHL E3 ligase holds promising potential in anti-cancer therapy due to its transcriptional relationship with intracellular hypoxia, a condition known to up-regulate pro-angiogenic genes.[15] The VHL tumor suppressor complex is comprised of elongins B and C, along with Cullin1 and ring box protein 1 (Rbx1).[16] Under normoxic conditions the complex constitutively ubiquinates hypoxia inducible factor 1α (HIF1α) by recognition of an internal hydroxylated proline located in a conserved 7-amino acid sequence.[17, 18]

Interestingly, coupling the HIV-tat translocation peptide to the HIF1α oxygen-dependent degradation domain (ODD) facilitates cellular entry with an accompanying angiogenic response along with induction of glucose transporter-1 gene expression.[19] This suggests that using the prolyl hydroxylation site in foreign

polypeptides can both serve as a VHL-E3 ligase substrate, and prevent HIFα from up-regulating its targeted genes. A candidate substrate for the PROTACs system is *de novo* source of the thymidine monophosphate (TMP): human thymidylate synthase (hTS, from this point on it will be referred to as TS unless otherwise noted).

As an overexpressed substrate in cancer, its potential applicability for PROTAC intervention is significant due to the following attributes: (i) TS represents a metabolic "bottleneck" for the pyrimidine TMP, thus presenting a pharmacological opportunity to induce cell death, (ii) TS possesses a large accessible array of modifiable quinazoline-based TS-directed antifolates. These antifolates can serve as the foundation for the TS-directed portion of the heterobifunctional PROTAC conjugate, and (iii) its [TS] intracellular stability is regulated by an internal bipartite degron and not direct ubiquitination.[20]

Selective chemical remodeling has already been demonstrated in potential TS targeted antimetabolites though elongation of the [antifolate] methylene bridge or through cyclopenta[γ]quinazoline diglutamyl arrangements at the carboxy-terminus.[21, 22] Of particular interest is the antifolate raltitrexed (RTX, Tomudex) and its nanomolar affinity toward TS. Previous attempts to modify RTX and its analogs with glutamic acid substrates successfully demonstrated the facile synthesis of gamma-modification to the terminal glutamic residue.[23-25] Here we describe our approach to the synthetic construction and *in vitro* potential of a gamma-linked TS-degradation directed RTX-PROTAC system using the VHL-E3 ligase directed HIF1α signal peptide (Figure 3.1). By affixing the HIF1α signal to the C-terminal carboxylate of RTX, the Ub-machinery is postulated to recognize the prolyl hydroxylated-peptide, induce TS-ubiquination and its

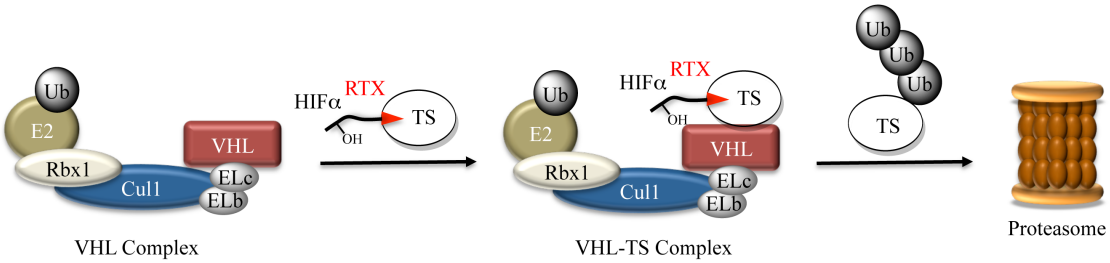

Figure 3.1 A general diagram illustrating the theoretical recognition of TS by the PROTAC HIFα hydroxyproyl moiety fused to TS bound-raltitrexed. Conferring substrate identity, the formation of the VHL-TS complex is accomplished with subsequent polyubiquination via the E2-congating subunit.

subsequent proteasomal degradation. This approach would prevent TS from escaping Ub-independent degradation, thus asserting intracellular control over the endogenous mechanism(s) that stabilize TS and promote cell death.

3.1 Results and Discussion

3.1.1 Synthesis of a TS-targeted PROTAC

Using the ALAPYIP peptide for E3-ligase recognition has been shown to serve as the minimum identification sequence for the VHL tumor suppressor protein.[18] Under hypoxic conditions HIF1α is not a VHL substrate and is therefore not post transnationally modified at P564.[26] Given that cancer cell lines function under hypoxic environments it was decided to omit the internal proline residue within the 8-mer-recognition [ALAPYIP] domain and synthesize the peptide with the VHL recognition residue, hydroxyproline (O). By circumventing the dependence of the intracellular hydroxylation of the HIF1α peptide we sought to remove any possibilities of generating an inert VHL substrate that would fail to result in (poly)ubiquitination. For the design of the TS-targeted PROTAC-1 we decided to rely upon the simple scaffolding features that solid phase peptide synthesis (SPPS) affords (Figure 3.2).[27]

A glycine trimer was coupled the C-terminus of **2** to generate **3a** in order to confer an unobtrusive linker and produce a stable chemical handle. Based on the crystal structure of a hyrodxylated HIFα bound to the VCB (VHL, elongin C, and B) complex, we hypothesized that the peptides structural arcing engendered by both the proline and hydroxyproline residues should be complimented with a ridged handle that orthogonally extends from the C-terminus away from the VCB complex (Figure 3.3).[18] The

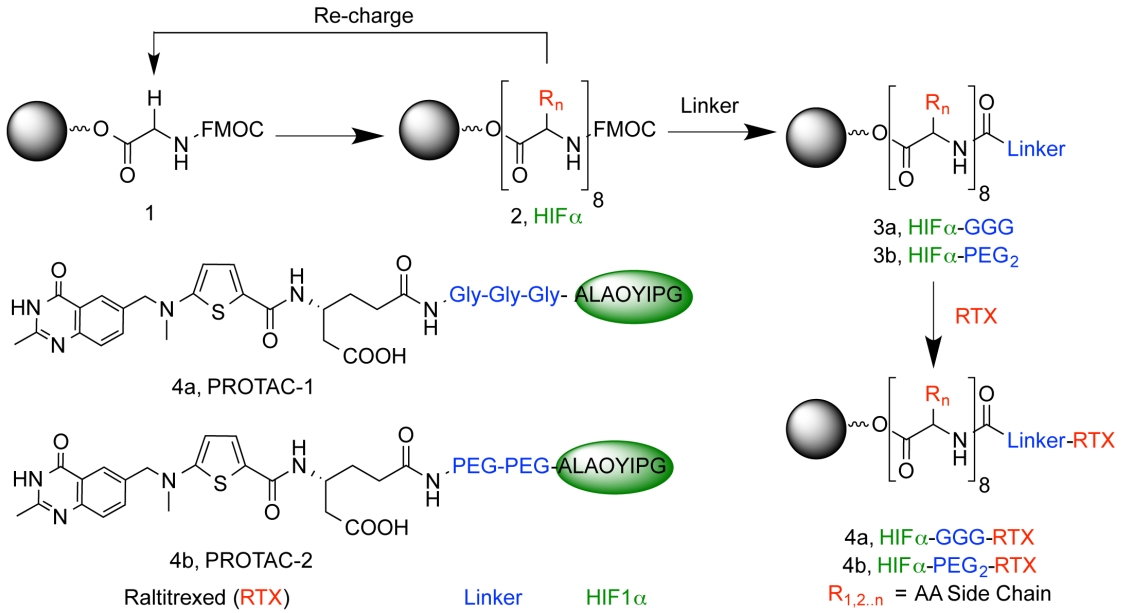

Figure 3.2 General schemes for the synthesis of both PROTAC-1 and PROTAC-2. Anatomies of both conjugates are shown with the gamma-carobxylate of raltitrexed tethered to a linker (blue), which presents the HIFα peptide (green) for VHL-E3 recognition.

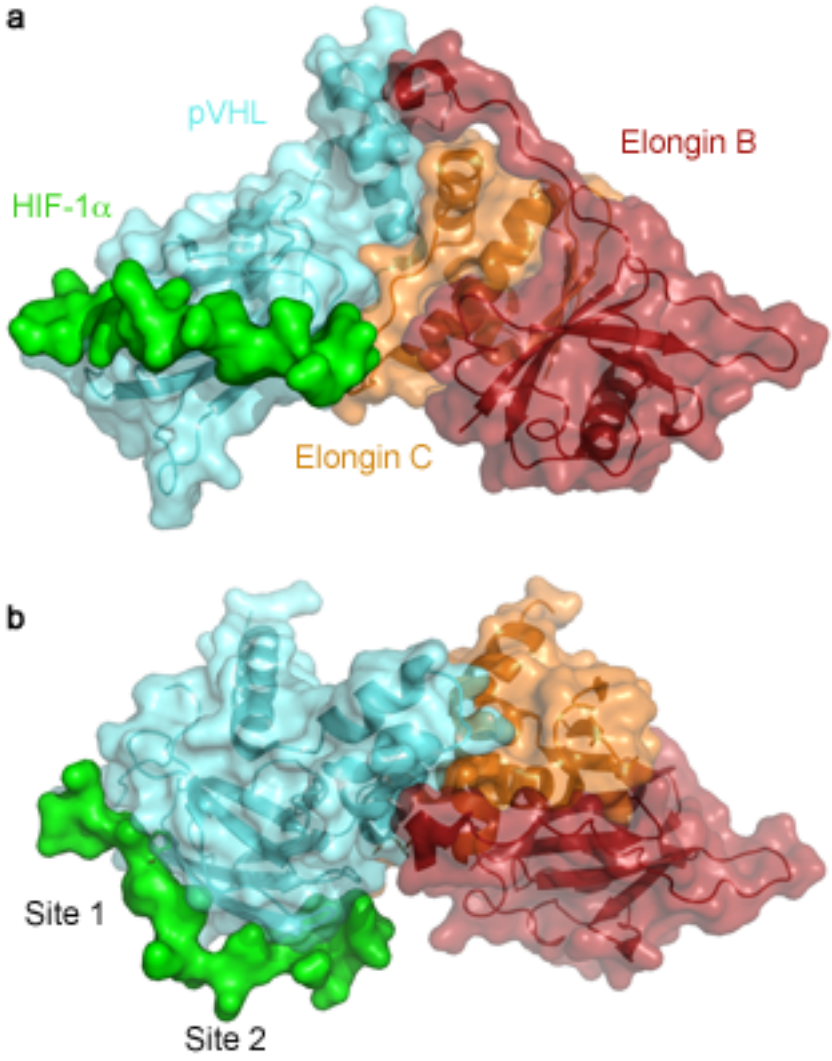

Figure 3.3 (a) Crystal structure of the VCB-COOD complex. The pVHL (blue) complexed to both elonging B (red) and elonging C (orange) with accompanying hydroxylated HIFα or carboxy-terminal oxygen-dependent degradation motif (COOD). Site 1 possesses the primary binding site where the hydroxyl modification to P564 binds to the pVHL's Hyp-binding pocket through an extensive hydrogen-bonding network mediated by water; whereas site 2 only interacts with one residue negating any sequence specificity and thus is omitted from the PROTAC sequence.

chemical synthesis of **4a** was completed upon ligation of raltitrexed to the C-terminus of **3a**. It's important to note, that no regioselectivity was conferred through the HOBt/HBTU coupling and thus both regioisomers are present. HPLC purification yielded **4a** (PROTAC-1) with a 78% recovery from **1** in 76% purity. Control peptides **2** and **3a** were synthesized in parallel to serve as *in vitro* controls (Figure 3.2). It was reasoned that triglycine-bridge may attract proteolytic digestion or may confer excessive structural rigidity that would prevent substrate identification, thus an alternative to the linker in **3a** was examined. Substituting for the triglycine linker, a flexible protease-resistant two-residue polyethylene glycol-FMOC (PEG) chain was coupled to **2** to give **3b** followed by direct coupling to RTX (**4b**, PROTAC-2).

3.1.2 PROTAC-1 in vitro Challenge

To demonstrate the inhibitory effects of PROTAC-1 we monitored TS expressing CHL^{-TS} pJZ205 and overexpressing CHL^{-TS} pJZ205/200 cell lines over a 4-day time course. PROTAC-1 had a moderate inhibitory effect, when compared to free RTX (IC_{50} 0.002 μM), on CHL^{-TS} pJZ205 cells, producing an IC_{50} of 0.20 μM (Figure 3.4). The TS-overexpressing cell line showed no effect upon administration of PROTAC-1, confirming the overabundance of TS had muted any growth inhibition or potential degradation.

To substantiate that growth inhibition was due to the presence of the PROTAC-1, both growth assays were repeated with a thymidine rescue added. It's reasoned that supplying the cell with free thymidine can reverse any deleterious pharmacological action upon TS, thus preventing a thymineless death. Under the auspice of a thymidine rescue, both cell lines remained resistant to the pharmacological effect of PROTAC-1,

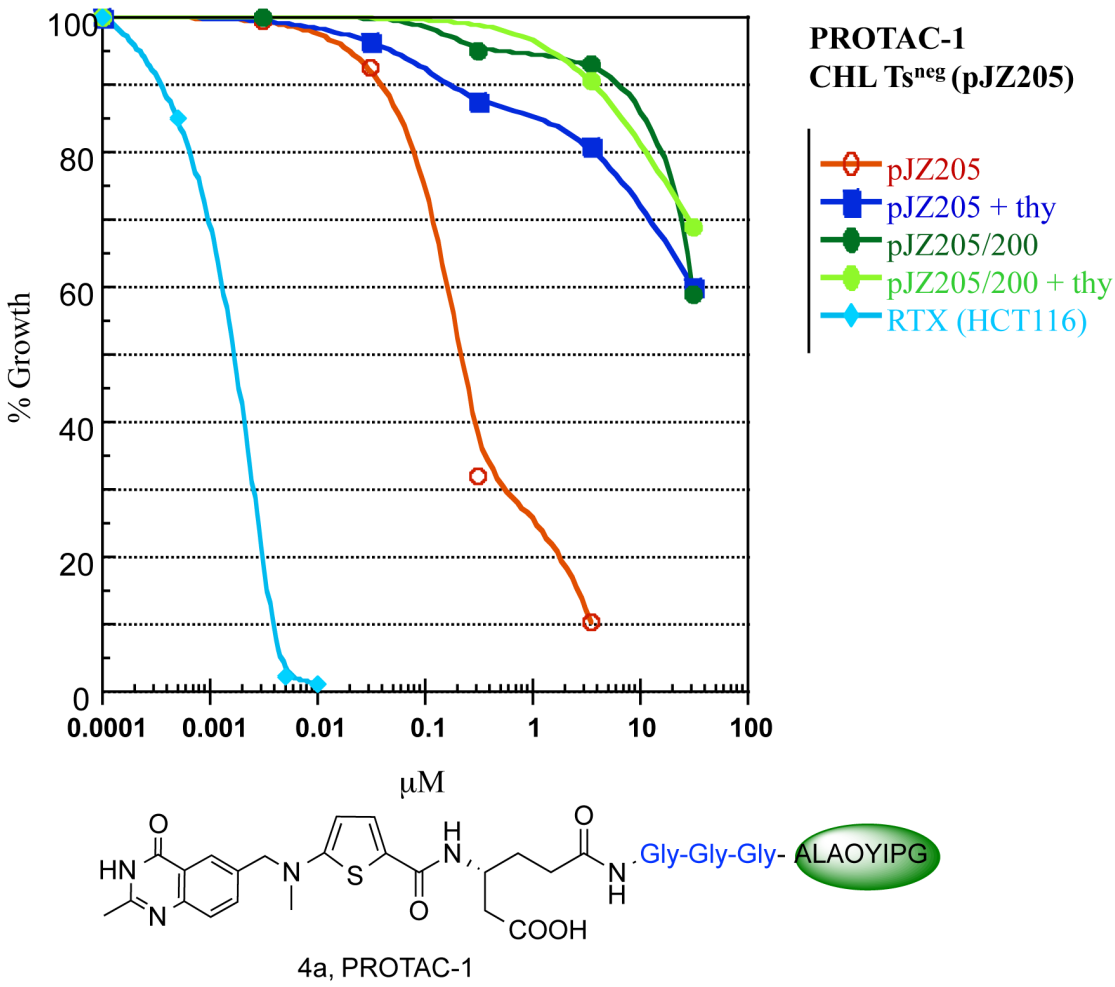

Figure 3.4 The IC_{50} performance of PROTAC-1 in CHL^{-TS} pJZ205 (red) and pJZ205/200 TS overexpressing cell lines (dark green) with concomitant thymidine rescues (blue and light green, respectively) as compared to free raltitrexed (light blue, IC_{50} = 0.002 μM).

confirming the inhibition is the result of the interaction between TS and PROTAC-1 (Figure 3.4). Although the rescue corroborated PROTAC-1's actions upon TS, it was still unknown if the effects were mediated through ubiquitin-depended proteasomal degradation or alternate mechanisms of cell death.[31]

3.1.3 PROTAC-1 Ubiquitin Analysis

To determine the extent of PROTAC-1's relationship with the VHL ligase, and thus the Ubiquitin Proteasomal System (UPS), TS expressing CHL^{-TS} pJZ205 cells were exposed to 1x and 10x the IC_{50} of PROTAC-1 in the presence of the proteasomal inhibitor, MG132 (Figure 3.5). In an effort to qualitatively assess the potential degradation of TS, RTX was used to act as a control due to its inherent ability to stabilize the TS complex (RTX•dUMP•TS), thus increasing TS intracellular concentration. Hence, cells were similarly exposed to 1× and 10× the IC_{50} of RTX (0.002 μM). Diminishing signal from TS was not observed in the western analysis under either concentration analyzed for PROTAC-1 (Figure 3.5A). Rather, each PROTAC-1 TS band closely paired with its RTX cognate both with and without M132 exposure.

Given the potential stabilizing effect of RTX, we next took measures to investigate whether the inhibitor effect of PROTAC-1 was attenuated due to poor VHL recognition and the UPS machinery was only capable of moderate signal suppression. The lysates were analyzed again under the preceding conditions, but probed for signals of UPS directed degradation of TS (Figure 3.5B). Under conditions free from MG132, no signal of TS degradation was apparent. Methods to extend the exposure time of the film failed to yield any qualitative evidence of PROTAC-1 facilitating the ubiquitination of

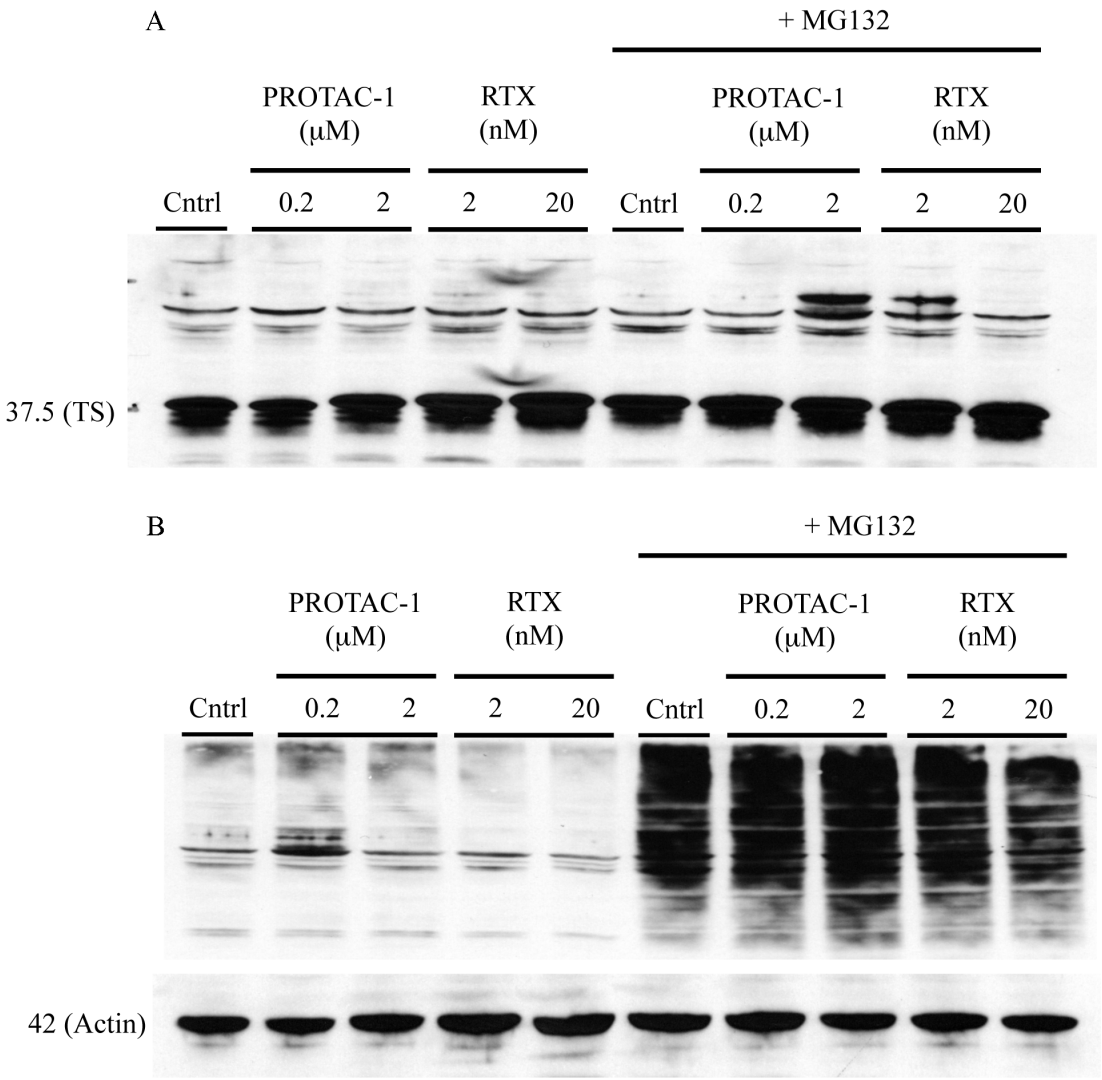

Figure 3.5 Western blot analyses of 1× and 10× PROTAC-1 cell lysates from CHL^{-TS} PJZ205 cells under MG132 inhibitor. (A) Only non-specific bands above TS (RTX-dUMP-TS) were noted with no indication of ubiquitin-promoted proteolysis in the presence of the proteasomal inhibitor MG132. (B) Lysates were analyzed again, but with ubiquitin specific antibody. No evidence of TS ubiquitination was realized.

TS. Because each signal in the western analysis closely resembled the stabilizing features of RTX, we sought to determine if RTX had been excised and was therefore free to bind TS. Intracellular stability of PROTAC-1 conjugates **2** and **3a** were analyzed in CHL^{-TS} pJZ205 cells to determine their potential effect upon TS inhibition (Figure 3.6). While PROTAC-1 reproduced its IC_{50} potential, no effects were observed for either conjugate **2** or **3a,** suggesting that the stabilization effect is due to RTX bound to TS. However, no evidence in the literature could be located regarding the expression levels of the VHL ligase in CHL^{-TS} pJZ205 cell lines. To alleviate these concerns, an identical Western blot analysis was repeated in the human colon cancer cell line HCT116. As with the first experiment in figure 3.5A, no discernable evidence of TS degradation was present (Figure 3.7).

Finally, we questioned whether PROTAC-1 was acting in accord of the pharmacokinetic action of RTX or inducing attenuated levels of degradation in an ubiquitin independent manner. To evaluate this concern, we measured the half-life of both RTX and PROTAC-1 over a 24 hr period in HCT116 cells. The dosimetry analysis for the half-life analyses concluded that PROTAC-1 exhibits a stabilizing effect up on TS, rendering the conjugate a less potent form of its free-from drug.

To this end, we explored the possibility that the tri-glycine linker was too rigid and performed a subsequent times course study on PROTAC-2 (Figure 3.8). Curiously, PROTAC-2 produced a 500-fold increase (> 100 μM IC_{50}) in stabilization in both CHL^{-TS} pJZ205 and overexpressing CHL^{-TS} pJZ205/200 cell lines compared to its counterpart, PROTAC-1 (IC_{50} = 0.20 μM). These results indicated that PROTAC-2 is ineffective due to the PEG linker. It's likely that its inherent flexibility and restricted atomic length

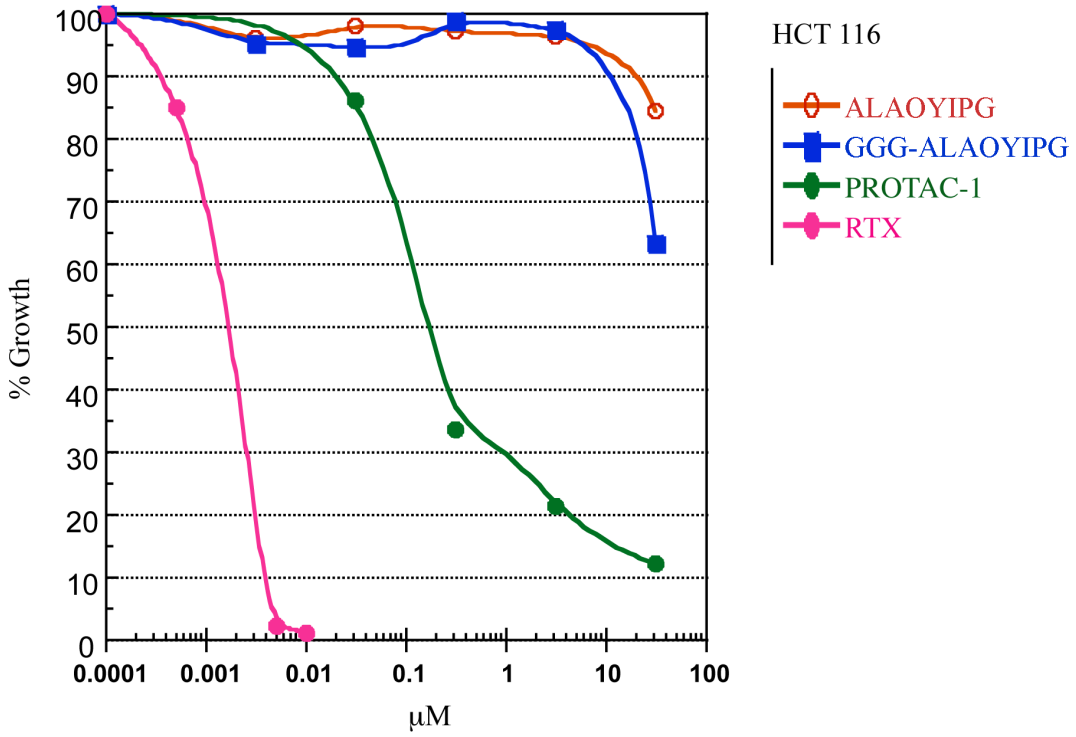

Figure 3.6 Representative plot for the IC_{50} of the HIFα peptide (red), HIFα with glycine linker (blue), and PROTAC-1 (green) versus free raltitrexed (pink, IC_{50} = 0.002 μM in HCT-116 cells. The lack of inhibitory potential of either the HIFα or HIFα-GGG peptide demonstrates the necessity of RTX in order to target TS and induce growth inhibition.

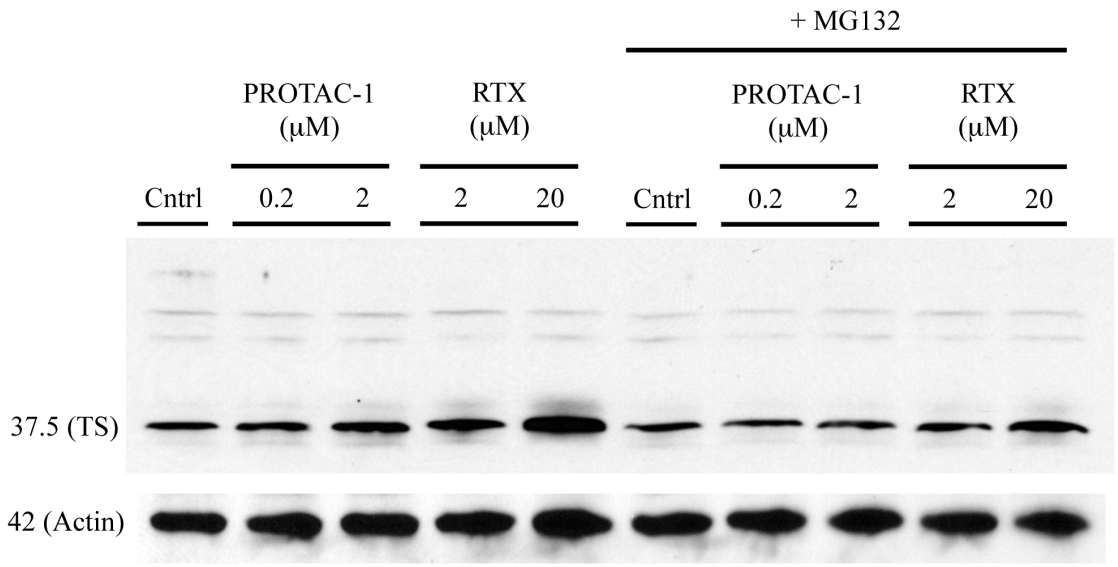

Figure 3.7 Western blot analyses of 1× and 20× PROTAC-1 IC_{50} concentration in HCT116 cells under MG132 inhibitor. No evidence of PROTAC-1 induced degradation of TS is apparent. All bands report RTX stabilized TS complexes.

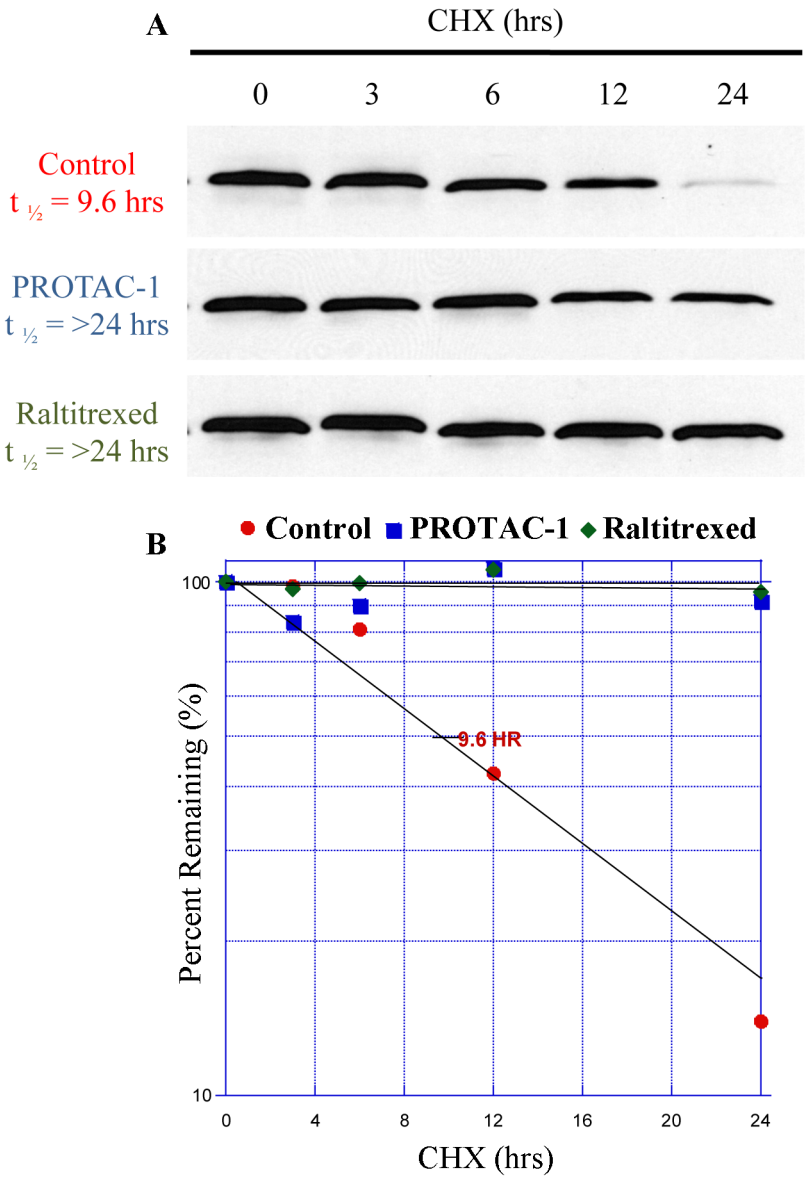

Figure 3.8 Half-life analysis of PROTAC-1 in HCT116 during 24-hour exposure to cyclohexamide. (A) Western blot analysis of control cells (red) yielded within the range of wtTS half-life (9.6 hrs) while PROTAC-1 (blue) mirrored the stabilizing effect of free raltitrexed (green). (B) Graphical representation of Western blot demonstrating the stabilization effect of PROTAC-1.

disrupts the conformational entropy required for proper ligand-active site docking. Provided that others have been unable to show TS in an ubiquitinated state, the assertion that TS follows an ubiquitin-independent proteasomal degradation pathway, stands.[32]

3.2 EXPERIMENTAL

3.2.1 General Procedure for Solid Phase Peptide Synthesis of PROTAC-1

To a 20 mL reactor cartridge was added ***Wang-Gly-Fmoc*** resin (330 mg, 0.20 mmol) followed by solvation in DMF. A fresh solution of 20% piperidine in DMF was added to the reactor and agitated for 30 min. The resin was then filtered and washed with DMF (3 × 5 mL) and filtered again. The following is the general procedure for each Fmoc-amino acid coupling: The resin was washed (3 × 5 mL) in DMF and filtered. To separate 50 mL flask was added ***Fmoc-amino acid*** (4 eq, 2.4 mmol), HBTU (2.9 eq, 1.74 mmol), NMM (4 eq, 2.4 mmol).

The reagents were dissolved in 10 mL of DMF, transferred tot he reaction cartridge and agitated for 45 min. A Kaiser test was administered to determine reaction completion.[29] The resin was washed (3 × 5 mL) in DMF and filtered. The resin was deprotected in 20% piperidine in DMF and agitated for 45 min after which a second Kaiser test was performed. The residues were added in the following order: Fmoc-Proline (×2), Fmoc-Isolucine, Fmoc-Tyrosine, Fmoc-Hydroxyproline (×2), Fmoc-Alanine, Fmoc-Leucine, Fmoc-Alanine for **2**, Fmoc-Glycine (3×) for **3a**.

For the synthesis of **4a** in 10 mL flask raltitrexed (2 eq, 0.215 mmol), HBTU (2.9 eq, 1.74 mmol), NMM (4 eq, 2.4 mmol) was dissolved in 7 mL of DMF. Reagents were transferred to each reaction cartridge with resin-bound deprotected **3a** and **3b** and

agitated for 60 min. The resin was washed (3 × 5 mL) in DMF, (3 × 5 mL) DCM, and (3 × 5 mL) in MeOH, filtered, and dried. Peptides **2**, **3a**, and **4a** were liberated from the resin under 9 mL of 95% TFA in H_2O for 2 hrs. The resins were drained and the eluent was collected. The resins were washed again in 9 mL of 95% TFA and pooled. Each was subsequently dried under N_2 until a yellow or white film appeared. To each was added ice-cold diethyl ether to form a precipitate. The precipitate was centrifuged at 9,000 RPMs at 4° C for 15 min. The clear eluent was decanted the remaining material was lyophilized overnight to yield the crude forms of **2** (26.3 mg, 35.3 μmol) **3a**, (41.7 mg, 42.2 μmol), **4a** (26.5 mg, 18.5 μmol).

All crude peptides were identified and purified by HPLC using a 250 × 10-mm, 5 μm RP C_{18} column at 5 mL min^{-1} from 10-65% ACN in 0.1% TFA for 65 min. Injections of 1.2 mL were monitored at 215, 276, and 304 nm. Fractions were pooled, concentrated, and lyophilized. Purified products were characterized using ESI LCMS over 150 × 2.0-mm, 3 μm RPC_{18} over 10-65% ACN (0.1% formic acid) gradient in 45 min. Products **2**, **3a**, and **4** were identified at $[M+H]^+$ 818, $[M+H]^+$ 988.7, and $[M+H]^+$ 1428.5, respectively.

3.2.2 General Procedure for Solid Phase Peptide Synthesis of PROTAC-2

To a 20 mL reactor cartridge was added ***Wang-Gly-Fmoc*** resin (166 mg, 0.10 mmol) followed by solvation in DMF. A fresh solution of 20% piperidine in DMF was added to the reactor and agitated for 30 min. The resin was then filtered and washed with DMF (3 × 5 mL) and filtered again. The following is the general procedure for each Fmoc-amino acid coupling: The resin was washed (3 × 5 mL) in DMF and filtered. To

separate 50 mL flask was added ***Fmoc-amino acid*** (2.9 eq, 0.29 mmol), HBTU (2.9 eq, 0.29 mmol), NMM (4 eq, 0.4 mmol). The reagents were dissolved in 10 mL of DMF, transferred tot he reaction cartridge and agitated for 45 min. A Kaiser test was administered to determine reaction completion.[29] The resin was washed (3 × 5 mL) in DMF and filtered. The resin was deprotected in 20% piperidine in DMF and agitated for 45 min after which a second Kaiser test was performed. The residues were added in the following order: Fmoc-Proline (×2), Fmoc-Isolucine, Fmoc-Tyrosine, Fmoc-Hydroxyproline (×2), Fmoc-Alanine, Fmoc-Leucine, Fmoc-Alanine for, Fmoc-AEEA (×2) for **3b**. The resin was deprotected in 20% piperidine in DMF and agitated for 45 min after which it was washed in DMF (3 × 5 mL), DCM (3 × 5 mL) and stored at 4 °C.

For the synthesis of **4b** in 10 mL flask RTX (46.5 mg, 0.101 mmol) was dissolved in 5 mL of DMF. To 45 mL of DCM in a 250 mL round bottom flask the 5 mL solution of RTX was added and jacketed over argon. The reaction mixture was cooled on ice for 10 minutes and bubbled with nitrogen. In 6 mL of DCM, DCC (21.1 mg, 0.102 mmol) was dissolved and added drop wise to the reaction over 30 min. The reaction incubated for 80 min at 4-10 °C under argon and then was brought to -40 °C on dry ice and acetonitrile. In 2 mL of DCM, DMAP (12.3 mg, 0.100 mmol) was dissolved and added to the reaction in four 500 μL aliquots. The resin bound **3b** was added in 3 mL of DCM and maintained at -40 °C for three hours and then allowed to reach room temp over night.

Resin bound **4b** was transferred to a reaction cartridge and washed in DCM (3 × 5 mL), filtered, and dried. Peptide conjugate **4b** were liberated from the resin under 10 mL of TFA for 2 hrs. The resin was drained and the eluent was collected. The resin was washed again in 10 mL of TFA and pooled and dried under N_2 until a yellow film

appeared. To the flask was added ice-cold diethyl ether to form a precipitate. The precipitate was centrifuged at 9,000 RPMs at 4 °C for 10 min. The clear eluent was decanted the remaining material was lyophilized overnight to yield the crude forms of **4b** (8.9 mg, 6.3 μmol). The **4b** crude was identified purified by HPLC using a 250 × 10-mm, 5 μm RP C_{18} column at 5 mL min^{-1} from 10-65% ACN in 0.1% TFA for 65 min. Injections of 1.2 mL were monitored at 269 and 341 nm. Fractions were pooled, concentrated, and lyophilized. Purified products were characterized using ESI LCMS over 150 × 2.0-mm, 3μM RPC_{18} over 10-65% ACN (0.1% formic acid) gradient in 45 min. Purified product **4b** (7.7 mg, 86.5%) was identified at $[M+H]^+$ 1402.7 m/z.

3.2.3 General Cell Preparation

All cells were provided by Dr. Franklin G. Berger (University of South Carolina, Department of Biological Sciences). All cells were grown in a T75 flask under 10% fetal bovine serum (FBS) in high glucose Dulbecco's Modified Eagle's medium (DMEM) with 100 U of penicillin-streptomycin (Pen-Strep) at 37 °C and humidified at 5% CO_2. Cell line RJK33.13, a TS-deficient derivative of V79 chinese hamster lung cells (CHL^{-TS} pJZ205, CHL^{-TS} pJZ205/200) were grown to confluency and passaged at either 1:10 or 1:20 with 0.25% trypsin.[33]

3.2.4 Growth Inhibition Studies for PROTAC-1 and PROTAC-2

To determine the growth inhibition response of compounds **2**, **3a**, **4a**, and **4b**, 500,000 cells/well of CHL^{-TS} pJZ205 and CHL^{-TS} pJZ205/200 were each plated in four 6

well plates and allowed to adhere over 4 hours before drug treatment with ranging concentrations of each compound were added in duplicate fashion. After five days, the number of surviving cells was counted with a hemocytometer after counter staining with Tyrpan Blue and the IC_{50} determined. The inhibition of the PROTAC conjugates was generously performed by Karen Barbour (University of South Carolina, Department of Biological Sciences).

3.2.5 Ubiqutination Analysis for PROTAC-1 in CHL^{-TS} pJZ205 and HCT116 Cells

Cells were plated in 100 mm dishes with 2×10^6 cells per plate. Cells analyzed for ubiquitinated products were pretreated with 25 mM MG132 4 hours before RTX and PROTAC-1 inoculation. Cells were then inoculated with 0.002 and 0.02 μM RTX with 0.2 and 2.0 μM of **4a**, to plates both with and without MG132, respectively. Cells were harvested with a rubber policeman and lysed with M-PER (ThermoFisher) and treated with 5 mM PMSF, 200 μg mL^{-1}, aprotinin, 100 μg mL^{-1} pepstatin, and 50 μg mL^{-1} leupeptin according to manufactures instructions. Crude lysates were centrifuged at 13,000 RPM for 15 min at 4 °C. The extracts were quantified using the Bio-Rad assay reagent with BSA standard.

Western analysis was performed under standard techniques. The blot was probed for TS and ubiquitin using a monoclonal antibodies provided by Dr. Franklin G. Berger (University of Southern Carolina, Department of Biological Sciences). Equal loading of the lysates was monitored by re-probing the nitrocellulose blots with an anti-actin monoclonal antibody (Sigma-Aldrich, Clone AC-40). For detection of TS the blots were visualized using the appropriate species dependent HRP-antibody with the ECL

chemiluminescence kit from Amersham Biosciences. All blots were run with exposure controls to correct for film exposure and normalized to actin via densiometric analysis using ImageJ software.

3.2.6 TS Half-Life Studies for PROTAC-1

The half-life of TS in HCT116 cells under exposure to 2 μM of **4b** and 0.2 μM RTX was assessed according to the protocol previously reported.[32]

3.3 REFERENCES

1. Cho, H.S. et al. Structure of the extracellular region of HER2 alone and in complex with the Herceptin Fab. *Nature* **421**, 756-760 (2003).
2. Baselga, J., Norton, L., Albanell, J., Kim, Y.M. & Mendelsohn, J. Recombinant humanized anti-HER2 antibody (Herceptin (TM)) enhances the antitumor activity of paclitaxel and doxorubicin against HER2/neu overexpressing human breast cancer xenografts. *Cancer Res.* **58**, 2825-2831 (1998).
3. Capdeville, R., Buchdunger, E., Zimmermann, J. & Matter, A. Glivec (ST1571, Imatinib), a rationally developed, targeted anticancer drug. *Nat. Rev. Drug Discov.* **1**, 493-502 (2002).
4. Wells, J.A. & McClendon, C.L. Reaching for high-hanging fruit in drug discovery at protein-protein interfaces. *Nature* **450**, 1001-1009 (2007).
5. Yin, H. & Hamilton, A.D. Strategies for targeting protein-protein interactions with synthetic agents. *Angew. Chem.-Int. Edit.* **44**, 4130-4163 (2005).

6. Schneekloth, J.S. et al. Chemical genetic control of protein levels: Selective in vivo targeted degradation. *J. Am. Chem. Soc.* **126**, 3748-3754 (2004).

7. Corson, T.W., Aberle, N. & Crews, C.M. Design and Applications of Bifunctional Small Molecules: Why Two Heads Are Better Than One. *ACS Chem. Biol.* **3**, 677-692 (2008).

8. Sakamoto, K.M. et al. Protacs: Chimeric molecules that target proteins to the Skp1-Cullin-F box complex for ubiquitination and degradation. *Proc. Natl. Acad. Sci. U. S. A.* **98**, 8554-8559 (2001).

9. Cockman, M.E. et al. Hypoxia inducible factor-alpha binding and ubiquitylation by the von Hippel-Lindau tumor suppressor protein. *J. Biol. Chem.* **275**, 25733-25741 (2000).

10. Buckley, D.L. et al. Targeting the von Hippel-Lindau E3 Ubiquitin Ligase Using Small Molecules To Disrupt the VHL/HIF-1 alpha Interaction. *J. Am. Chem. Soc.* **134**, 4465-4468 (2012).

11. Pray, T.R. et al. Cell cycle regulatory E3 ubiquitin ligases as anticancer targets. *Drug Resist. Update* **5**, 249-258 (2002).

12. Jia, L. & Sun, Y. SCF E3 Ubiquitin Ligases as Anticancer Targets. *Curr. Cancer Drug Targets* **11**, 347-356 (2011).

13. Puppala, D., Lee, H., Kim, K.B. & Swanson, H.I. Development of an aryl hydrocarbon receptor antagonist using the proteolysis-targeting chimeric molecules approach: A potential tool for chemoprevention. *Mol. Pharmacol.* **73**, 1064-1071 (2008).

14. Rodriguez-Gonzalez, A. et al. Targeting steroid hormone receptors for ubiquitination and degradation in breast and prostate cancer. *Oncogene* **27**, 7201-7211 (2008).

15. Kaelin, W.G. The von Hippel-Lindau tumour suppressor protein: O-2 sensing and cancer. *Nat. Rev. Cancer* **8**, 865-873 (2008).

16. Kamura, T. et al. Rbx1, a component of the VHL tumor suppressor complex and SCF ubiquitin ligase. *Science* **284**, 657-661 (1999).

17. Ivan, M. et al. HIF alpha targeted for VHL-mediated destruction by proline hydroxylation: Implications for O-2 sensing. *Science* **292**, 464-468 (2001).

18. Hon, W.C. et al. Structural basis for the recognition of hydroxyproline in alpha IF-1 alpha by pVHL. *Nature* **417**, 975-978 (2002).

19. Willam, C. et al. Peptide blockade of HIF alpha degradation modulates cellular metabolism and angiogenesis. *Proc. Natl. Acad. Sci. U. S. A.* **99**, 10423-10428 (2002).

20. Jarmula, A. Antifolate Inhibitors of Thymidylate Synthase as Anticancer Drugs. *Mini-Rev. Med. Chem.* **10**, 1211-1222 (2010).

21. Bavetsias, V. et al. Design and synthesis of cyclopenta g quinazoline-based antifolates as inhibitors of thymidylate synthase and potential antitumor agents. *J. Med. Chem.* **43**, 1910-1926 (2000).

22. Wang, L. et al. Synthesis and Biological Activity of 6-Substituted Pyrrolo 2,3-d pyrimidine Thienoyl Regioisomers as Inhibitors of de Novo Purine Biosynthesis with Selectivity for Cellular Uptake by High Affinity Folate Receptors and the

Proton-Coupled Folate Transporter over the Reduced Folate Carrier. *J. Med. Chem.* **55**, 1758-1770 (2012).

23. Bavetsias, V. et al. Quinazoline antifolate thymidylate synthase inhibitors: gamma-Linked L-D, D-D, and D-L dipeptide analogues of 2-desamino-2-methyl-N-10-propargyl-5,8-dideazafolic acid (ICI 198583). *J. Med. Chem.* **39**, 73-85 (1996).

24. Bavetsias, V., Bisset, G.M.F., Kimbell, R., Boyle, F.T. & Jackman, A.L. Synthesis of novel quinazoline-based antifolates with modified glutamate side chains as potential inhibitors of thymidylate synthase and antitumour agents. *Tetrahedron* **53**, 13383-13396 (1997).

25. Forsch, R., Bader, H. & Rosowsky, A. Synthesis of L-2-(N-pteroylamino)-3-(N-phosphonoacetyl)amino-propanoic acid as an analogue of the putative phosphorylated intermediate in the gamma-glutamation of folic acid by folylpolyglutamate synthetase. *Pteridines* **10**, 39-46 (1999).

26. Epstein, A.C.R. et al. C-elegans EGL-9 and mammalian homologs define a family of dioxygenases that regulate HIF by prolyl hydroxylation. *Cell* **107**, 43-54 (2001).

27. Wellings, D.A. & Atherton, E. in Solid-Phase Peptide Synthesis, Vol. 289. (ed. G.B. Fields) 44-67 (Elsevier Academic Press Inc, San Diego; 1997).

28. Konig, W. & Geiger, R. Racemization in Peptide Synthesese. *Chem. Ber.-Recl.* **103**, 2024-2024 (1970).

29. Kaiser, E., Colescot.Rl, Bossinge.Cd & Cook, P.I. Color Test For Detection of Free Terminal Amino Groups in Solid-Phase Synthesis of Peptides. *Anal. Biochem.* **34**, 595-595 (1970).

30. Coin, I., Beyermann, M. & Bienert, M. Solid-phase peptide synthesis: from standard procedures to the synthesis of difficult sequences. *Nat. Protoc.* **2**, 3247-3256 (2007).

31. Barbour, K.W. & Berger, F.G. Cell death in response to antimetabolites directed at thymidylate synthase. *Cancer Chemother. Pharmacol.* **61**, 189-201 (2008).

32. Pena, M.M.O., Xing, Y.Y., Koli, S. & Berger, F.G. Role of N-terminal residues in the ubiquitin-independent degradation of human thymidylate synthase. *Biochem. J.* **394**, 355-363 (2006).

33. Nussbaum, R.L., Walmsley, R.M., Lesko, J.G., Airhart, S.D. & Ledbetter, D.H. Thymidylate Synthase-Deficient Chinese-Hamster Cells - A Selection System for Human-Cbromosome 18 and Experimental System for the Study of Thymidilate Synthase Regulation and Fragile-X Expression. *Am. J. Hum. Genet.* **37**, 1192-1205 (1985).

CHAPTER 4

COMBINATORIAL DEVELOPMENT OF HYDROPHOBIC-TAGGED RALTIREXED

4.0 INTRODUCTION

The traditional routes of probing or modulating protein function have directed their scope toward alterations at the transcriptional level to engineer or solicit a desired phenotype. Within this subtext are chemical modifiers that induce or suppress gene expression either at the level of transcription, translation, or through post-translational control. These levels of control afford a strict regulation over the dynamic processes that modulate the invoked protein phenotype. Through RNAi mediated tools, the conditional knockdown of specific protein phenotypes has emerged as popular and highly desirable approach for manipulating post-translational events and their resultant gene products. However, RNAi still cannot afford the spatial-temporal control necessary to achieve a post-translational effect capable of delivering a sustained degradation response. Thus, to meet this precise and defined metric, many small molecules have been tailored to selectively delineate protein function in order to exert a degradation effect, as opposed to inhibitory, upon their substrates. Selective estrogen-receptor modulators (SERDS) such as fulvestrant, is a pure agonist that promotes the nuclear degradation of the estrogen receptor (Er) via proteasomal proteolysis. When co-administered with the proteasomal

inhibitor bortezomib aggregation of nascent cytosolic Er is promoted activating the pro-apoptotic mechanism of the UPR.[1] Mediated by a series of chaperone complexes, similar drug-induced ubiquitination-degradation was observed when the tyrosine kinase inhibitor CI-1033 irreversibly alkylates a cysteine specific to the ErbB2/Her2 receptor.[2] These examples bring specificity to their targets and mediate a global intracellular response significant enough to induct the UPS pathway through nonnative signaling. While they demonstrate the therapeutic potential of induced protein degradation, their utility is narrowed to the intrinsic nature of inhibitors rather than the synergistic exploitation of the UPS pathway. With the utility of the UPS pathway, a robust system that actively promotes the ablation of target proteins in an adaptable chemical-induced manner has yet to emerge.

Several approaches to formulate a proteolytic-inducing small molecule system have shown promise. Crews and co-workers have developed a heterobifunctional small molecule capable of inducing proteasomal mediated protein degradation of multiple proteins of various cellular locations and capabilities. This PROTAC (PROteolysis TArgeting Chimera) only requires a targeting motif, rather than possessing any inhibitory action, and a ligand for and E3-ligase separated by a chemically inert linker. The PROTAC can then form a ternary complex joined by both the ligand specific POI and the E3-ligase. Thus, the multi-protein E3-ligase ubiquitin-promoting complex can actively sort and identify foreign substrates for ubiquitination and subsequent proteolysis. This adaptable system has been used to target and degrade the androgen and estrogen receptors, peptidase MetAP-2, the immune-regulator FKBP12, and the aryl hydrocarbon receptor using various E3-ligase specific ligands.[3-7]

Recently, a stimuli-responsive PROTAC was developed, where in response to mitogenic signaling, RTK dimerize and initiate a series of transautophosphyorylation events through their tyrosine residues within their intracellular domain. This event recruits a series of substrates that posses PTP and SH2 domains. This phosphoPROTAC (phosphate PROteolysis TArgeting Chimera) was designed to posses the phosphorylated tyrosine signaling domain from the NGF receptor, TrkA, and a VHL-binding sequence. The inactive phosphoPROTAC is phosphorylated by the RTK in response to mitogen activation. Once the phosphoPROTAC is activated it generates a binding site for the SH2 or PTB-domain-containing effector protein of fibroblast growth factor receptor substrate 2α (FRS2α) and is subsequently polyubiquinated and transported to the proteasome for proteolysis. Upon treatment of NGF-stimulated PC12 cells the authors observed roughly a 90% knockdown of the effector/substrate FRS2α.

Encouraged by these results, the authors fabricated another phosooPROTAC capable of targeting the PI3K receptor using a peptidic sequence from the ErbB2 receptor, which is phosphorylated by ErbB3 in response to neuregulin.[8] This model produced dose-depended toxicity in MCF-7 cells and was successfully applied in a mouse xenograft model yielding a 40% reduction in tumor volume.[8] Although these and the aforementioned PROTACS have proven to be effective modulators of protein degradation, they rely on the capability of the E2-ligase to transfer Ub to the POI. In the case where the ε-amino group is blocked or inactivated by surrounding residues, the E2 ligase is incapable of Ub-conjugation.

A rapid and highly tunable method regulate intracellular concentrations of a specific protein involves the expression of fusion proteins coupled to an unstable degron-

domain. With in the cell, the degron domain that remains unstable transfers this instability to its fusion partner. Upon exposure to a degron specific ligand, the domain is rescued and thus stabilized, whereas the absence of ligand facilitates its proteolysis.[9, 10] Although functionally useful, this system necessitates genetic intervention to supply protein degradation. In the past few years a novel application toward the development of direct ligand-mediated protein degradation has been introduced. Taking advantage of the general stabilizing factors that govern protein folding and internal cohesion, some groups have used various hydrophobic moieties conjugated to known potent inhibitors to pull down endogenous proteins.[11,12]

Interestingly, Hedstrom and co-workers have constructed a system that is capable of Ub-indpendent degradation by affixing a hydrophobic Boc_3Arg group to the covalent (EA, ethacrynic acid) and non-covalent (TMP, trimethoprim) inhibitors of glutathione S-transferase (GST) and *E. coli* dihydrofolatereductase (eDHFR), respectively. By mimicking an unfolded protein, through hydrophobic exposure, both EA and EA-Boc_3Arg inactivate GST. However, EA-Boc_3Arg yielded a degradation effect, degrading roughly 80% of GST in whole cells, whereas TMP-Boc_3Arg only achieved a 30% knockdown.[11] The adaptable and tunable approach of mimicking hydrophobic exposure as a means of translational control has also been shown using fusion constructs, which possess a high affinity for a hydrophobic-tagged ligand (Figure 4.1).[12] Under the auspice of the work performed by Hedstrom and co-workers, we sought to apply hydrophobic-tagging against human thymidylate synthase (TS), a high value cancer target. In colorectal cancer (CRC), TS is overexpressed in the crypt cells of the gut where this *de novo* source of deoxythymidine monophosphate (dTMP) maintains large pools of

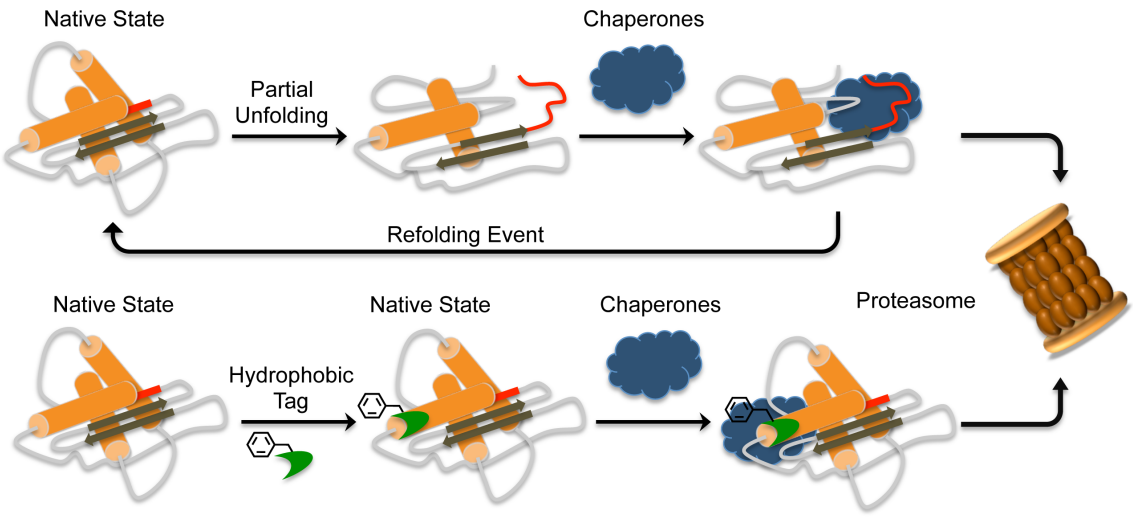

Figure 4.1 General schematic for the hydrophobic tagging of stable proteins.

dTMP for DNA replication. This action has subsequently shown to yield routes of resistance to TS specific inhibitors in established cell lines making it difficult to manipulate its intracellular levels.[13]

We previously established the insensitivity of TS against an RTX based PROTAC, which failed to demonstrate ubiquitination. Thus, investigating the potential of hydrophobic exposure through TS directed hydrophobically tagged ligand provided the means to avoid any dependency on either the conjugation or ligation enzymes of UPS. By working from a known TS inhibitor, raltitrexed, we synthesized a small array of hydrophobically diversified chemical tags to screen for potential RTX-based compounds that will recruit the cellular machinery responsible for identifying misfolded proteins and promote TS-proteasomal degradation.

4.1 Results and Discussion

4.1.1 Induction of Hydrophobic Exposure to TS Structure Inherent

In order to measure the response of TS to potential hydrophobic exposure, we induced two point mutations on the solvent exposed helices at residues R115 and D116 (Figure 4.2). Single point mutations for both positions with tryptophan and isoleucine destabilized TS and decreased its half-life by 30%. However, double point mutation R115W/D116W and R115I/D116I decreased the half-life of TS by 90%. This level of degradation indicated that TS is responsive to aberrant hydrophobic exposure, thus establishing possibility that a TS targeting ligand with the proper level of hydrophobic exposure may induce proteasomal degradation.

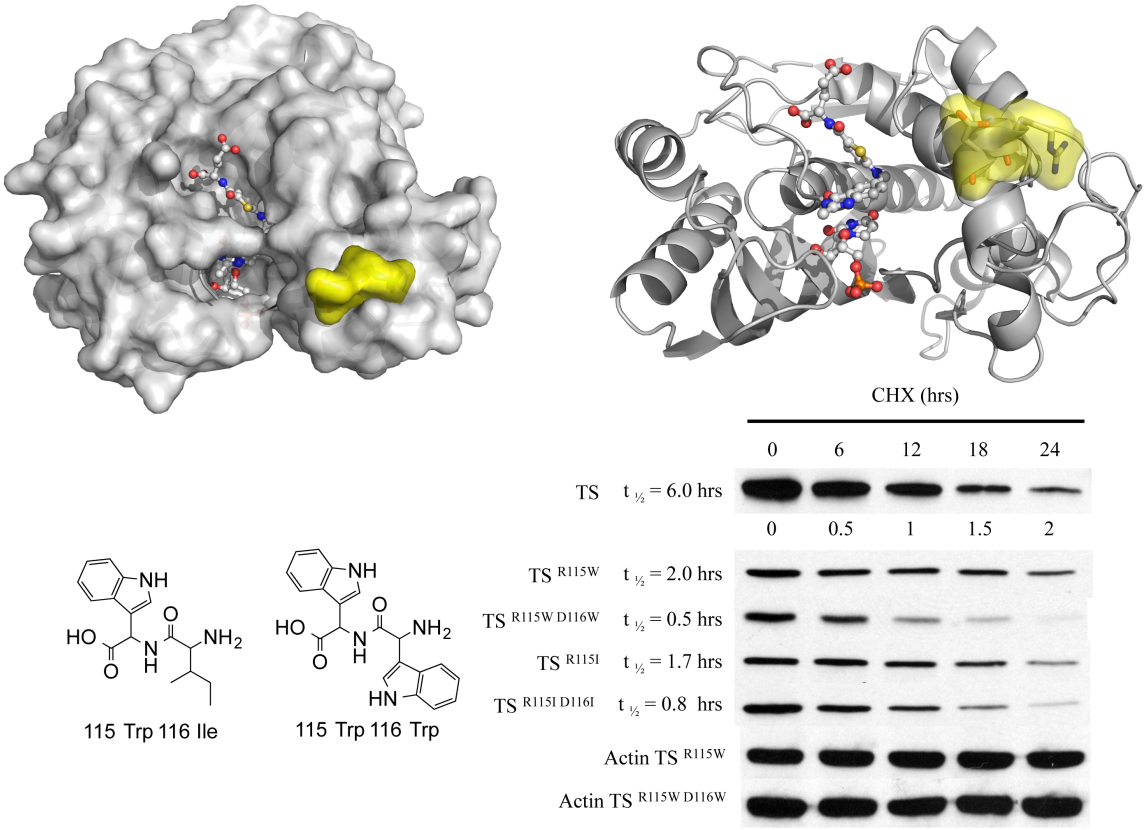

Figure 4.2 Induction of hydrophobic exposure by site directed mutagenesis of TS (PDB 1HYV). The solvent exposed residues Arg115 and Asp116 were substituted for the hydrophobic amino acids Trp and Ille (yellow) in both single and double point mutations. The double R115W/D116W mutant demonstrated a significant instability with a 12-fold decrease in half-life as compared to wtTS (6 hrs).

4.1.2 Raltitrexed Dipeptide Analysis

Quinazolinone based TS inhibitors rely on their poly-γ-glutamate metabolites for their increased intracellular residency and antitumor activity. It has been established that these metabolites are more potent inhibitors than their parent monoglutamate compounds. The addition of one glutamate residue on the γ-carboxyl of 2-desamino-2-methyl-N^{10}-propargyl-5,8-dideazafolic acid (ICI 198583) resulted in stronger binding to TS by approximately 30-fold.[14] For these reasons we were interested in the potential inhibitory effect of raltitrexed (RTX, ICI D1695) in a similar manner. The crystal structure of the RTX•dUMP•TS complex shows the γ-carboxylate of RTX (**1a**) is coordinated through the hydrogen-bond network of water, which resides on the exterior of the binding pocket. Based on this observation, we designed a small set of RTX-dipeptides that would represent the various classes of amino acids: acidic (**1b**, RTX-Glu), basic (**1c**, RTX-Arg), hydrophobic-sterically restrictive (**1d**, RTX-Tyr), and hydrophobic-sterically unrestrictive (**1e**, RTX-Gly). Each conjugate was prepared under standard Fmoc solid phase peptide synthesis (SPPS) and their respective regioisomers were purified by HPLC. Enantiomeric purity of the conjugates was not considered of vital importance provided that neither stereocenter in the dipeptide affects TS analog fidelity or inhibition, only serum stability is, in this regard, of vital importance to inhibitor stability.

To evaluate the potential inhibitory effects upon TS, incubation of each conjugate was performed over a 4-day time course in CHL^{-TS} pJZ205 cells (Figure 4.3). When compared to **1a**, we found that both **1b** and **1d** produced a significant modulation in the inhibitory signature of TS with a moderate 5.5 and 14-fold increase in IC_{50} (Figure 4.3A). Conversely, both hydrophobic residues were considerably less effective than their

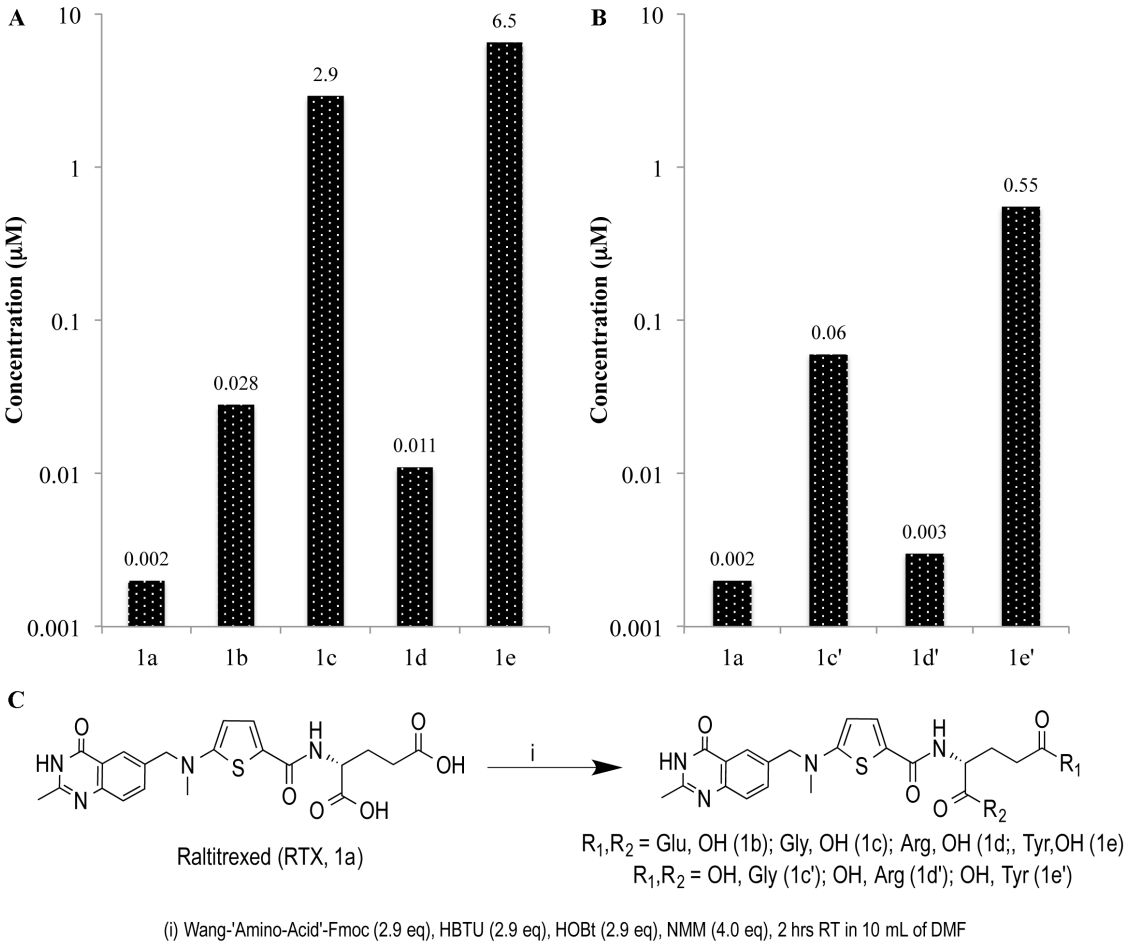

Figure 4.3 (A) The relationship between the inhibitory characteristics (IC_{50}) of free **1a** and the γ-linked dipeptide conjugates 1b-e. (B) The relationship between the inhibitory characteristics (IC_{50}) of free **1a** and the α-linked dipeptide conjugates 1c'-e'. (C) General scheme for the synthesis of each α/γ-conjugate of **1a**.

hydrophilic counterparts. Both **1c** and **1e** yielded a substantial 1450 and 3250-fold increase in IC_{50} values compared to **1a**. Although not unanticipated for **1e** as its calculated partition coefficient (LogP) was 0.77, indicating hydrophobic character, the similar result of **1c** appeared to be unrelated to this same feature (calculated logP = -1.01). The failure of these two dipeptides to assert any modest inhibitory action could be for a number of reasons: (i) the hydrophobic character prevented uptake by the RFC, (ii) without a free γ-carboxylate, neither is a substrate for FPGS, thus their cellular retention is compromised, and (iii) their direct binding with TS is obstructed due to their anti-polar nature or steric bulk. Interestingly, when we profiled the α-dipeptide conjugates of **1a,** we found a substantial inhibitory effect for all compounds (Figure 4.3B).

We reasoned that the drastic suppression in IC_{50} values could not confer the failure of **1c** and **1e** as a result of impaired reduced folate carrier (RFC) uptake; rather, the positional modification of the α-carboxylate may have allowed for FPGS processing at the γ-position, thus reinstating polyglutamylation. However, previous research with methotrexate dipeptides revealed the significance behind the role of the α-carboxylate.[15] In order to be a substrate for FPGS, the terminal α-carboxylate must be present regardless of the condition of the initial α-carboxylate.[15] Given this evidence, it's therefore reasonable to deduce that the enhanced suppressive effect of the α-conjugates is not due to FPGS processing.

The potency for compound **1d** and **1d'** is believe to stem from targeting both TS and FPGS, although the later is unlikely to target FPGS due to the occlusion of its terminal α-carboxylate. Previous research has shown that modification of quinazolinone - based inhibitors with ornithine act as powerful inhibitor of FPGS and TS.[16, 17]

4.1.3 Biological Evaluation of Di-,Tri-, and Tetraglutamates of Raltitrexed

The intracellular metabolism activity of **1a** plays a distinct role in both its cellular residence and substrate avidity. It has been shown that that successive intracellular glutamylation by FPGS of **1a** occurs with 90% conversion to the mono-, di-, tri-, and tetraglutamates being formed within the first 30 minutes of exposure. The reported amount of material lost was approximately 30% with the remaining undergoing further processing to tetra-, penta-, and to a lesser extent, hexaglutamates.[18]

Based on these results, we synthesized the di-, tri-, and γ-tetraglutamates (**1a**, **2a**, and **2c**, respectively) using standard SPPS followed purification by HPLC. To analyze their potential to serve as a possible scaffold for hydrophobic tagging, we examined each conjugates' TS binding ability and pharmacological impact in CHL^{-TS} pJZ205 cells and respective lysates (Figure 4.4 and 4.5). Inhibition analysis of **1a**, **2a**, and **2c** showed a trending increase in resistance as glutamate addition progressed with **2c** potency decreasing 232 fold (Figure 4.4A).

However, the triglutamate conjugate, **2a**, resisted this trend and maintained its potency. Isothermal titration calorimetry correlated with the inhibition analyses and **2a** did not deviate from the inhibition characteristics of the parent monoglutamate (**1a**). Finally, the half-life of each conjugate was assessed to determine if the each conferred the stabilizing effect of **1a**. None of the conjugates transformed the extreme stabilization to the extent of **1a**. The di- and tetraglutamate showed marginal reduction the half-life status of TS with a 2 and 2.4 fold increase in half-life, respectively, with conjugate **2a** reporting a 1.7 fold increase (Figure 4.5).

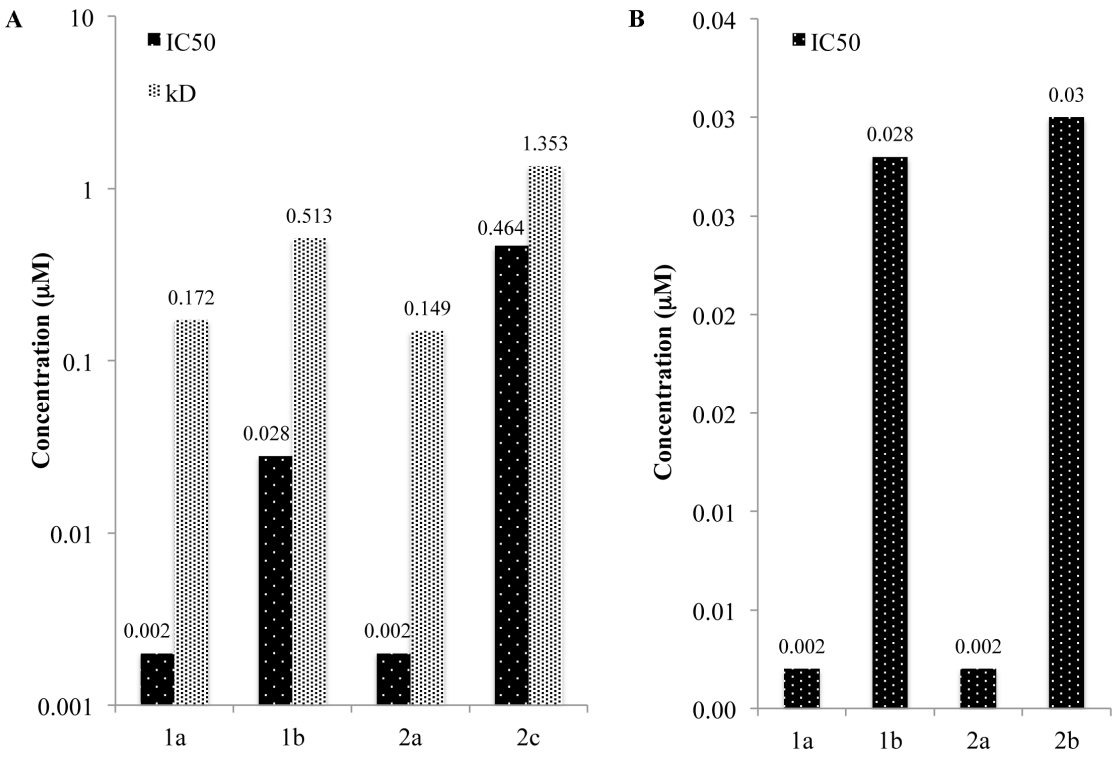

C

Glutamate(s)	RTX Conjugates	Fold Change Vs RTX IC_{50}	Fold Change Vs RTX k_D
Mono-glu	RTX (1a)	0.002	0.172
Di-glu	RTXγ-E (1b)	14↑	3↑
Tri-glu	RTXγ-Eγ-E (2a)	NC	NC
Tri-glu	RTXγ-Eα-E (2b)	15↑	N/A
Tetra-glu	RTXγ-Eγ-Eγ-E (2c)	232↑	8↑

Figure 4.4 (A) The effect of conjugating one, two, and three γ-linked glutamic acid residues upon **1a** as measured by the binding ability (K_d) and growth inhibitory characteristics (IC_{50}) in CHL^{-TS} pJZ205 cells. (B) The effect between α and γ regiochemistry between the triglutamates **2a** and **2b** of **1a** as measured by growth inhibition (IC_{50}) in CHL^{-TS} pJZ205 cells. (C) Values of each conjugate measured against the fold change of **1a**.

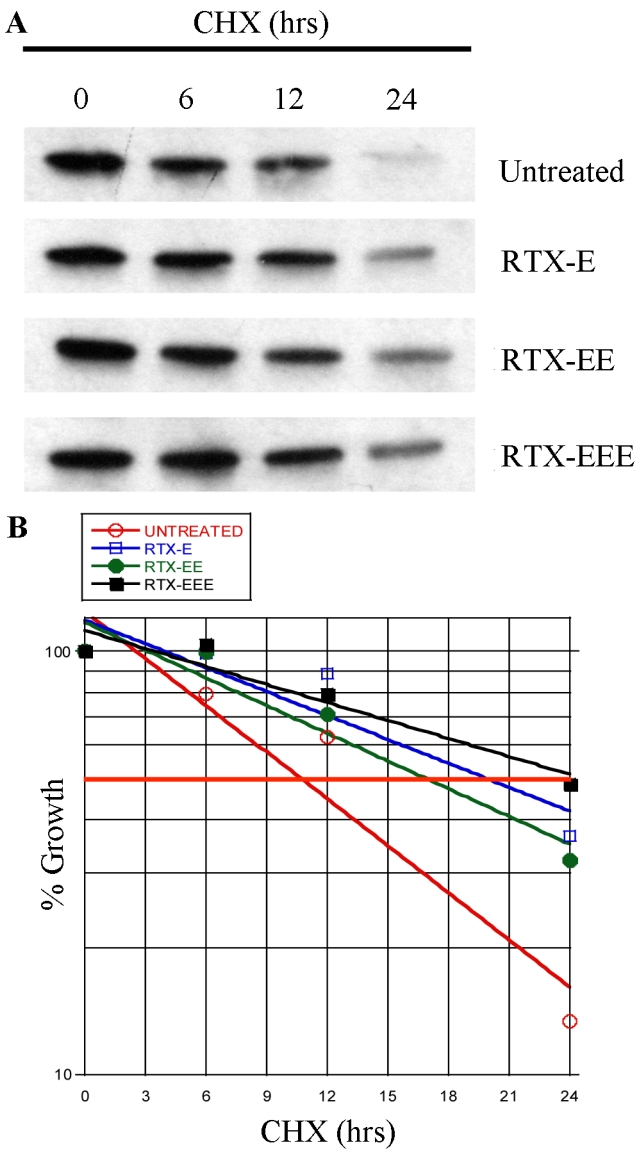

Figure 4.5 The relationship between the stability of TS and the effect of successive γ-glutamylation on **1a.** (A) Western blot analyses as measured by the half-life in CHL^{-TS} pJZ205 cells of di- (RTX-E), tri- (RTX-EE), and tetraglutamates (RTX-EEE) of **1a**. (B) Graphical representation of TS stability (red) against di- (blue), tri- (green), and tetraglutamates (black) of **1a**. (E = γ-glutamic acid)

To examine the stability of regioisomers between di- and triglutamate conjugates, we prepared a α-connected triglutamate and assessed its impact on *in vitro* inhibition of TS (Figure 4.4B). The α-triglutamate conjugate **2b** potency reverted to that of the diglutamate **1b**, highlighting the innate importance of the regiochemical linkage between residues two and three in the triglutamate conjugate and its relationship to *in vitro* efficacy. Furthermore, the biophysical measurements of all conjugates were evaluated to determine the major driving force behind the stability of **1b** (Figure 4.6).

As shown in Figure 4.6, both panels A and B show favorable relationships between the thermodynamic reaction potential (ΔG) and the general order and alignment of van der Waals and hydrogen bonding (ΔH) of the RTX conjugates to TS. Maximum ligand alignment is evidenced by their observed exothermic behavior ($\Delta H < 0$), which reflects the correct placement of the conjugate at the binding interface (Figure 4.6B). However, entropic forces become non-ideal as the as the final glutamate or isoleucine unit is appended to the triglutamate conjugate (Figure 4.6C). This is likely a consequence chain extension, which increases the disordered nature of chain as residues are added. Hence, the entropic costs for binding these extended conjugates is high.[19]

4.1.4 Safety-Catch SPPS Synthesis of Raltitrexed-Triglutamate-Hydrophobic Tags

Based on our synthetic efforts with polyglutamylation of **1a**, we were interested in building a small library of hydrophobic-tagged compounds with **2a** serving as the main scaffold-binding unit. However, given that traditional Fmoc SPPS methods build from the amino to the carboxy-terminus, the ability to construct a library based on **2a** was prohibitive. As such, we investigated the potential of the Kenner "Safety-Catch" solid

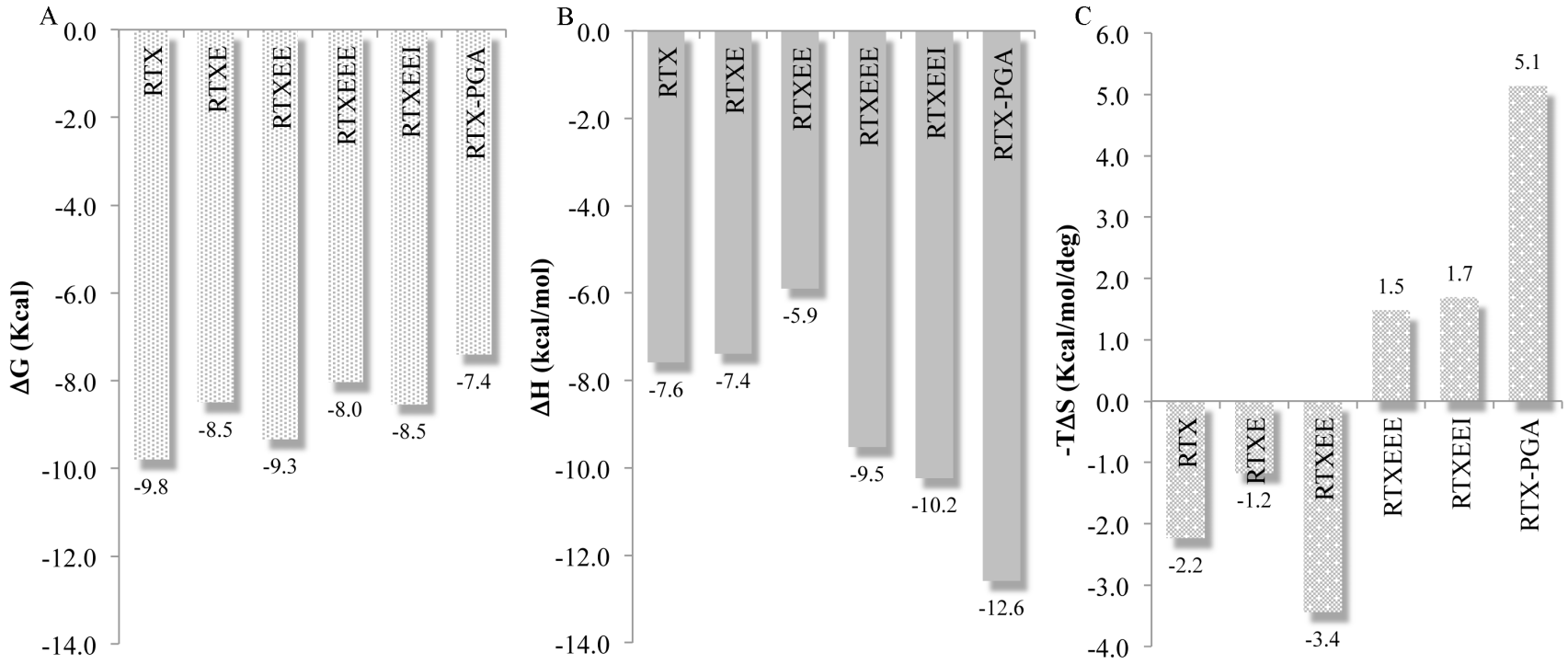

Figure 4.6 Biophysical analyses of raltitrexed conjugates by isothermal titration calorimetry against TS and dUMP. (A) The calculated change in Gibbs free energy (all are exergonic, $\Delta G < 0$), (B) measured change in enthalpy (all are exothermic, $\Delta H < 0$), and (C) the calculated change in entropy for the binding of each conjugate to the dUMP•TS complex, respectively. The transformation from RTX-EE to RTX-EEE illustrates the increase in disorder ($\Delta S > 0$) as related to their binding and their increase in length and size (PgA), which follows a concomitant decrease in enthalpy for those conjugates (B, C).

phase support (Figure 4.7).[20] The alkanesulfonamide handle was quantitatively charged to high loading aminomethyl resin using commercially available 3-carboxypropanesulfonamide. Gram quantities for the Safety-Catch (**5**) resin were prepared using standard DICI (*N,N'*-diiso-propylcarbodiimide) and HOBt (*N*-hydroxybenzotriazole) coupling conditions monitored by a bromophenol blue test (Figure 4.8).[21] Linker oligomerization does not occur as the alkanesulfonamide linker is unreactive to HOBt esters.[22] Optimization of the first Fmoc-Glu-OtBu with high loading efficiency was initially preformed at low temperatures with PyBOP [bromotris(pyrrolidino)phosphonium hexafluorophosphate] and a tertiary base i-Pr_2EtN (Diispropylethylamine) as acylation with HATU reportedly leads to significant levels of racemization.[22]

Loading efficiencies for coupling of the first Fmoc-Glu-OtBu (**6**) produced extremely low yields for the first charge, with no improvement upon a second charge. Continued efforts to increase yields were examined by increasing the reaction temperature to -20 °C from -40 °C, using DMF to fully swell the resin, and increasing the equivalents of PyBOP and Fmoc-(GluOtBu) (Table 4.1, entry 2). Additional efforts were made to maintain the swelling properties of the resin using DMF with reaction volume restriction did not abrogate the low yields. Questioning the reactivity of our alkanesulfonamide support we switched to commercial Aryl safety-catch resin, however, results did not improve (Table 4.1, entry 3)

Although reports state that the active intermediate during coupling with PyBOP at low temperature is the O-acyl phosphonium adduct, we found that coupling to an extended methylene bridged carboxylate did not warrant low temperatures.[23] We then

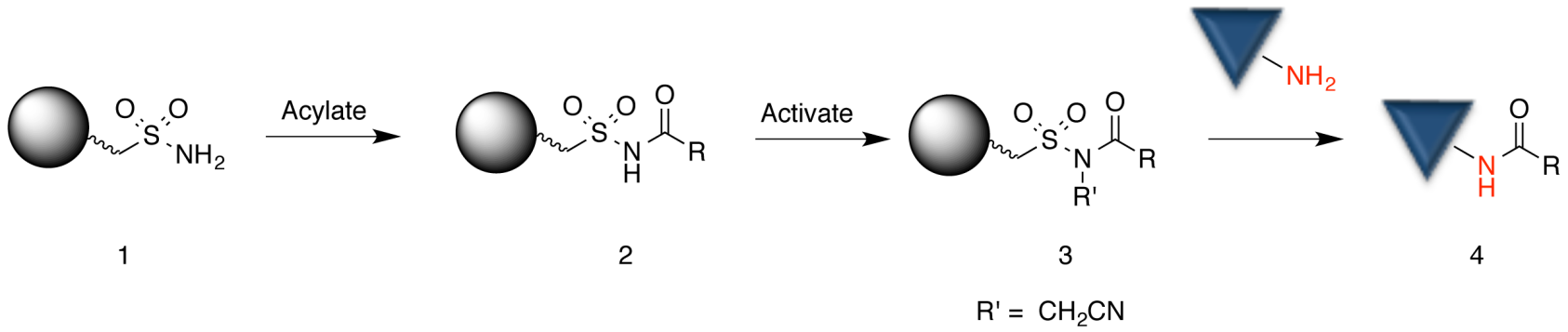

Figure 4.7 General scheme for the Kenner safety-catch resin and the alkanesulfonamide linker (**1**) with subsequent acylation (**2**), activation (**3**) and release of the peptide conjugate through nucleophilic displacement by a potent primary amine (**4**).

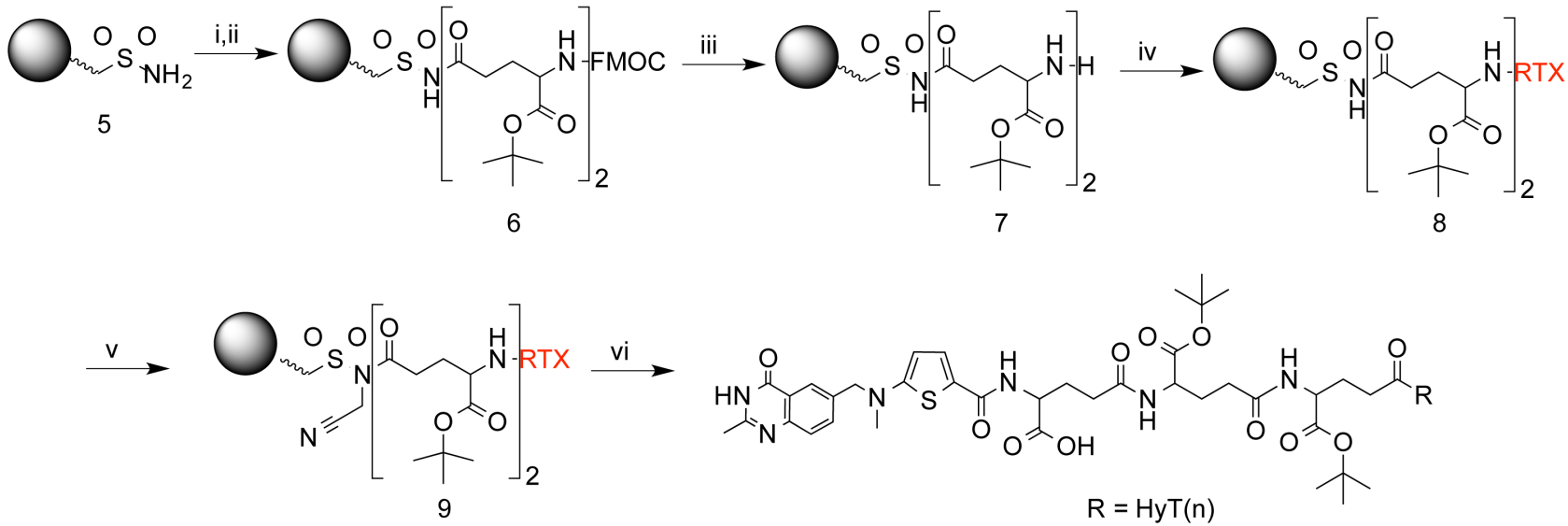

Figure 4.8 General scheme for building raltitrexed triglutamate scaffold. (**i** & **ii**) FMOC-Glu-OtBu (8 eq), PyBop (8 eq), DIPEA (14 eq), RT, 15 hrs; (**iii**) 50% piperdine in DCM, 3x 5-10 mg 1 hr Abs @ 301 nm; (**iv**) RTX (5 eq), PyBOP (5 eq), DIPEA (10 eq), 2-4 hrs (**v**) ICH_2CN (20 eq) in NMP, RT, 24 hrs; (**vi**) 5 eq of HyT in 5% DMF in THF, 25 °C, 16 hrs. (**1a**, RTX = raltitrexed)

Table 4.1 Preliminary Safety-Catch reaction parameters. Abbreviations: AlkaneS = Alkanesulfonaminde; ArylS: Arylsulfonaminde; DIPEA = diisopropylamine; $CHCl_3$ = chloroform; DMF = *N',N'*-dimethylformamide; RT = room temperature; N/A = not applicable; DICI = *N,N'*-diisopropylcarbodiimide; HOBt = *N*-hydroxybenzotriazole; PyBOP = bromotris(pyrrolidino)phosphonium hexafluorophosphate.

							Initial Coupling[1]		Second Coupling[1]		Third Coupling[1]	
Entry	Resin	AA	EQ (FMOC-E/PyBOP/DIPEA)	Temp (°C)	Time (hrs)	Solvent	mmol g-1	% Yield	mmol g-1	% Yield	mmol g-1	% Yield
1	AlkaneS	FMOC-GluOtBu-OH	3.5/3.5/6	-40	8	20 mL CHCl3	0.004	0.7	0.19	19.1	0.34	46.9
2	AlkaneS	FMOC-(GluOtBu)-OH	4/4/6	-20	8	3 mL DMF	0.012	1.6				
3	ArylS	FMOC-GluOtBu-OH	3/3/5	-20	8	3 mL DMF	0.015	2.6	0.034	6.6		
4	AlkaneS	FMOC-GluOtBu-OH	8/8/13	RT	2.5	1 mL Dry DMF	0.271	45.7	N/A	N/A	0.531	89.5
5	AlkaneS	FMOC-GluOtBu-OH	8/8/13	-20	8	3 mL DMF	0.055	6.1				
6	AlkaneS	FMOC-GluOtBu-OH	9/9/14	-20	7.5	1.7 mL CHCl3	0.127	21.6	0.203	34		
7	AlkaneS	FMOC-GluOtBu-OH	9/9/14	RT	2.75	1.7 mL Dry	0.147	24.8	0.386	65	0.405	68
8	AlkaneS	FMOC-GluOtBu-OH	8/8/14	RT	14	1 mL DMF	0.322	54.3				
9	AlkaneS	FMOC-GluOtBu-OH	10/10/20 (HOBt/FMOC-E/DICI)	RT	14	1 mL DMF	0	0				

(1)PyBOP = Added Dry, (2) Rxn in 8 mL DMF

compared the same reactions using 0.044 mmol of resin under both -20 °C and room temperature to generate a 13% and 58% yield, respectively (Table 4.1, entry 4). The reaction was duplicated and charged twice to improve yields to 68% (Table 4.1, entry 7). Given the moderate increase in substitution, entry 4 was examined for additional coupling followed by Fmoc cleavage (**7**) managed to stabilize coupling yields (57%) (Table 4.1). Further optimization was not carried out and raltitrexed (**8**) was coupled under lower equivalents followed by ICH_2CN activation (**9**). The conjugate was cleaved from the resin using 1 equivalent of PgA to yield pro-RTX-EE-PgA (43%).

Encouraged by our improvements, we decided to use the Quest210 synthesizer to meet our combinatorial needs. Our initial attempt at primary coupling of Glu-OtBu-OH was met with low yields (~20%), although a second and third charge elevated coupling up to 87% (Table 4.2, entries 10a-d). In order to improve coupling efficiency for the attachment of the second glutamic acid the incubation time was increased to 27 hours. The first round of the second attachment improved average yields to 37%, however a second charge did not alter coupling (Table 4.2 entries 11a-d).

Low yields were not suitable for further advancement to generate hydrophobic-tagged library, thus the reaction capacity was increased 5-fold to 0.6 mmol batch reactions. A dramatic improvement in yield and a reduction in charging, from three to two, resulted for both glutamate residues (Table 4.2, entries 12 and 13).

4.1.5 Pilot Study for Safety-Catch Raltitrexed-Triglutamate-Hydrophobic Tags

A small pilot library was constructed using seven various hydrophobic tags fitting with active primary amines based on their known reactivity's, boiling points, and their

Table 4.2 Safety-Catch reaction parameters for Quest210. Abbreviations: AlkaneS-E = Alkanesulfonaminde-GluOtBu-OH; AlkaneS-EE = Alkanesulfonaminde-[GluOtBu-OH] (×2); DIPEA = diisopropylamine; DMF = *N',N'*-dimethylformamide; RT = room temperature; N/A = not applicable; DICI = *N,N'*-diisopropylcarbodiimide; HOBt = *N*-hydroxybenzotriazole; PyBOP = bromotris(pyrrolidino)phosphonium hexafluorophosphate; RTX = raltitrexed.

							Initial Coupling		Second Coupling		Third Coupling	
Entry	Resin	AA	Equivilents	Temp (°C)	Time (hrs)	Solvent	mmol g-1	% Yield	mmol g-1	% Yield	mmol g-1	% Yield
10a	AlkaneS-E	FMOC-GluOtBu-OH	8/8/14 (PyBop/FMOC-E/DIPEA)	RT	15	1 mL DMF	0.112	18.9	0.38	64.1	0.581	87.3
10b	AlkaneS-E	FMOC-GluOtBu-OH	8/8/14 (PyBop/FMOC-E/DIPEA)	RT	15	1 mL DMF	0.098	16.5	0.443	74.7	0.468	79.0
10c	AlkaneS-E	FMOC-GluOtBu-OH	8/8/14 (PyBop/FMOC-E/DIPEA)	RT	15	1 mL DMF	0.089	15.1	0.465	78.4	0.414	69.9
10d	AlkaneS-E	FMOC-GluOtBu-OH	8/8/14 (PyBop/FMOC-E/DIPEA)	RT	15	1 mL DMF	0.076	12.9	0.563	94.9	0.441	74.4
11a	AlkaneS-EE	FMOC-GluOtBu-OH	8/8/8 (DICI/FMOC-E/HOBt)	RT	27	1 mL DMF	0.231	43.2	0.195	36.2		
11b	AlkaneS-EE	FMOC-GluOtBu-OH	8/8/8 (DICI/FMOC-E/HOBt)	RT	27	1 mL DMF	0.185	34.7	0.173	32.4		
11c	AlkaneS-EE	FMOC-GluOtBu-OH	8/8/8 (DICI/FMOC-E/HOBt)	RT	27	1 mL DMF	0.207	38.9	0.200	37.4		
11d	AlkaneS-EE	FMOC-GluOtBu-OH	8/8/8 (DICI/FMOC-E/HOBt)	RT	27	1 mL DMF	0.18	33.8	0.162	30.4		
12	AlkaneS-E	FMOC-GluOtBu-OH	8/8/14 (PyBop/FMOC-E/DIPEA)	RT	18	1 mL DMF	0.38	64.1	0.484	81.6		
13	AlkaneS-EE	FMOC-GluOtBu-OH	8/8/14 (PyBop/FMOC-E/DIPEA)	RT	16	1 mL DMF	0.431	80.8	0.465	87.0		
14	AlkaneS-EE	RTX	5/5/10 (PyBOP/FMOC/DIPEA)	RT	16	1 mL DMF						

calculated partition coefficients (logP) (Figure 4.9A). Each was activated for 24 hrs, washed and displaced with nucleophile/hydrophobic tags 1-7 (HyT1-7) and purified by HPLC. A parallel synthesis, performed by our colleague, using selective amidation methods previously developed by our lab, yielded three highly pure γ-selective hydrophobic-tagged raltitrexed-conjugates with various polyethylene glycol (PEG) linkers (Figure 4.9B).

These conjugates were produced to measure the general nature of the glutamic acid bridge, however, ITC analyses of the three conjugates failed to produce any thermodynamic results when challenged against the dUMP•TS complex (data not shown). This strongly suggests the ability, if any, of HyT(9-11) to produce a binding event or exhibit any inhibitory is not promoted by any enthalpic promoted mechanism.

4.1.6 Biological Evaluation of Hydrophobic-Tagged Raltitrexed

The biological impact of RTX-HyT(1-10) were examined over a 4-day time course in CHL^{-TS} pJZ205 cells (Figure 4.10). Conjugates prepped using the both the safety-catch resin and selective amidation reported elevated IC_{50}'s, exceeding their parent compounds (**2a** and **1a**, respectively) cellular efficacy by an average of 2.5×10^{6} fold. Compounds HyT(7) and HyT(8) produced the lowest inhibition values of 2.3 and 3.7 μM as shown in figures 4.10A and 4.10B.

The inhibition values were followed up with a half-life assay to determine if the either of the conjugates had promoted TS destabilization through mimicked hydrophobic exposure (Figure 4.11). Compound HyT(9) produced a half-life of approximately 14 hours, 1.3 fold higher than the DMSO vehicle (wtTS). However, when compared to **2a**

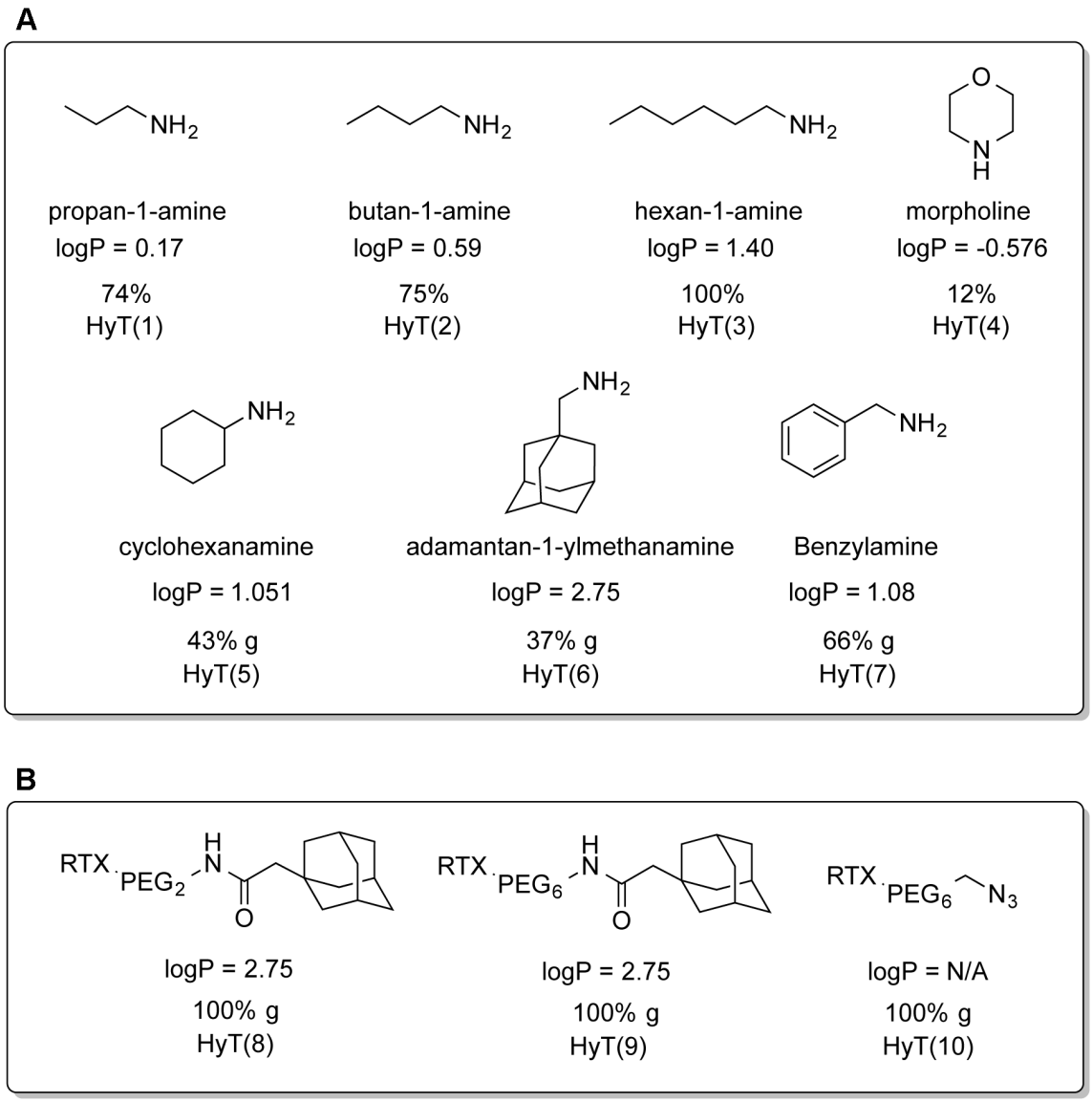

Figure 4.9 (A) Hydrophobic tags (HyT) used for pilot study with RTX-EE Kenner safety-catch resin with alkanesulfonamide linker. (B) RTX-PEG$_n$-HyT synthesized via DCC/DMAP coupling with various pegylated linkers.

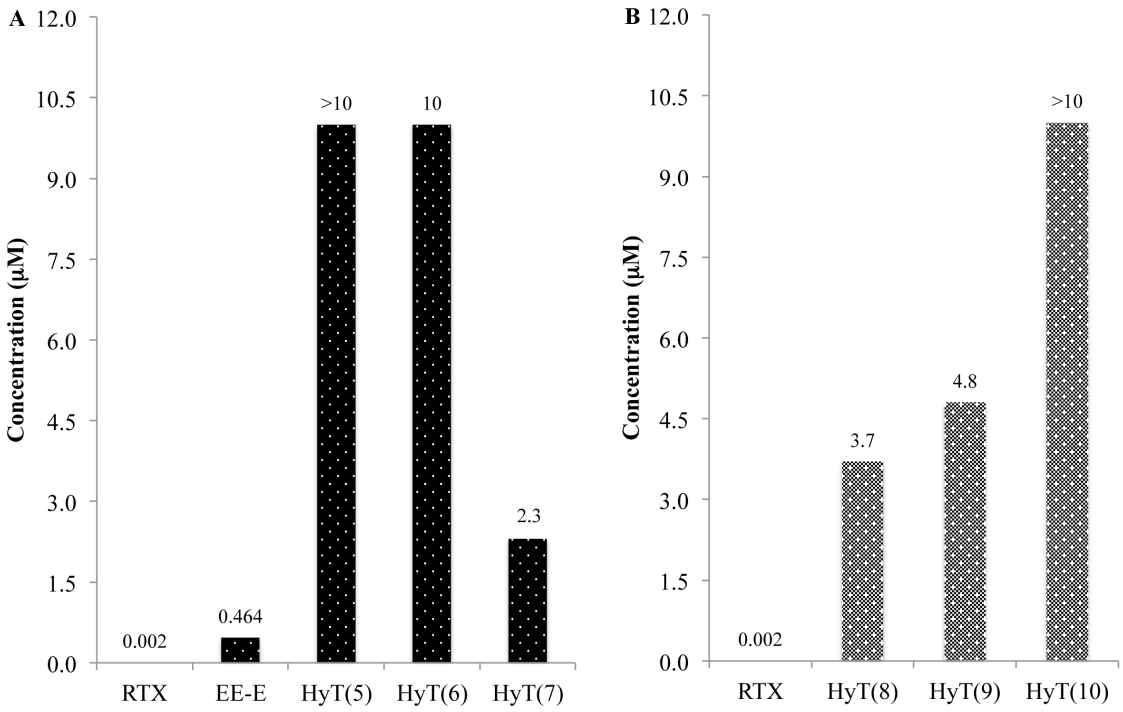

Figure 4.10 Growth inhibition analyses of RTX conjugates with HyT's 5-7 and 8-10 with triglutamate (A) and pegylated linkers (B), respectively.

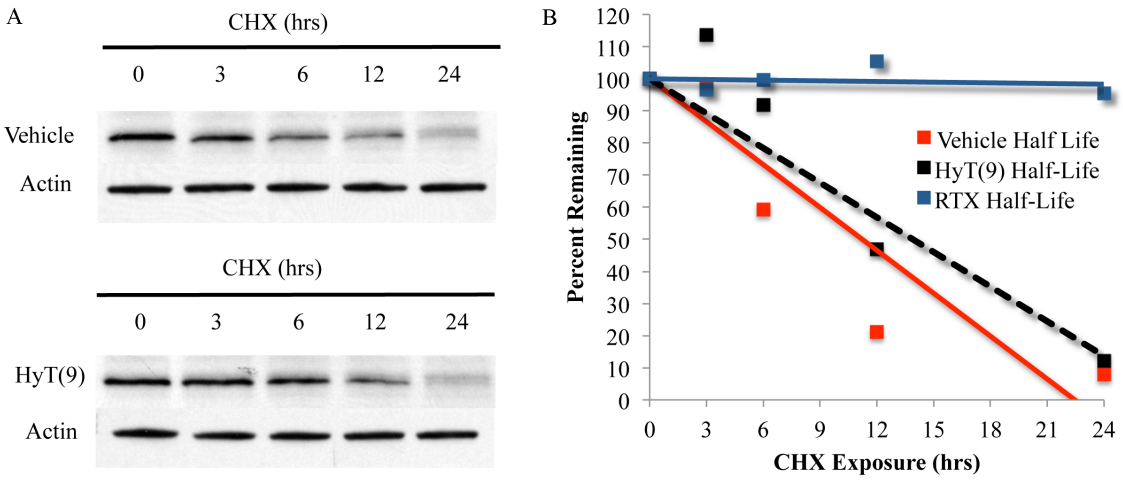

Compound ID	Half-Life (hrs)
Vehicle	10.7
RTX	>24
RTX-PEG$_2$HyT(9)	14

Figure 4.11 (A) Western-blot analysis of RTX-PEG$_6$-HyT(8) half-life. (B) Graphical representation of the half-life of raltitrexed (blue), RTX-PEG$_6$-HyT(8) (black), and wtTS DMSO vehicle (red).

the effect HyT(9) displays is casually lower, indicating its action is the result of TS destabilization. Additional input in necessary to determine if HyT(9) activity can impose dose-dependent degradation and if this effect is linked to the proteasome.

4.1.7 Advanced Study for Safety-Catch Raltitrexed-Triglutamate-Hydrophobic Tags

The preliminary results of the pilot study encouraged the development of larger in-depth analysis, which examined the spatial nature of the HyT's and their respective inherent physical properties (logP) and inhibitory capacities (IC_{50}) against TS (Table 4.3). Group I was predicted to demonstrate an inhibitory relationship directly proportional to its chain length (logP) due to the increase in potential hydrophobic surface area (Figure 4.12). However, this relationship was not observed, rather HyT(4), the methylated γ-carboxylate, yielded the lowest IC_{50}.

Interestingly, HyT(11) with its 9-methylene chain, also produced and IC_{50} resembling **1b** (Figure 4.4). The inhibitory impact by HyT(4) is likely due to the modest alteration. However, the response to HyT(11) may have maintained the low inhibition threshold of **1b** due to its chain extension, which may not interact directly with the surface of TS, but allows for surface recognition for degradation. Additional studies determining each tags roll in degradation is needed.

Further analysis of group II and III compared the effect of methylene spacers (1, 2, or 3) and the effect of benzylic heteroatoms (HyT(19)), along with electron withdrawing (EWG) and donating groups (EDG), HyT(17, 22) and HyT(18, 21), respectively. Hydrophobic tags 7, 18, and 20 demonstrated poor inhibition with values exceeding 10 μM (Figure 4.12). Interestingly, HyT(19), HyT(22), and HyT(23) showed

Table 4.3 List of corresponding HyT's used to synthesize their respective RTX-EE-HyT(n) conjugates. Yields are based on spectrophotometric measurement of RTX (**1a**). Inhibition was measured after 48 hrs in CHL^{-TS} pJZ205 cells. (N/A: Not Available)

HyT ID#	Compound (HyT)	% Yield	IC_{50} (μM)
1	n-propylamine	>100	N/A
2	Butylamine	71.5	0.33
3	1-heptylamine	63.6	0.19
4	methylamine	71.5	0.05
5	hexylamine	95.8	1.48
6	adamantanemethylamine	93.6	0.20
7	Benzylamine	>100	>100
11	1-Nonanamine	>100	0.06
12	(-)-cis-myrtanylamine	67.7	0.25
13	6-Aminohexanitrile	93.7	0.55
14	4-pentynylamine	59.5	N/A
15	Propargylamine	72.7	0.28
16	diphenylmethylamine	73.7	0.43
17	4-(Trifluoromethyl)benzylamine	81.1	5.38
18	4-Methylbenzylamine	90.3	>100
19	4-(Aminomethyl)pyridine	>100	0.16
20	3-Phenyl-1-propylamine	87.3	19.56
21	N-Phenylethylenediamine	83.1	3.32
22	2-(4-Chlorophenyl)ethylamine	81.1	0.16
23	2-Phenethylamine	80.8	0.06

HyT(n)	IC_{50} (μM)	LogP	CH_2 Spacer	
				Group I: Aliphatic HyT's
4	0.05	-0.65	1	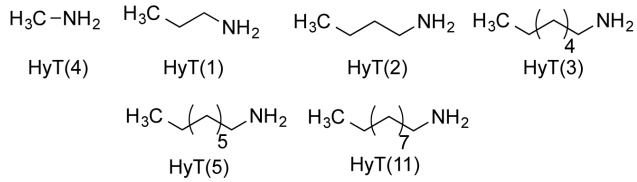 HyT(4) HyT(1) HyT(2) HyT(3) HyT(5) HyT(11)
1	N/A	0.17	3	
2	0.33	0.59	4	
3	0.19	1.40	6	
5	1.48	1.84	7	
11	0.06	2.26	9	
				Group II: Aromatic HyT's
19	0.16	-0.26	1	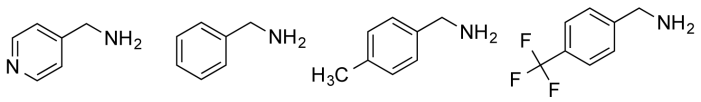 HyT(19) HyT(7) HyT(18) HyT(17)
7	>100	1.08	1	
18	>100	1.57	1	
17	5.38	2.00	1	
				Group III: Extended Aromatic HyT's
21	3.32	0.63	3	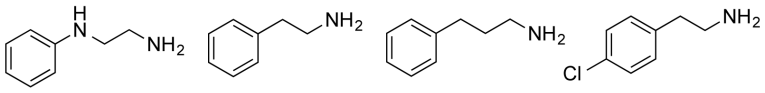 HyT(21) HyT(23) HyT(20) HyT(22)
23	0.06	1.36	2	
20	19.56	1.78	3	
22	0.16	1.92	2	
				Group IV: Large HyT's
12	0.25	1.40	1	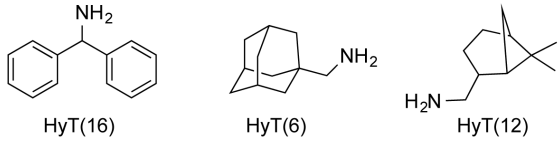 HyT(16) HyT(6) HyT(12)
16	0.45	1.79	0	
6	0.20	2.75	1	
				Group V: Functional Aliphatic HyT's
13	0.55	-0.65	5	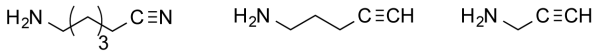 HyT(13) HyT(14) HyT(15)
14	N/A	0.17	3	
15	0.28	0.59	1	

Figure 4.12 Structural relationship between HyT's conjugates (RTX-EE-HyT(n)) with their partition coefficients (logP) and inhibitory capacity toward TS (IC_{50}). (N/A: Not Available)

similar results to that of HyT(4) and HyT(11). Hydrophobic tags 22 and 23 indicated that spacer length might be critical to inhibition when compared to HyT(7), HyT(17), and HyT(20) with the optimal length set at 2 methylene units (Table 4.12, II and III). Moreover, strong intra-chain-EDG's, HyT(21), may also play a role in muting hydrophobic response. The EDG and EWG of benzylic (single methylene spacers) tags appear to be deleterious (HyT 17 and 18) with IC_{50}'s reported greater than 5 μM.

Groups V hydrophobic tags possessed some of the lowest IC_{50}'s when compared to **1b** and the other group's intra-inhibitory results. Here, their "spherical" nature, rather than the aromaticity displayed by members groups III and IV, appears to parallel their respective partition coefficients (Table 4.12, V). Although aromatic, the dual nature of biphenyl moiety of HyT(16) seems to be beneficial and may override its single aryl homolog HyT(7). Lastly, group VI, a series of potential CuAAC conjugates, and a cyano-terminated aliphatic amine offer modest results with 2× the inhibitory capacity of **1b**. Although it should be noted that HyT(13) does have a surprisingly low IC_{50} when its hydrophilic partition coefficient is taken into consideration.

While many of these conclusions are based on the structural activity relationship (SAR) between the architecture of the hydrophobic tag and both its theoretical logP and observed IC_{50}, it should be noted that additional analyses should be performed to substantiate the preliminary SAR. The development of the **1b** scaffold, its biological evaluation, and the construction of the HyT library do, however, provide a useful insight for further investigation to the degradative potential of hydrophobic tags upon thymidylate synthase.

4.2 EXPERIMENTAL

4.2.1 General Cell Preparation

All cells were provided by Dr. Franklin G. Berger (University of South Carolina, Department of Biological Sciences). Cells were grown in a T75 flask under 10% fetal bovine serum (FBS) in high glucose Dulbecco's Modified Eagle's medium (DMEM) with 100 U of penicillin-streptomycin (Pen-Strep) at 37 °C and humidified at 5% CO_2. Cell line RJK33.13, a TS-deficient derivative of V79 Chinese hamster lung cells (CHL^{-TS} pJZ205, CHL^{-TS} pJZ205/200) were grown to confluency and passaged at either 1:10 or 1:20 with 0.25% trypsin.[24]

4.2.2 TS Half-Life Studies

The half-life of thymidylate synthase in RJK33.13 cells under exposure to HyT(9) was assessed according to the protocol previously reported.[25] The half-life of the conjugates **1a**, **2a**, and **2c** was generously performed by Karen Barbour (University of South Carolina, Department of Biological Sciences).

4.2.3 Growth Inhibition Studies

The growth inhibition response of all compounds, unless otherwise stated, was assessed according to the protocol previously reported.[13] This work was generously performed by Karen Barbour (University of South Carolina, Department of Biological Sciences). The growth inhibition of RTX-EE-HyT 1-7 and 11-23 in CHL^{-TS} pJZ205 cells was calculated after 48 hours of triplicate drug conjugate incubation at 37 °C with 5% humidity using CyQuant Direct Cell Proliferation Assay (Life Technologies, P/N

C35011). Inhibition analysis was implemented per the manufactures instructions unless otherwise noted and calculated using Prisim 6 Trial Software.

4.2.4 Solid Phase Peptide Synthesis of Raltitrexed Glu, Gly, Arg, and Tyr Conjugates

Unless otherwise noted, all reactions were carried out using an Argonaut Quest 210 Organic Synthesizer. The following stoichiometric parameters were followed for all reaction: to a 5 mL reaction cartridge was added ***Wang-aminoacid-Fmoc*** (0.05 mmol) and 4 mL of DMF. The resin was allowed to swell for 60 minutes before it was drained and deprotected in 20% piperidine in DMF followed by agitation 45 min after which a second Kaiser test was performed.[26] The resin was then filtered and washed with DMF (3 × 5 mL) and filtered again. RTX (**1a**) (4.0 eq, 0.20 mmol) was dissolved in 5 mL of DMF with HBTU (2.9 eq, 0.145 mmol), HOBt (2.9 eq, 0.145 mmol), NMM (4.0 eq, 0.20 mmol) then added to the reaction. The reaction was agitated for 2 hrs then filtered and washed with DMF (3 × 5 mL) then MeOH (1 × 5 mL) and dried.

Raltitrexed-peptide conjugates were liberated from the resin under 2 mL of 98% TFA in water for 2 hrs. The resin was drained and the eluent was collected. The resin was washed again in 5 mL of 98% TFA in water then pooled and dried under N_2 until a yellow film appeared. To the flask was added ice-cold diethyl ether to form a precipitate. The precipitate was centrifuged at 9,000 RPMs at 4 °C for 10 min. The clear eluent was decanted the remaining material was lyophilized overnight to yield the crude forms of **1b** (18.6 mg, 36.0 μmol)**, 1e,** (30.7 mg, 49.4 μmol) **1c** (25.5 mg, 40.9 μmol)**,** and **1d** (25.1 mg, 40.8 μmol). Each crude was purified by HPLC using a 250 × 10-mm, 5 μm RP C_{18} column at 5 mL min^{-1} from 10-65% ACN in 0.1% TFA for 65 min. Injections of 1.0 mL

were monitored at 269 and 341 nm. Fractions were pooled, concentrated, and lyophilized. Purified products were characterized using ESI LCMS over 150 × 2.0-mm, 3 μM RP C_{18} over 10-65% ACN (0.1% formic acid) gradient in 45 min. Purified γ-products **1b** (1.1 mg, 5.2%)**, 1e** (2.3 mg, 7.5%) **1c** (1.2 mg, 5.7%)**,** and **1d** (1.2 mg, 4.8%) and their corresponding Purified α-products **1b'** (1.1 mg, 5.2%)**, 1e'** (3.4 mg, 11.1%) **1c'** (1.2 mg, 5.7%)**,** and **1d'** (1.4 mg, 5.6%) were identified at $[M+H]^+$ 588, 623, 516, and 616 m/z by ESI LCMS.

4.2.5 Solid Phase Peptide Synthesis of Di-, Tri-, and Tetraglutamates

To a 20 mL reactor cartridge was added ***Wang-GluOtBu-Fmoc*** resin (101 mg, 0.05 mmol) followed by solvation in DMF. A fresh solution of 20% piperidine in DMF was added to the reactor and agitated for 30 min. The resin was then filtered and washed with DMF (3 × 5 mL) and filtered again. The following is the general procedure for each Fmoc-GluOtBu acid coupling: To separate 50 mL flask was added Fmoc-GluOtBu (4.0 eq, 0.20 mmol), HBTU (2.9 eq, 0.146 mmol), HOBt (2.9 eq, 0.146 mmol), NMM (4 eq, 0.2 mmol). The reagents were dissolved in 10 mL of DMF, transferred to the reaction cartridge and agitated for 45 min. The resin was then filtered and washed with DMF (3 × 5 mL) and filtered again. A Kaiser test was administered to determine reaction completion.[26]

To a separate vial, **1a** (4.0 eq, 0.20 mmol) was dissolved in 10 mL of DMF followed by HBTU (2.9 eq, 0.146 mmol), HOBt (2.9 eq, 0.146 mmol), and NMM (4 eq, 0.2 mmol) and then added to the reactor cartridge. The reaction was agitated for 2 hrs then filtered and washed with DMF (3 × 5 mL) then MeOH (1 × 5 mL) and dried *in*

vacuo for 45 minuntes. Raltitrexed-Glu conjugates were liberated from the resin under 10 mL of TFA for 45 minutes. The resin was drained and the eluent was collected. The resin was washed again in 5 mL of TFA then pooled and dried under N_2 until a yellow film appeared. To the flask was added ice-cold diethyl ether to form a precipitate and was stored at -20 °C for 30 min. The precipitate was centrifuged at 9,000 RPMs at 4 °C for 10 min.

The clear eluent was decanted the remaining material was lyophilized overnight to yield the crude forms of **1b** (24.2 mg, 41.2 μmol), **2a**, (33.2 mg, 46.7 μmol), **2c** (29.7 mg, 35.1 μmol), **2b** (12.8 mg, 17.8 μmol). Each crude was was purified by HPLC as previously mentioned in 4.2.3. Purified γ-products were **1b** (6.5 mg, 27.3%), **2a**, (4.8 mg, 14.3%), **2c** (29.7 mg, 12.1%), **2b** (3.8 mg, 29.8%) and identified by LCMS as noted in section 4.2.4 by their $[M+H]^+$ 588, 717, 846, and 717 m/z.

4.2.6 Safety-Catch Resin and RTX-EE-HyT Conjugates

The synthesis of the safety-catch alkane sulfonamide linker and all pilot RTX-EE-HyT conjugates were performed according to the protocols previously reported.[22] Reactions carried out for Table 4.1 were completed in a 50 mL round bottom glass whereas all reactions in Table 4.2 were performed on an Argonaut Quest 210 Organic Synthesizer.

The advanced Safety-Catch study was performed as previously reported with various alterations.[27] Briefly, using the alkanesulfonamide linker from the pilot study, we successively built the RTX-EE platform and prepared approximately 50 mg (0.020 mmol) for activation (ICH_2CN (20 eq), DIPEA (40 eq) in NMP, RT, 24 hrs, no light) and

release with 5 eq (0.10 mmol) of each HyT's 1-7 and 11-23 at RT for 64 hrs. Free amines were captured with high loading tosyl chloride resin (125 mg, 0.3 mmol) and Et_3N (84 μL, 0.60 mmol) per reaction in 1 mL of DCM and agitated on an orbital shaker at 150 RPM's overnight at 27 °C.

The triethylamine salts were free based with K_2CO_3 (5.2 mmol, 700 mg) for 15 hours at 33 °C at 150 RPM's. The salts were gravimetrically filtered and washed with DCM. The filtrates were dried *in vacuo*, resuspended in 2 mL of Xylene and washed with 2 mL of acetone and filtered again. The filtrate was dried *in vacuo* and washed with 2-4 mL of BuOH and dried again until dry.

Protecting groups were cleaved with TFA/H_2O/TIPS [95:0.5:0.5] for 1 hour then dried under N_2 for 20 minutes. The conjugates were resuspended in 1 mL of 10% ACN in water then diluted at 1:25 in 100 μL of DMSO. Each conjugate was quantitated by UV/Vis based on the adsorption of RTX at both 269 and 341 nm, respectively. The bulk filtrates in 10% ACN in water were subsequently lyophilized, massed, and their yields calculated (Table 4.3) followed by their resuspension in DMSO to yield a 10 mM solution of each conjugate for biological evaluation.

4.2.7 Safety-Catch Resin and RTX-PEG$_n$-HyT Conjugates

The synthesis of the RTX-PEG$_n$-HyT conjugates was performed by our colleague, Enoch Adogla, under Dr. Qian Wang's mentorship (Department of Chemistry and Biochemistry, University of South Carolina).

4.2.8 Isothermal Titration Calorimetry

Isothermal titration calorimetry (ITC) was performed on a VPITC instrument (Microcal Corp.) with a 250 μL syringe. All ITC measurements were carried out at in degassed solutions at 26 °C. Approximately fifty-two, 5 μL injections were made with 6-second duration and 120 seconds spacing. The macromolecule (TS) concentration was 15 μM in 50 mM Tris-HCl, pH 7.4 with 1 mM EDTA and 20 μM BME, which is referred to as "Buffer A." Titration was carried out in buffer A with the following reagents: 100 μM dUMP and 300 μM of conjugate(s). The data was processed using the manufactures software ORIGIN.

4.3 REFERENCES

1. Ishii, Y. et al. Bortezomib Enhances the Efficacy of Fulvestrant by Amplifying the Aggregation of the Estrogen Receptor, Which Leads to a Proapoptotic Unfolded Protein Response. *Clin. Cancer Res.* **17**, 2292-2300 (2011).
2. Citri, A. et al. Drug-induced ubiquitylation and degradation of ErbB receptor tyrosine kinases: implications for cancer therapy. *Embo J.* **21**, 2407-2417 (2002).
3. Sakamoto, K.M. et al. Protacs: Chimeric molecules that target proteins to the Skp1-Cullin-F box complex for ubiquitination and degradation. *Proc. Natl. Acad. Sci. U. S. A.* **98**, 8554-8559 (2001).
4. Sakamoto, K.M. et al. Development of protacs to target cancer-promoting proteins for ubiquitination and degradation. *Mol. Cell. Proteomics* **2**, 1350-1358 (2003).

5. Schneekloth, J.S. et al. Chemical genetic control of protein levels: Selective in vivo targeted degradation. *J. Am. Chem. Soc.* **126**, 3748-3754 (2004).

6. Bargagna-Mohan, P., Baek, S.H., Lee, H., Kim, K. & Mohan, R. Use of PROTACS as molecular probes of angiogenesis. *Bioorg. Med. Chem. Lett.* **15**, 2724-2727 (2005).

7. Puppala, D., Lee, H., Kim, K.B. & Swanson, H.I. Development of an aryl hydrocarbon receptor antagonist using the proteolysis-targeting chimeric molecules approach: A potential tool for chemoprevention. *Mol. Pharmacol.* **73**, 1064-1071 (2008).

8. Hines, J., Gough, J.D., Corson, T.W. & Crews, C.M. Posttranslational protein knockdown coupled to receptor tyrosine kinase activation with phosphoPROTACs. *Proc. Natl. Acad. Sci. U. S. A.* **110**, 8942-8947 (2013).

9. Banaszynski, L.A., Chen, L.C., Maynard-Smith, L.A., Ooi, A.G.L. & Wandless, T.J. A rapid, reversible, and tunable method to regulate protein function in living cells using synthetic small molecules. *Cell* **126**, 995-1004 (2006).

10. Pratt, M.R., Schwartz, E.C. & Muir, T.W. Small-molecule-mediated rescue of protein function by an inducible proteolytic shunt. *Proc. Natl. Acad. Sci. U. S. A.* **104**, 11209-11214 (2007).

11. Long, M.J.C., Gollapalli, D.R. & Hedstrom, L. Inhibitor Mediated Protein Degradation. *Chem. Biol.* **19**, 629-637 (2012).

12. Neklesa, T.K. et al. Small-molecule hydrophobic tagging-induced degradation of HaloTag fusion proteins. *Nat. Chem. Biol.* **7**, 538-543 (2011).

13. Barbour, K.W. & Berger, F.G. Cell death in response to antimetabolites directed at thymidylate synthase. *Cancer Chemother. Pharmacol.* **61**, 189-201 (2008).

14. Jackman, A.L. et al. The Biochemical Pharmacology of the Thymidylate Synthase Inhibitor, 2-Desamino-2-methyl-N-10-Propargyl-5,8-dideazafolic acid (ICI-198583). *Biochem. Pharmacol.* **42**, 1885-1895 (1991).

15. Moran, R.G., Colman, P.D., Forsch, R.A. & Rosowsky, A. A Mechanism for the Addition of Multiple Moles of Glutamate by Folylpolyglutamate Synthaetase. *J. Med. Chem.* **27**, 1263-1267 (1984).

16. Singh, S.K. et al. Symthesis and Biological Evaluation of N-alpha-(5-deaza-5,6,7,8-tetrahydropteroyl)-L-Ornithine. *J. Med. Chem.* **35**, 2002-2006 (1992).

17. Rosowsky, A., Forsch, R.A. & Moran, R.G. Inhibition of folylpolyglutamate synthetase by substrate analogues with an ornithine side chain. *J. Heterocycl. Chem.* **33**, 1355-1361 (1996).

18. Gibson, W. et al. The Measurement of Polyglutamate Metabolites of the Thymidylate Synthase Inhibitor ICI-D1694, In Mouns and Human Cultured-Cells. *Biochem. Pharmacol.* **45**, 863-869 (1993).

19. Kamb, A., Moore, J.F., Calvert, A.H. & Stroud, R.M. Structural Basis for Recognition of Polyglutamyl Folates by Thymidylate Synthase. *Biochemistry* **31**, 9883-9890 (1992).

20. Kenner, G.W., McDermot.Jr & Sheppard, R.C. Safety Catch Principle in Solid Phase Peptide Synthesis. *Journal of the Chemical Society D-Chemical Communications*, 636-637 (1971).

21. Krchnak, V., Vagner, J., Safar, P. & Lebl, M. Amino-Acids and Peptides .206. Nonivasive Continous Monitoring of Solid-Phase Peptide-Synthesis by Acid-Base Indicator. *Collect. Czech. Chem. Commun.* **53**, 2542-2548 (1988).

22. Backes, B.J. & Ellman, J.A. An alkanesulfonamide "safety-catch" linker for solid-phase synthesis. *J. Org. Chem.* **64**, 2322-2330 (1999).

23. Kim, M.H. & Patel, D.V. BOP as a Reagent for Mild and Efficient Preparation of Esters. *Tetrahedron Lett.* **35**, 5603-5606 (1994).

24. Nussbaum, R.L., Walmsley, R.M., Lesko, J.G., Airhart, S.D. & Ledbetter, D.H. Thymidylate Synthase-Deficient Chinese-Hamster Cells - A Selection for Human-Chromosome 18 and Experimental System for the Study of Thymidylate Synthase Regulation and Fragile-X Expression. *Am. J. Hum. Genet.* **37**, 1192-1205 (1985).

25. Pena, M.M.O., Xing, Y.Y., Koli, S. & Berger, F.G. Role of N-terminal residues in the ubiquitin-independent degradation of human thymidylate synthase. *Biochem. J.* **394**, 355-363 (2006).

26. Kaiser, E., Colescot.Rl, Bossinge.Cd & Cook, P.I. Color Test for Detection of Free Terminal Amino Groups in Solid-Phase Synthesis of Peptides. *Anal. Biochem.* **34**, 595-& (1970).

27. Backes, B.J., Harris, J.L., Leonetti, F., Craik, C.S. & Ellman, J.A. Synthesis of positional-scanning libraries of fluorogenic peptide substrates to define the extended substrate specificity of plasmin and thrombin (vol 18, pg 188, 2000). *Nat. Biotechnol.* **18**, 559-559 (2000).

CHAPTER 5

5.0 SUMMARY AND CONCLUSION

Here, we described two approaches' to systematically degrade human thymidylate synthase through both an ubiquitin-dependent and independent mechanism. Through our synthetic endeavors (Table 2.2), we were able to characterize and develop a raltitrexed (RTX) γ-selective TS-specific probe and pursue *in vitro* TS tracking through the *in situ* application of CuAAC chemistry (Figure 2.12 and 2.14). Applying our previous synthetic approaches, we used the TS-specific antifolate raltitrexed to synthetically construct a TS-HIFα heterobifunctional ligand (PROTAC-1 and -2) that would bind to TS and recruit the VHL E3-ligase complex for proteasomal degradation. It was hypothesized that PROTAC-1 and/or -2 would engender the polyubiquitination of TS necessary to induce ubiquitin-dependent proteasomal degradation. This strategy was perceived to be superior to the direct systemic administration of antimetabolites used to pharmacologically inhibit TS action and function independently of the internal TS degron.

We found that neither PROTAC-1 or -2 enabled the targeted ubiquitination of TS, rather, only moderate inhibition (0.20 μM IC_{50}) of the TS ternary complex (PROTAC-1•dUMP•TS) was achieved with half-life stabilities resembling those of free RTX (Half-Life > 24 hrs). The failure of our PROTAC to systematically degrade (through

ubiquitination) TS could potentially be the result of: (i) the relative short length of the linker, both triglycine and PEG, may have restricted the presentation of the HIFα signal peptide and allowed for its non-specific interaction with the surface of TS, (ii) the regioselectivity of RTX to the linker may have impaired the ability of RTX to successfully dock with TS as only the γ-carboxylate of RTX has been shown to yield high binding affinity, or (iii) the lack of active surface lysine moieties on TS has likely rendered PROTAC's a moot endeavor, whereas if the VHL E3-ligase were recruited, the absence of a viable ligation partner (ε-amino group) for the E2-conjugating enzyme would not accommodate proteasomal degradation via the UPS.

However, the PROTAC served as a translational probe of the innate properties of TS degradation. Previous results have shown TS degradation is independent to Ub even the conditions of TS lysine-null mutant. Our results corroborate the inherent resistance of TS to Ub and substantiate its status as proceeding via ubiquitin-independent proteasomal degradation.

Notwithstanding, we sought to explore an alternate approach to ligand-directed degradation of TS. We hypothesized that appending a hydrophobic moiety or "tag" to raltitrexed functionalize RTX to act as a direct post-translational degradation ligand, whereas free RTX only stabilizes intracellular TS. Again, using our previous synthetic efforts, we recruited the Kenner Safety-Catch resin for the construction of multiple TS-directed ligand-based hydrophobic tag conjugates. The Safety-Catch resin was well suited for our efforts as the acylation at the terminal end of our RTX-EE (**1b**) conjugate was impractical under standard N→C solid phase peptide synthesis. With this resin, we were able to introduce compounds with active primary amines and varying degrees of

hydrophobicity as determined by their theoretical partition coefficients (LogP). Furthermore, this approach accommodated the relatively high-throughput requirements needed to produce complicated compounds with workable yields (60-100%) and apply them in high-volume manner for their biological evaluation (Table 4.3). We examined 23 prospective hydrophobic tags (HyT) based on their LogP, low molecular weight (> 250 amu), and whether they possessed and active primary or secondary amine. Structurally, we were interested in the effects of increasing HyT length (surface area) under aliphatic compounds, aromatic substituents with 1, 2, or 3 methylene spacers from their active amine, and spherical or elliptical non-aromatic compounds.

The relatively small library was constructed through various stages of method development and each of the 23 HyT's was used to generate a RTX-EE-HyT conjugate capable of targeting TS (Figure 4.8 and 4.12). Post synthesis, we evaluated each compound in triplicate fashion by monitoring their ability to inhibit cell proliferation in CHL-TS pJZ205 cells. We found this metric (IC_{50}) to be the most useful as it was easily scaled for high-throughput analyses and could provide insight as to the potential of each compound.

Based on our preliminary data, we found no correlation with the increasing surface area of the aliphatic HyT's (Figure 4.12, group I) where only the shortest and longest aliphatic chains recorded inhibition numbers comparable to free **1b** (Figure 4.4A). The structure activity relationship (SAR) of benzylated HyT's (Figure 4.12, group II and III) indicated that both chain length from the active amine to the benzene moiety and moderate tailoring of benzene with weak electron withdrawing groups were among the attributes that contributed to the inhibitory characteristics of each conjugate. The

remaining tags, group IV and VI, demonstrated excellent and mixed conclusions, respectively. Group IV consisted of the spherical non-aromatic compounds such as adamantane. This compound has already demonstrated potential as a hydrophobic tag, however, the mechanism involved relied upon the genetic assault of the targeted organism through the direct transfection of a stable fusion construct specifically targeted by the adamantly-ligand. Under our expertise, we found that the adamantyl moiety and two of its homologs (HyT's 12 and 16) reported excellent inhibition values when compared to the parent compound **1b**. Hence, group IV offered the most potential for further investigation toward the specific involvement of the proteasome.

Taken together, we showed that although TS undoubtedly follows an ubiquitin-independent pathway toward proteasomal degradation, we demonstrated the direct value in TS degradation through hydrophobic tagging. Unlike several other degradation methods, which require genetic intervention, hydrophobic tagging would allow for the direct targeting of TS and circumvent the stabilizing effect of RTX (or other antifolates with free carboxylates) to potentially promote what would likely be a concentration dependent reduction of intracellular TS.

APPENDIX A – PERMISSION REQUEST FOR ADAPTATION FOR TABLE 1.1

SPRINGER LICENSE
TERMS AND CONDITIONS

Oct 24, 2014

This is a License Agreement between Daniel J Menasco ("You") and Springer ("Springer") provided by Copyright Clearance Center ("CCC"). The license consists of your order details, the terms and conditions provided by Springer, and the payment terms and conditions.

All payments must be made in full to CCC. For payment instructions, please see information listed at the bottom of this form.

License Number	3495201077431
License date	Oct 24, 2014
Licensed content publisher	Springer
Licensed content publication	Springer eBook
Licensed content title	The Role of the Reduced-Folate Carrier and Metabolism to Intracellular Polyglutamates for the Activity of ICI D1694
Licensed content author	Ann L. Jackman
Licensed content date	Jan 1, 1993
Type of Use	Thesis/Dissertation
Portion	Figures
Author of this Springer article	No
Order reference number	None
Original figure numbers	Tables 1 and 2
Title of your thesis / dissertation	Toward the combinatorial development of hydrophobic-tagged anitfolate-directed degradation of human thymdylate synthase
Expected completion date	Nov 2014
Estimated size(pages)	150
Total	0.00 USD
Terms and Conditions	

Introduction
The publisher for this copyrighted material is Springer Science + Business Media. By clicking "accept" in connection with completing this licensing transaction, you agree that the following terms and conditions apply to this transaction (along with the Billing and Payment terms and conditions established by Copyright Clearance Center, Inc. ("CCC"), at the time that you opened your Rightslink account and that are available at any time at

APPENDIX B – PERMISSION REQUEST FOR ADAPTATION FOR FIGURE 1.4

NATURE PUBLISHING GROUP LICENSE TERMS AND CONDITIONS

Oct 24, 2014

This is a License Agreement between Daniel J Menasco ("You") and Nature Publishing Group ("Nature Publishing Group") provided by Copyright Clearance Center ("CCC"). The license consists of your order details, the terms and conditions provided by Nature Publishing Group, and the payment terms and conditions.

All payments must be made in full to CCC. For payment instructions, please see information listed at the bottom of this form.

License Number	3495201359484
License date	Oct 24, 2014
Licensed content publisher	Nature Publishing Group
Licensed content publication	Nature
Licensed content title	An unusual mechanism of thymidylate biosynthesis in organisms containing the thyX gene
Licensed content author	Eric M. Koehn, Todd Fleischmann, John A. Conrad, Bruce A. Palfey, Scott A. Lesley et al.
Licensed content date	Apr 16, 2009
Volume number	458
Issue number	7240
Type of Use	reuse in a dissertation / thesis
Requestor type	academic/educational
Format	print and electronic
Portion	figures/tables/illustrations
Number of figures/tables/illustrations	1
High-res required	no
Figures	Figure 1a, the traditional hTS mechanism.
Author of this NPG article	no
Your reference number	None
Title of your thesis / dissertation	Toward the combinatorial development of hydrophobic-tagged anitfolate-directed degradation of human thymdylate synthase
Expected completion date	Nov 2014
Estimated size (number of	150

APPENDIX C – PERMISSION REQUEST FOR REPRODUCTION FOR FIGURE 1.8

NATURE PUBLISHING GROUP LICENSE TERMS AND CONDITIONS

Oct 23, 2014

This is a License Agreement between Daniel J Menasco ("You") and Nature Publishing Group ("Nature Publishing Group") provided by Copyright Clearance Center ("CCC"). The license consists of your order details, the terms and conditions provided by Nature Publishing Group, and the payment terms and conditions.

All payments must be made in full to CCC. For payment instructions, please see information listed at the bottom of this form.

License Number	3495060176554
License date	Oct 23, 2014
Licensed content publisher	Nature Publishing Group
Licensed content publication	Nature
Licensed content title	Molecular chaperones in protein folding and proteostasis
Licensed content author	F. Ulrich Hartl, Andreas Bracher, Manajit Hayer-Hartl
Licensed content date	Jul 20, 2011
Volume number	475
Issue number	7356
Type of Use	reuse in a dissertation / thesis
Requestor type	academic/educational
Format	print and electronic
Portion	figures/tables/illustrations
Number of figures/tables/illustrations	1
High-res required	no
Figures	Original Paper: Fig 6. Thesis: Fig 1.7.
Author of this NPG article	no
Your reference number	None
Title of your thesis / dissertation	Toward the combinatorial development of hydrophobic-tagged anitfolate-directed degradation of human thymdylate synthase
Expected completion date	Nov 2014
Estimated size (number of pages)	150

APPENDIX D – PERMISSION REQUEST FOR REPRODUCTION FOR FIGURE 3.3

NATURE PUBLISHING GROUP LICENSE TERMS AND CONDITIONS

Oct 27, 2014

This is a License Agreement between Daniel J Menasco ("You") and Nature Publishing Group ("Nature Publishing Group") provided by Copyright Clearance Center ("CCC"). The license consists of your order details, the terms and conditions provided by Nature Publishing Group, and the payment terms and conditions.

All payments must be made in full to CCC. For payment instructions, please see information listed at the bottom of this form.

License Number	3497260267296
License date	Oct 27, 2014
Licensed content publisher	Nature Publishing Group
Licensed content publication	Nature
Licensed content title	Structural basis for the recognition of hydroxyproline in HIF-1[alpha] by pVHL
Licensed content author	Wai-Ching Hon, Michael I. Wilson, Karl Harlos, Timothy D. W. Claridge, Christopher J. Schofield et al.
Licensed content date	Jun 5, 2002
Volume number	417
Issue number	6892
Type of Use	reuse in a dissertation / thesis
Requestor type	academic/educational
Format	print and electronic
Portion	figures/tables/illustrations
Number of figures/tables/illustrations	1
High-res required	no
Figures	I would like permission to reproduce the structure in figure 1a and b.
Author of this NPG article	no
Your reference number	None
Title of your thesis / dissertation	Toward the combinatorial development of hydrophobic-tagged anitfolate-directed degradation of human thymdylate synthase
Expected completion date	Nov 2014